UNIVERSIDADE DE SÃO PAULO

FACULDADE DE FILOSOFIA, CIÊNCIAS E LETRAS DE RIBEIRÃO PRETO

PROGRAMA DE PÓS-GRADUAÇÃO EM BIOLOGIA COMPARADA

# 3D skull modelling and description of a new baurusuchid (Crocodyliformes, Mesoeucrocodylia) from the Late Cretaceous (Bauru Basin) of Brazil

# Modelagem craniana 3D e descrição de um novo baurusuquídeo (Crocodyliformes, Mesoeucrocodylia) do Cretáceo Tardio (Bacia Bauru) do Brasil

GUSTAVO DARLIM DE OLIVEIRA

Dissertação apresentada à Faculdade de Filosofia, Ciências e Letras de Ribeirão Preto da Universidade de São Paulo, como parte das exigências para obtenção do título de Mestre em Ciências, obtido no Programa de Pós-Graduação em Biologia Comparada.

RIBEIRÃO PRETO - SP

2020

UNIVERSIDADE DE SÃO PAULO

FACULDADE DE FILOSOFIA, CIÊNCIAS E LETRAS DE RIBEIRÃO PRETO

PROGRAMA DE PÓS-GRADUAÇÃO EM BIOLOGIA COMPARADA

# 3D skull modelling and description of a new baurusuchid (Crocodyliformes, Mesoeucrocodylia) from the Late Cretaceous (Bauru Basin) of Brazil

GUSTAVO DARLIM DE OLIVEIRA

Dissertação apresentada à Faculdade de Filosofia, Ciências e Letras de Ribeirão Preto da Universidade de São Paulo, como parte das exigências para obtenção do título de Mestre em Ciências, obtido no Programa de Pós-Graduação em Biologia Comparada.

Orientador: Max Cardoso Langer

RIBEIRÃO PRETO - SP

2020

Oliveira, Gustavo Darlim de

3D skull modelling and description of a new baurusuchid (Crocodyliformes, Mesoeucrocodylia) from the Late Cretaceous (Bauru Basin) of Brazil. Ribeirão Preto, 2020.

111 p.

Dissertação de Mestrado apresentada à Faculdade de Filosofia, Ciências e Letras de Ribeirão Preto/USP. Área de concentração: Biologia Comparada.

Orientador: Langer, Max Cardoso

1. Mesoeucrocodylia. 2. Baurusuchidae. 3. CT scan. 4. Skull
5. Tomography

Name: OLIVEIRA, Gustavo Darlim

Title: 3D skull modelling and description of a new baurusuchid (Crocodyliformes, Mesoeucrocodylia) from the Late Cretaceous (Bauru Basin) of Brazil. Ribeirão Preto, 2020.

Dissertação apresentada à Faculdade de Filosofia, Ciências e Letras de Ribeirão Preto-USP, como parte das exigências para obtenção do título de Mestre em Ciências, obtido no Programa de Pós-Graduação em Biologia Comparada.

Approved in:

Evaluation Board

Prof. Dr. _____Instituição: _____

Veredict: _____ Signature:_____

Prof. Dr. _____Instituição: _____

Veredict: _____Signature:_____

Prof. Dr. _____Instituição: _____

Veredict: _____Signature:_____

Prof. Dr. _____Instituição: _____

Veredict: _____Signature:_____

**Acknowledgements**

First, I would like to thank my Family: my father, Renato, my mother, Maria Helena and my brother Juliano for all the love, care, and support to every decision I have made. I can't put in words how hard my family has worked to give me the best conditions to study and work with what I love. I hope I can be as good as they one day. Thank you, and I love you. Without you, it would not be possible.

I want to thank my friend, Prof. Dra Manoela Marinho, who gave me opportunities to grow in science and research. As all the member of the ichthyology session of MZUSP, who provides me an amazing, friendly work environment. Miss you all.

To all my friends and colleagues of the Laboratório de Paleontologia de Ribeirão Preto (Paleolab): Prof. Annie, Julio, Mari, Ana Laura, Blair, Felipe, Flávia, Julian, Loboda, Paulo, Roque, Silvia, Wafinha, Pedro (Tomate), Giovanne, Bete and Marcos.

A special thanks to my closest friends, for all the daily conversations, laughs and good moments: Xico, Gabriel, João, Bruna, Fellipe, Silvio, Gabriel (Fumaça), and Guilherme (Squirtle). Love you guys.

To my friend from graduation (to life), Luiza. I love you and thank you for being you.

A special thanks to Guilherme (Squirtle), Gabriel (Fumaça), Mario Bronzati (Roque), Pedro Godoy (Tomate), Julio to all the suggestions and improvements to my project.

To Gabriel Ferreira (Fumaça), who helped me to get new opportunities in my professional life.

To my co-supervisor Prof. Dr. Felipe Montefeltro for all the conversations, suggestions and all the knowledge about baurusuchids. Thank you for improving so much the dissertation.

To my paleolab friends for the help and the company for the collection visits: Fellipe, Julian, Tati, Schumi. Thank you guys for helping me and for the amazing time.

For access to collections, I want to thank Prof. Dr. Thiago Marinho (CCCP, Peirópolis), Prof. Ismar Carvalho, and to the museologists Penélope and Flávia (UFRJ), Rafael (DNPM) and Dra. Sandra Tavares (MPMA).

To the Program of Comparative Biology from Faculdade de Filosofia, Ciências e Letras de Ribeirão Preto.

To secretary Vera Cicilini de Luca for the help with all the bureaucracy, for the patience and good laugh.

To the Coordenação de Aperfeiçoamento de Pessoal de Nível Superior (CAPES) for the scholarship during my first year and to Fundação de Amparo a Pesquisa do Estado de São Paulo (FAPESP- 2019/ 06311-4) for the scholarship during my second year on masters degree for funding meetings and travels for collection visiting.

To Dr. Flávio Junior de Oliveira and Dr. Marcel Koenigkam Santos (Centro das imagens e Física Médica – CCIFM) for authorize the use of the tomograph at Hospital das Clínicas-USP.

And I am thankful to my supervisor, Professor Max Cardoso Langer, who gave me the opportunity to start working with paleontology. Thank you for all the suggestions, the field works, the conversation and to proportionate a friendly and productive environment to work, and how the lab is opening doors for me to grow in paleontology. I am very grateful.

**“Porque não vivo nem no meu passado, nem no meu futuro. Tenho apenas o presente, e ele é o que me interessa. Se puder permanecer sempre no presente, então será um homem feliz”**

- O Alquimista. Paulo Coelho, 1988

**Resumo**

A família Baurusuchidae representa um dos mais diversos grupos de notossúquios Sul-Americanos, registrados em depósitos do Cretáceo Superior do Brasil e Argentina. O grupo é caracterizado pela fórmula dentária reduzida, rostro comprimido látero-medialmente e quadrado verticalizado, representando os predadores de topo de suas paleobiotas. A morfologia do crânio é historicamente a ferramenta mais utilizada para entender a evolução dos baurussuquídeos, tendo em vista que a maioria das espécies foram descritas com base primariamente em elementos cranianos. O presente estudo apresenta a descrição de uma nova espécie em Baurusuchidae da Bacia Bauru, Cretáceo do Brasil, e discute a sua posição filogenética no grupo. Ademais, o estudo disponibiliza a primeira reconstrução digital tridimensional para ossos craniano individuais de Notosuchia. A nova espécie difere dos demais baurusuquídeos por apresentar uma depressão na porção posterior do nasal com uma crista central, uma crista infraorbital do jugal se estendendo até a margem anterior do lacrimal, ausência de crista e depressão longitudinais no frontal e margem lateral das abas do esquamosal convexas participando da placa occipital do crânio. O novo táxon é consistentemente posicionado como grupo-irmão de um clado que inclui todos os Baurusuchinae, mas as relações entre *Aplestosuchus sordidus*, *Baurusuchus albertoi* e *Stratiotosuchus maxhechti* permanecem não resolvidas. Adicionalmente, os novos caracteres de valor filogenético foram identificados e novas variações morfológicas foram reconhecidas para as subfamílias Baurusuchinae e Pissarrachampsinae. A nova espécie apresenta características em comum com esses dois subgrupos, sugerindo a ocorrência de "Zonas de Variabilidade" na origem de Baurusuchidae.

Palavras-chave: Mesoeucrocodylia, Baurusuchidae, CT scan, crânio, Cretáceo

**Abstract**

Baurusuchidae is one of the most diverse groups of South American notosuchians, recorded in Late Cretaceous deposits of Brazil and Argentina. The group is characterized by a reduced tooth formula, a lateromedially compressed rostrum, and a verticalized quadrate, representing the top predators of their faunas. The morphology of the skull is historically the most employed tool to investigate the phylogeny of baurusuchids, as most of the species have been described based primally on cranial remains. The present study describes a new baurusuchid species from the Bauru Basin of Brazil, discussing its phylogenetic position within the group. Furthermore, the study provides the first tridimensional digital reconstruction of individual skull bones for Notosuchia. The new species differs from all the other known baurusuchids by a depression on the posterior portion of nasal bearing a crest, a infraorbital crest of the jugal that extends until the anterior margin of the lacrimal, the absence of a longitudinal crest or depression on the dorsal surface of the frontal, and the lateral convexity of the squamosal prongs taking part of the occipital wall. The new taxon is consistently positioned as sister to a clade including all other baurusuchines, but the relations among *Aplestosuchus sordidus*, *Baurusuchus albertoi*, and *Stratiotosuchus maxhechti* remain unresolved. The phylogenetic data matrix includes newly proposed characters, which hep in the differentiation between Baurusuchinae and Pissarrachampsinae. Yet, the new species shares morphological features with both groups, suggesting the occurrence of "Zones of Variability" in the origin of Baurusuchidae.

Keywords: Mesoeucrocodylia, Baurusuchidae, CT scan, Skull, Cretaceous

**SUMMARY**

## 1. Introduction

Baurusuchidae is a group of terrestrial and cursorial Crocodyliformes that were top predators during the Cretaceous where today is South America. The fossil record of the group is mostly limited to the Adamantina Formation in Brazil and the Bajo de La Carpa Formation in Argentina. The group was originally proposed by Price (1945) to encompass only *Baurusuchus pachecoi* and defined by the unique combination of morphological features of that single species (e. g. reduced tooth formula, laterally compressed rostrum, ziphodont dentition, verticalized quadrate, and large ectopterygoids participating on the borders of the internal narial openings). Later discoveries revealed Baurusuchidae as the most diverse group of Crocodyliformes in the Adamantina Formation (Riff et al. 2013; Godoy et al., 2014; Montefeltro 2019), including seven other species: *Stratiotosuchus maxhechti* Campos et al. (2001), *B. salgadoensis* Carvalho et al. (2005), *B. alberoi* Nascimento & Zaher (2010), *Campinasuchus dinizi* Carvalho et al. (2011), *Pissarrachampsa sera* Montefeltro et al. (2011), *Gondwanasuchus scabrosus* Marinho et al. (2013), and *Aplestosuchus sordidus* Godoy et al. (2014). Also, two Argentinean species are assigned to Baurusuchidae, *Cynodontosuchus rothi* Woorward (1896) and *Wargosuchus australis* Martinelli & Pais (2008), as well as a potentially Pakistani species, *Pabwehshi pakistanensis* (Wilson et al., 2001), and a third plausible Argentinean baurusuchid, *Pehuenchesuschus enderi* (Turner & Calvo, 2005), which also is closely related to Sebecosuchia, highlighting not only the affinities of Patagonian baurusuchids (Leardi et al., 2018), but also the exuberance of the group in the Late Cretaceous of Gondwana.

*Cynodontosuchus rothi* was, historically, the first baurusuchid to be described, but it was initially related to *Notosuchus terrestris* (Woodward, 1896). The exact provenance of the holotype and only specimen of *C. rothi* is not known, but due its association with *N. terrestris*, is inferred to be the Bajo de La Carpa Formation (Martinelli & Pais, 2008). The material is composed of a poorly preserved rostrum and morphological features such the absence of maxillary and premaxillary caniniform teeth indicate that the species is valid, but also raise questions about its possible juvenile status (Leardi et al., 2018). The other Argentinean species, *W. australis*, is also represented by a fragmentary skull, with portions of the premaxilla and skull roof. The species is diagnosed by the presence of a longitudinal sulcus on the anterior portion of the frontal dorsal surface, the prefrontals approaching but not contacting one another medially, allowing the nasal-frontal contact, and the presence of an enlarged last premaxillary tooth. Furthermore, new fragmentary skull and postcranial remains have been recognized as baurusuchids from Bajo de la Carpa Formation more recently (Leardi et al., 2018), but the

fragmentary condition of the material hampered a taxonomic association, as indicated by the floating position of the new specimens on the phylogeny. The incompleteness of all those taxa reveals a gap on the knowledge, but at the same time a work in progress about the Argentinean baurusuchid diversity. However, the fact that there are unquestionable baurusuchids outside Brazil is important for understanding the original paleogeographical distribution of the group.

As for the Brazilian baurusuchids, all the species were unearthed from the Adamantina Formation in the states of São Paulo and Minas Gerais. *S. maxhechti,* discovered in the municipality of Irapuru-SP, was the first baurusuchid described after *B. pachecoi*, representing one of the largest baurusuchids ever recorded (Campos et al., 2001; Godoy et al., 2016). In its heavily ornamented skull, sutures are mostly untraceable and the supraorbital fenestrae is not present. Unfortunately, the choanal structures are very damaged, and the mandible is mostly not preserved, but features such the presence of three premaxillary teeth, frontal not entering the supratemporal fossa, ventral notch in the posterior portion of the jugal orbital border, and enlarged foramen incisivum in the premaxilla-maxilla suture allow diagnosing the taxon (Campos et al., 2011; Montefeltro et al., 2011). The second *Baurusuchus* species to be described was *B. salgadoensis*, which is also relatively large in comparison to the other bauruschids, although not as much as *S. maxhecthi*, and included the first complete skull described for the genus. Two main features diagnose the species, the paired ventral ridges of the basisphenoid anteroventrally convergent and a ridged border of the angular medial surface not overcoming the anterior edge of the mandibular fenestra (Montefeltro et al., 2011). More recently, Nascimento & Zaher (2010) provided the first comprehensive description of the postcranial anatomy of a baurusuchid, focused on the third *Baurusuchus* species, *B. albertoi* from Fazenda Buriti, near the district of Prudêncio e Morais, General Salgado-SP, the same site that yielded *B. salgadoensis*. *B. albertoi* lacks significant portions of the skull, and is diagnosed by a concave anterior surface of the squamosal prong, and a well-developed ventromedial crest on the quadrate (*sensu* Montefeltro et al., 2011). These subtle features hamper the precise individualization of the species. In fact, Nascimento (2014) mentioned that the first feature can be doubtful due a broken area on the specimen and that the condition can also be related to individual variation.

In 2011, *C. dinizi* and *P. sera* were discovered in Minas Gerais, both in the municipality of Campina Verde. Interestingly, those species have morphological features clearly distinct from those of other baurusuchids, but similar between them, especially regarding their choanal anatomy. Montefeltro et al. (2011) proposed the definition of two subgroups of Baurusuchidae,

Baurusuchinae and Pissarrachampsinae, based on synapomorphies present on the nasal, prefrontal, and frontal bones. Apart from *P. sera* and *C. dinizi*, Pissarrachampsinae includes the Argentinean *W. australis*. The remaining two species of the group are somehow intriguing. As for *G. scabrosus*, described based on a partial skull. This taxon is significantly smaller than the taxa in Pissarrachampsinae and Baurusuchinae, and presents a unique condition among baurusuchids, the presence of deep and wide apicobasal sulci that converge apically on premaxillary and maxillary dentition. Also, the species has a more posteriorly positioned external mandibular fenestra, starting posterior to the level of the anteriormost portion of the orbit, which is conspicuously large and more anteriorly directed when compared with those of its group relatives (Marinho et al., 2013). Consequently, the infraorbital ramus of the jugal forms a dorsoventrally thin bar. Furthermore, the anterior margin of the premaxilla is more prominent anteriorly, than that of the mandible, it possesses a marked dorsal depression on the nasal, and the prefrontals do not contact one another medially, allowing the nasal-frontal contact. Marinho et al. (2013) mention that the species could represent a subadult of a small to medium-sized baurusuchid.

The last described baurusuchid was *A. sordidus* (Godoy et al, 2014), based on an almost complete single skeleton, but only the skull was described in detail, which is dorsoventrally compressed, preventing the external exposure of some of the bones. A marked crest on the posterior portion of the nasal, a frontal longitudinal ridge reaching the midline contact between the prefrontals, and a palatine bar with crested ventral surface distinguish the species from other baurusuchids. It is interesting to mention that *A. sordidus* and *G. scabrosus* were discovered in the same set of outcrops as *B. salgadoensis* and *B. albertoi*. In addition, the area also yielded other crocodyliform materials, including eggs and the sphagesaurids Armadillosuchus arrudai (Marinho & Carvalho 2009) and *Caipirasuchus stenognathus* (Pol et al. 2014).

That recent phylogenetic definition of Baurusuchidae proposed by Montefeltro et al. (2011) consists in the least inclusive clade containing *C. rothi*, *P. sera*, *S. maxhechti*, and *B. pachecoi*, as long as it does not include *N. terrestris* Woodward, 1896, *Mariliasuchus amarali* Carvalho & Bertini, 1999, *Armadillosuchus arrudai* Marinho & Carvalho, 2009, *Araripesuchus gomesi* Price, 1959, *Sebecus icaeorhinus* Simpson 1937, *Bretesuchus bonapartei* Gasparini, Fernandez & Powell, 1993, *Peirosaurus tormini* Price, 1955, or *Crocodylus niloticus* Laurent, 1768. The group presents the following combination of morphological features: laterally compressed rostrum, no antorbital fenestra, notch in the rostrum for the reception of the dentary caniniform tooth, approximation of prefrontals towards midline, well developed palatine bar,

anterior extension of palatine not reaching the level of the anterior margin of suborbital fenestra, ectopterygoid forming the choanal border, posteroventral depressions in the mandibular symphysis, anterodorsal orientation of the mandibular symphysis terminus (at approximately 45 degrees to the jaw line), quadratojugal extending dorsally as a broad sheet contacting most of the postorbital portion of the postorbital bar, vertical quadrate, reduced number of teeth, hypertrophied maxillary tooth, and ziphodont dentition (Price, 1945; Colbert, 1946; Gasparini, 1972; Gasparini, 1981; Prasad & Lapparent de Broin, 2002; Carvalho *et al*., 2005; Turner & Calvo, 2005; Martinelli & Pais, 2008; Montefeltro et al. 2011).

In 2012 an expedition of the Laboratório de Paleontologia, FFCLRP-USP, to the municipality of Jales, São Paulo State, resulted in the discovery of a new specimen (LPRP/USP 0697) of Baurusuchidae from the Adamantina Formation. The material composed of an almost complete skeleton can be easily referred to the group due to its reduced maxillary tooth formula, verticalized quadrate, and mediolaterally compressed rostrum. The Fazenda Furnas outcrop, where the specimen was found, also yielded other baurusuchid specimens, including a nearly complete articulated tail (Avilla et al., 2004) and a series of vertebrae articulated with a partial pelvic girdle (Araújo & Marinho, 2013). Also, eggs possibly associated to Baurusuchidae were found in the same outcrop (Oliveira et al., 2011).

### *1.1 Geology and Paleontology of the Adamantina Formation*

During the opening of the Atlantic Ocean, the continental break up produced a huge depression where southeastern Brazil is today, allowing the accumulation of sediments into the so-called Bauru Basin, which covers large areas of the Paraná, São Paulo, Mato Grosso do Sul, Mato Grosso, Goiás, and Minas Gerais states (Fernandes & Coimbra, 1996). Two groups compose the lithostratigraphic framework of the basin: the Caiuá Group, tentatively given a Cenomanian-Turonian age, which includes the Rio Paraná, Goio Erê, and Santo Anastácio formations; and the Bauru Group, including the Adamantina, Uberaba, Araçatuba, and Marilia formations, dated as Turonian-Maastrichtian (Dias-Brito et al., 2001; Batezelli et al., 2003; Paula e Silva et al., 2003). Such ages were partially based on biostratigraphic data from ostracods and Charophyta algae, as well as vertebrates such as titanosaur sauropods (Santucci & Bertini 2001). In a recent work, Castro et al. (2018) provided the first radioisotopic age for the Bauru Group, a high precision dating using U-Pb geochronology for the Adamantina Formation in General Salgado-SP resulted in a possible post Conician to Maastrichthian age.

The Adamantina Formation was defined by Soares et al. (1980), and is exposed in the states of Goiás, Mato Grosso do Sul, Minas Gerais, and São Paulo. It is recognized by deposits usually composed of fine-grained sandstones and subordinate mudstones, with granulometric patterns that suggest a fluvial sedimentation in meandering canals (Paula e Silva et al, 2005), associated with a semi-arid climate. A progressive increase in aridity due the persistence of a hot climate, and topographic heights surrounding the basin, resulted in the establishment of alluvial plains, braided rivers, and small ponds (Fernandes, 1998; Fernandes & Coimbra, 1996; Dias-Brito et al., 2001).

The paleontological record of the Adamantina Formation is extensive, comprising algae, mollusks, crustaceans, anurans, turtles, lizards, snakes, non-avian dinosaurs, mammals, birds, and an exuberant diversity of crocodyliforms (Carvalho & Bertini, 1999; Dias-Brito et al., 2001; Arruda et al., 2004; Carvalho et al., 2005; Castro et al., 2018). The mesoeucrocodylian taxa have been most frequently recognized in Minas Gerais and São Paulo, including notosuchian groups such as Sphagesauridae and Baurusuchidae. This record emphasizes the importance of the studies in this area, in order to better understand crocodyliform evolution, distribution, and paleoecology (Figure 1)

The area where LPRP 0697 was collected, the Furnas Farm, is also known for other baurusuchid records (Avilla et al., 2004; Araújo & Marinho, 2013). Araújo & Marinho (2013) provided a lithofaciological analysis indicating a succession of floodplain deposits. Their studied specimens came from the uppermost layer of the 20m thick profile, composed of very fine sandstones with carbonate cementation.

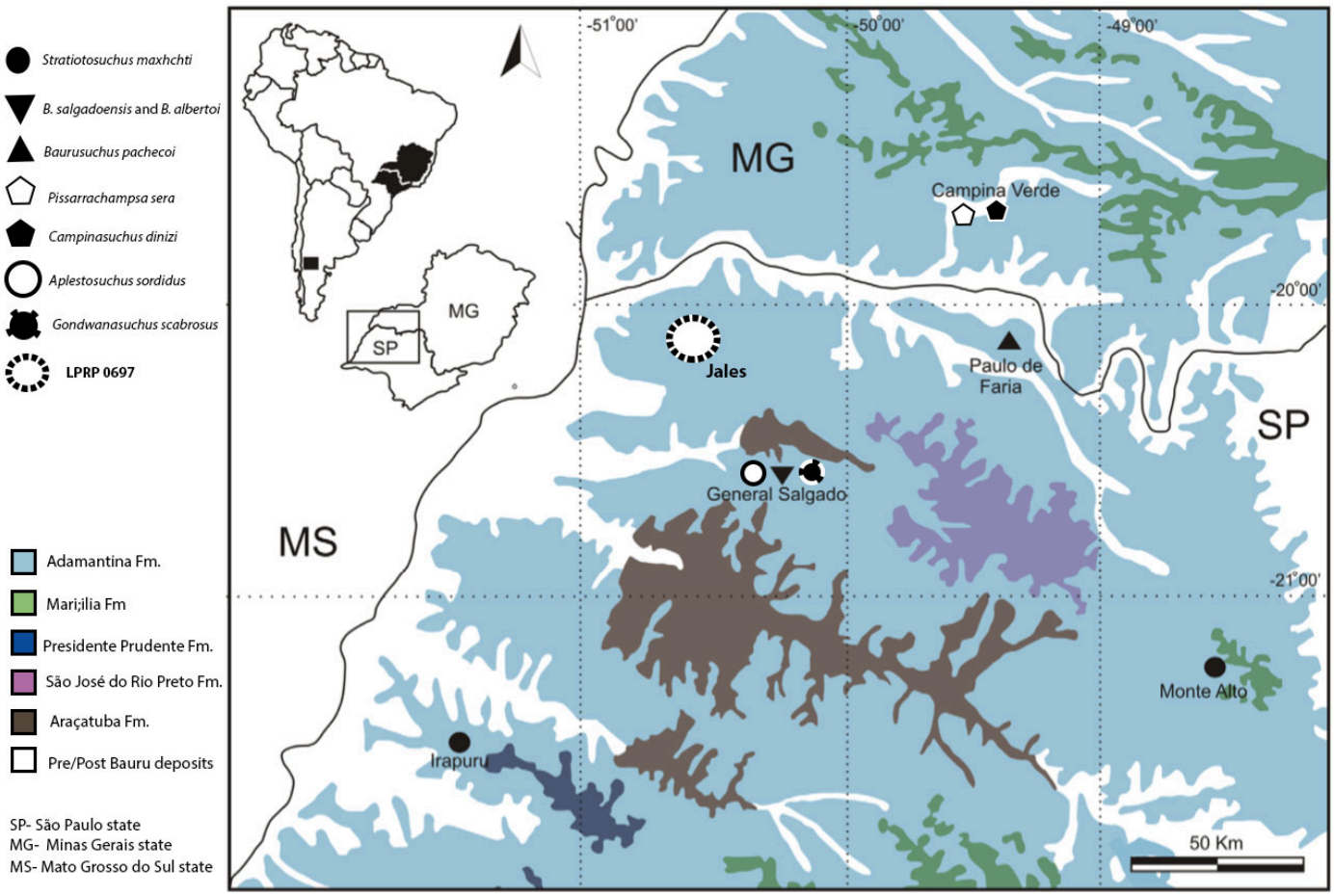


**Figure 1.** Bauru group formations distribution. Northern of São Paulo state, showing the localities of all Brazilian baurusuchids were collected. (map modified from Fernandes, 2004 and Montefeltro et al., 2011).

### *1.2 Baurusuchidae phylogenetic relationships*

The phylogenetic relationships of Baurusuchidae have been discussed for the past decades. *B. pachecoi* has an important and central role for understanding the evolutionary and biogeographic patterns of Mesozoic Crocodyliformes due its unique morphological features and well-preserved skull bones (Turner, 2004; Montefeltro et al., 2011). For many years, *B. pachecoi* was the only known baurusuchid, and as such was included as comparative material in most phylogentic studies of Crocodyliformes. In a broader aspect, Baurusuchidae is nested within Metasuchia, a group of non-Thalatosuchia mesoeucrocodylians, which includes living crocodiles as well as Notosuchia, a clade mainly composed of terrestrial forms from Gondwana (Benton & Clark, 1988). Two main hypotheses have been proposed regarding the relationships

of the first Metasuchia. Traditionally, *Baurusuchus* and *Sebecus* were included in a clade called Sebecosuchia, but given a series of conflict in characters, Benton & Clark (1988) suggested a second hypothesis, in which *Sebecus* would be more closely related to Neosuchia (including Eusuchia) that to *Baurusuchus*. Nonetheless, the Sebecosuchia hypothesis carried on being supported by later studies (Gasparini et al., 1991. Tykoshi et al., 2002), even when Cenozoic non-south-american sebecids are included in the analyses (Gasparini et al., 1993; Langston, 1965; Buffetaut, 1989; Ortega et al., 1996). In more recent analysis, containing a broader number of taxa, the composition of Sebecosuchia became even more uncertain. Larsson & Sues (2007) recovered *Sebecus* more closely related to the peirosaurids, composing a clade named Sebecia, whereas *Baurusuchus* was positioned as the sister-group of Neosuchia + Sebecia. Sereno & Larsson (2009) also did not corroborate Sebecosuchia, recovering *Baurusuchus* within Notosuchia. However, two other recent studies recovered that clade (Turner & Sertich, 2010; Pol & Powell, 2011; Pol et al., 2014; Kellner et al., 2014; Leardi et al., 2015, 2018), highlighting the still prevailing uncertainty on the matter.

Phylogenetic studies including a diverse array of Baurusuchidae became more common in the last decade, all of which corroborating the monophyly of the group (Sereno & Larsson, 2009; Nascimento & Zaher, 2011; Pol & Powell, 2011; Montefeltro et al., 2011, 2013, Godoy et al., 2016, Iori et al., 2013, Leardi et al., 2019). Nacimento & Zaher (2011) and Pol & Powell (2011) found two clades within Baurusuchidae, one composed of the *Baurusuchus* species and the other of *S. maxhecthi* + *P. pakistanensis*. In recent studies, Pol et al., (2012) did not recover the latter clade, with *S. maxhecthi* and *P. pakistanensis* forming a polytomy together with *C. rothi* instead. The uncertain position of the last taxon was also recovered by Pol & Powell (2011), with the taxon positioned in a polytomy with Baurusuchidae and a clade including Sebecidae, *Bergisuchus*, and *Iberosuchus*.

Montefeltro et al. (2011) proposed the existence of two subfamilies within Baurusuchidae, with synapomorphies related to the morphology of the nasal, prefrontal, and frontal bones. The Pissarrachampsinae correspond to all Crocodyliformes that share a more recent common ancestor with *P. sera* than with *S. maxhechti*, *B. pachecoi*, *N. terrestris*, *M. amarali*, *Ar. arrudai*, *Ara. gomesi*, *Se. icaeorhinus*, *Br. bonapartei*, *Pe. tormini*, and *Cr. niloticus*. Baurusuchinae is defined as all Crocodyliformes that share a more recent common ancestor with *B. pachecoi* than with, *P. sera*, *N. terrestris*, *M. amarali*, *Arm. arrudai*, *Ara. gomesi*, *S. icaeorhinus*, *Br. bonapartei*, *Pe. tormini*, and *Cr. niloticus*. In this phylogenetic proposal, *C. rothi* is recovered outside this dichotomy, being the sister-group of the clade

formed by both subfamilies. The author also redefined Baurusuchia (Walker, 1968) as including all Crocodyliformes more closely related to *B. pachecoi* than to *Notosuchus*, *Mariliasuchus*, and *Armadillosuchus* and presenting the same diagnostics characters as Baurusuchidae.

An updated matrix presented by Godoy et al. (2014) included the newly described *A. sordidus* and new characters. The analysis resulted in the paraphyly of *Baurusuchus*, within Baurusuchinae, with *B. albertoi* recovered in a clade with *A. sordidus*, which is the sister-group to a clade including *S. maxhetchi*, *B. salgadoensis*, and *B. pachecoi*. This analysis also included the then recently described *C. dinizi* and *G. scabrosus*. The first was placed within Pissarrachampsinae, whereas *G. scabrosus* was placed as the sister-group of the clade including both subfamilies. As for *C. rothi*¸ it was recovered as the earliest diverging baurusuchid branch. It is interesting to notice that the two species recovered outside the Baurusuchinae-Pissarrachampsinae clade are known from material with juvenile features (Marinho et al., 2013).

### *1.3 Morphological CT scan analysis in Baurusuchidae*

All phylogenetic analysis mentioned in the last section have been mostly based on cranial morphological characters. In order to refine such anatomical inferences, new tools such as tridimensional images from computed tomography are helpful. These allow both the virtual removal of sediment from the bones and the better visualization of bony structures without damaging them. This methodology is based on a series of X-ray slices taken in different views, which allow the identification of individual bones and their 3D digital reconstruction. Furthermore, soft structures, such as bloody vessels and nerves, the inner ears and the skull endocast can be reconstructed. Those studies are rather common for Dinosauria (e.g., Rogers, 1998; Franzosa & Rowe, 2005; Witmer et al., 2008; Ösi et al., 2014; Bronzati et al., 2017; Bronzati et al., 2019a,b; Cuesta et al., 2018; Chapelle & Choiniere 2018; Chapelle et al., 2019), with the authors providing 3D virtual models of the skull and its bones. For fossil Crocodyliformes, there has been also several studies using CT scan data, starting with the pioneering description of *Calsoyasuchus valliceps* (Tykoski et al. 2002) and including more recent works such as the description of *Pakasuchus kapilimai* digitally detailing the heterodont dentition of the species (O'Connor et al., 2010), the study of the *Simosucuhs clarki* skull, which only used 2D slice images to visualize different views of the skull instead of a 3D reconstruction (Kley et al., 2010), and the reconstruction of the endocranium of *Rukwasuchus yajabalijekundu*

(Sertich & O'Connor, 2014). Also, for a taxon more phylogenetic close to Baurusuchidae, Dias et al. (2019) analyzed the nasal cavities of the sphagsaurid *Caipirasuchus montealtensis*, in order to understand the pterygoid fenestration and the air passages in the inner cavities of the skull.

Few studies have used CT scan data to produce 3D models of baurusuchid bones. Vasconcellos (2009) digitally reconstructed both cranial and postcranial elements of *B. salgadoensis* in order to analyze morphofunctional aspects of the species, but such study did not include the description of individual bones from the 3D digital images. Fonseca et al. (2020) published a study about the encodracanial cavity of *C. dinizi*, which was the first work to describe the morphology of such structures for baurusuchids. The study explores the internal cranial anatomy, analyzing the paranasal and paratympanic sinuses, the internal structures of the nostril, the endocast, and the semicircular canals of the inner ear. The authors also made inferences about the paleoecology and physiology of *C. dinizi*. It is importance to mention that Montefeltro et al. (2019) used tridimensional images of LPRP 0697 for Finite Element Analyses (FEA) in order to understand how the bite forces operate on the skull of baurusuchids.

## 2. Material and Methods

### *2.1 Collection*

The specimen LPRP 0697 was found and partially collected in first semester of 2012 at Fazenda Furnas, in the municipality of Jales-SP. The field work was conducted to collect a previously found material composed of sacral bones referred to *Armadillosuchus arrudae* (LPRP 0774), but LPRP 0697 was found during the process, in the trench dug to isolate LPRP 0774. Its skull and front part of the body was then collected in a single block of sediments by Max Langer, Julio Marsola, and Felipe Montefeltro. A second collection team, this time composed of Julio Marsola, Pedro Godoy, Giovanne Mendes, Fernando Adorni, Gabriel Taixeira, and Geovani Ferreira came back to the locality also by first semester 2012 and collected the remaining postcranial parts, which were taken to the lab in four main blocks. Three trunk vertebrae (V-VII) were lost during the collection of the fossil, due the mechanical division of the skull and postcranial blocks. The specimen is housed at the Laboratório de Paleontologia de Ribeirão Preto collection, FFCLRP-USP, Ribeirão Preto-SP.

### *2.2 Fossil preparation*

In the period between 2012 and 2018, the material was prepared mostly by Geovani Ferreira, using pneumatic tools (*Paleo-aro* and *Micro-jack*), removing rock matrix from most of the skull and the entire dorsal surface of the main postcranal block. The ventral surface of such block remains associated with a rock matrix platform to support the skeleton. In 2018, I continued the preparation of the main postcranium blocks, exposing dorsolaterally the caudal and sacral vertebrae, the right pes elements and removing the excess of sediment around the postcranium. Also, the two isolated blocks containing caudal vertebrae were also prepared, exposing its dorsal and lateral surfaces. The bones were hardened with paraloid B-72.

### *2.3 LPRP 0697*

The specimen is composed of an almost complete skeleton, preserved in four main blocks (Figure 2). The first is composed of the skull, associated with atlas, axis, and six other cervical vertebrae (III-VIII) with ribs. That block also includes the first to fourth trunk vertebrae (I-IV), a sagittal row of paired parasagittal osteoderms, two almost complete scapulae and the articulated coracoids, the right of which is heavily damaged, with only the articular portion preserved. The second block contains most of the articulated postcranium, composed of nine trunk vertebrae (VIII-XVI), the three sacral, and the first nine caudal vertebrae. As also seen in the skull block, starting from cervical vertebrae VII, all vertebrae of the main postcranial block are covered by a pair of parasagittal osteoderms associated with each neural spine. Most ribs are articulated with the vertebrae in trunk elements VI-XIV; the gastralia is also preserved, and possible gastrolites are seen near its posterior portion. Only the right forelimb is articulated with the trunk, comprising radius, ulna, carpal elements, metacarpals, and phalanges of five manual digits. A partial left humerus is preserved, but isolated of the rest of the postcranium, along with the left radius, ulna, and manus. The pelvic girdle is completely preserved and articulated with the rest of the body. Both ischia are still partially covered by rock matrix, and both pubis are displaced ventrally, anteriorly reaching the posterior portion of the gastralia. The right hindlimb is almost completely preserved, with all the bones exposed, except for digits I and II. From the left side, the proximal portion of tibia and fibula and four falanges were found isolated from the block. The third block is much smaller, preserving caudal vertebrae X-XV, all associated with

ostederms. The fourth block is also small, preserving nine more distal caudal vertebrae. Yet, it is not clear if these follow the numeration from the previous block, because the anteriormost vertebrae are very damaged. Furthermore, isolated from the four blocks, there are two very small caudal vertebrae, also bearing tiny osteoderms. Also, rib fragments are found isolated, but cannot be assigned to specific vertebrae.

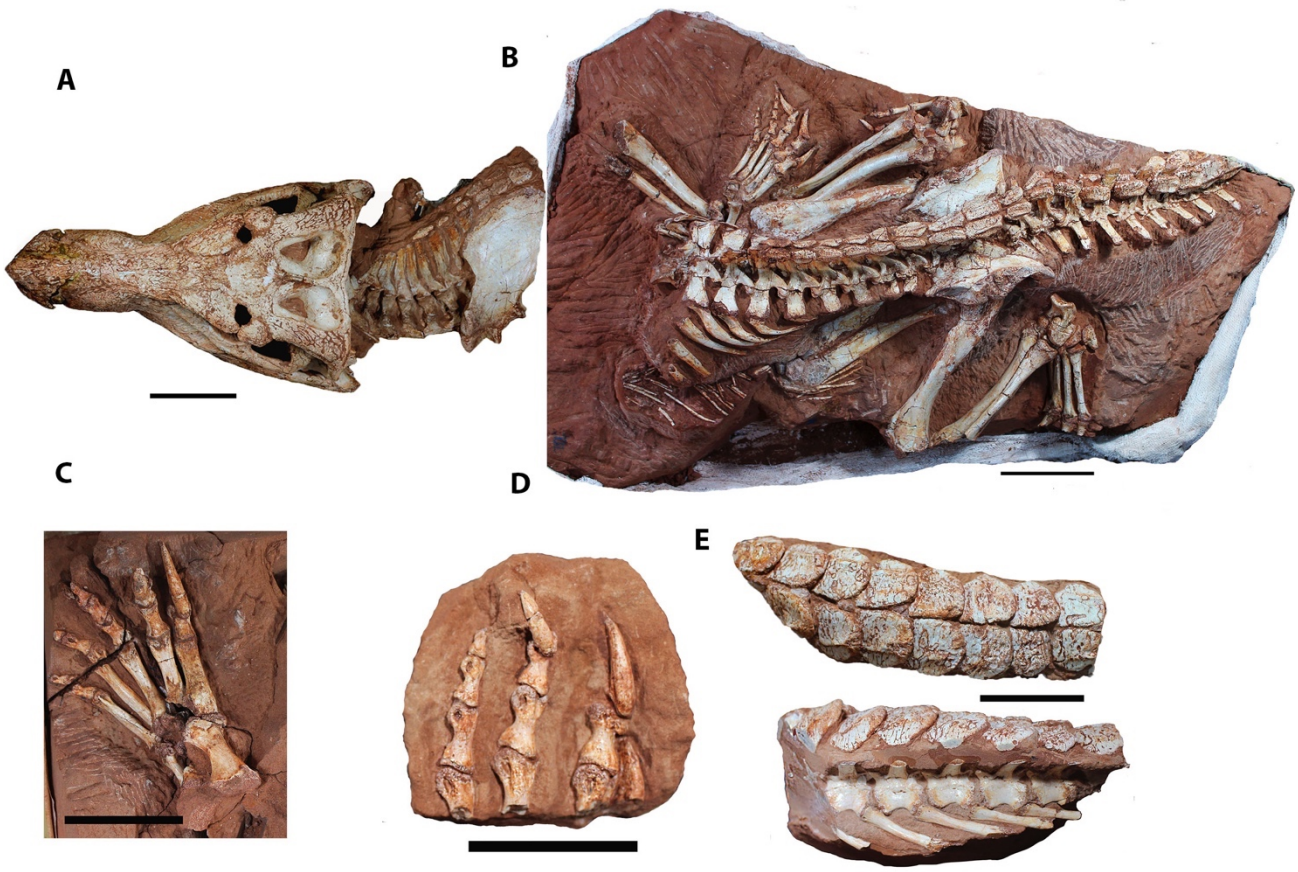


**Figure 2.** Postcranium elements of LPRP 0697. (A) cranium in dorsal view associated with cervical vertebrae; (B) second main block containing most of the articulated postcranium; (C) articulated left manus; (D) pedal elements of left pes; (E) dorsal and lateral views of caudal vertebrae articulated with osteoderms. Scale bars: 5cm (C-E) and 10 cm (A, B).

### *2.4 Computed tomography (CT Scan)*

The computed images of LPRP 0697 were acquired by the tomograph *Toshiba Aquilion Prime*, at Centro de Ciências das Imagens e Física Médica (CCIFM), Hospital das Clínicas da Faculdade de Medicina de Ribeirão Preto, Universidade de São Paulo, authorized by the

CCIFM coordinator Dr. Flávio Junior de Oliveira and Dr. Marcel Koenigkam Santos. The X-ray parameters were established as 120KV and 150μA, and slices have 0.5 mm thickness. The images were segmented and the 3D model was renderized using the software *Avizo 7.0*.

### *2.5 Institutional abbreviations*

**CPPLIP**- Centro de Pesquisas Paleontológicas, L.I. Price, Uberaba; **DGM**- Museu de Ciências da Terra do Departamento Nacional de Produção Mineral, Rio de Janeiro; **LPRP**- Laboratório de Paleontologia de Ribeirão Preto; **MPMA**- Museu de Paleontologia de Monte Alto, Monte Alto; **UFRJ DG**- Departamento de Geologia da Universidade Federal do Rio de Janeiro.

### *2.6 Comparative material*

For the comparative description of LPRP 0697, the following notosuchian specimens from the Bauru Basin were studied firsthand (holotypes are highlighted in bold).

Table 1. List of species and collection identification

| Species | Collection identification |
|---|---|
| *Aplestosuchus sordidus* | **LPRP 0229**[a] |
| *Armadillosuchus arrudai* | **UFRJ DG 303R**, MPMA 64-0001-04 |
| *Baurusuchus pachecoi* | **DGM 299-R** |
| *Baurusuchus salgadoensis* | **MPMA 62-001-02**, 64-0005-04;UFRJ DG 285-R, 288-R, 307-R, 308-R, 341-R, 386-R. |
| *Campinasuchus dinizi* | **CPPLIP 1235**, 1234, 1236, 1237, 1435, 1436, 1437 |
| *Gondwanasuchus scabrosus* | **UFRJ DG 408-R** |
| *Mariliasuchus amarali* | **UFRJ DG 50R,** 105R, 106R |
| *Pissarrachampsa sera* | **LPRP 0019**, 0018, 0020 |
| *Stratiotosuchus maxhechti* | **DGM 1477** |

*2.7 Phylogenetic analysis*

LPRP 0697 was included in the data matrix of Godoy et al. (2014), which is an updated version of that by Montefeltro et al. (2011), which is the only phylogenetic dataset built exclusively to investigate baurusuchid relationships. The original taxon/character matrix was composed of 66 characters and 10 taxa; seven baurusuchids and the outgroup composed of *Armadillosuchus arrudai*, *Mariliasuchus amarali*, and *Notosuchus terrestris*, the last one as the primary outgroup taxon. Godoy et al. (2014) added eight characters to the dataset (67 to 74; see Appendix 2), and also expanded the taxon sampling adding *A. sordidus*, *C. dinizi*, and *G. scabrosus*.

The software *Mesquite v.3.6* was used to score LPRP 0697, as well as to incorporate six new morphological characters (75-80; Appendix 2). The phylogenetic analysis follows the parameters of the previous works (Montefeltro et al., 2011; Godoy et al., 2014), using equally weighted parsimony in *TNT v.1.1* (Goloboff et al., 2008) based on the implicit enumeration search algorithm. The bootstrap method of random resampling was run on *TNT v.1.1* to infer node support and only values higher than 50% were indicated on the trees. Bremmer support (Bremer, 1994) values were calculated using the available *TNT v.1.1* script. Characters 5, 11, 12, 22, 27, 32, and 41 were treated as additive, following Godoy et al. (2014).

First, LPRP 0697 was simply scored in the original matrix of Godoy et al. (2014), but a second analysis was run with the six new characters (75 to 80) added to the dataset. Also for this second run, two characters (20 and 24) were rescored for *B. pachecoi* and eight for *G. scabrosus* (6, 8, 10, 15, 28, 30, 43 and 73), based on a first-hand analysis of the holotypes. The character state modifications and the new characters can be found in the supplementary material and the phylogenetic trees were summarized in the consensus tree.

*2.8 Terminology*

The nomenclature for the supratemporal fenestra and fossa follows Montefeltro et al. (2011); cranial shape classification follows Busbey (1995); crest nomenclature of the ventral surface of quadrate follows Iordanski (1973); teeth classification follows Prasad & de Broin (2002); anatomical nomenclature follows Smith & Dodson (2003); nomenclature of meatal chamber structures follows Montefeltro et al., (2016); nomenclature of pharyngeal tubes follows Dufeau

& Witmer (2015); numbering of cervical vertebrae follows Pol (2005); nomenclature for adductor muscles of quadrate follows Holliday & Witmer (2007).

## 3. Objectives

The objectives of this dissertation are:

- Comparatively describe the external anatomy of the LPRP 0697 skull in detail;
- Taxonomically evaluate LPRP 0697 in the context of known Baurusuchidae diversity;
- Define and discuss the phylogenetic position of LPRP 0697 within Baurusuchidae;
- Provide and analyze the Computed tomography images of LPRP 0697 in order to help its anatomical description by digitally reconstructing each skull bone.

## 4. Results

### *4.1 Systematic Paleontology*

**Crocodylomorpha** Hay, 1930 *sensu* Walker, 1940

**Crocodyliformes** Benton & Clark, 1988

**Mesoeucrocodylia** Whestone & Whybrown 1983 *sensu* Benton & Clark, 1988

**Notosuchia** Gasparini, 1971 *sensu* Sereno et al., 2001

**Baurusuchidae** Price, 1945 *sensu* Montefeltro et al., 2011

**Baurusuchinae** Montefeltro, Larsson & Langer 2011

**Gen. et sp. nov.**

**Type locality.** Furnas Farm, ca. 7 km south from Jales-SP, Brazil. The geographic coordinates were not taken during the fieldwork, but the digging spot was later identified in satellite images by the collectors as -20°20'25''S -50°32'54''W. Such coordinates indicate similar locality as those of Avilla et al., 2004; Araújo & Marinho, 2013.

**Age and horizon.** Adamantina Formation, Bauru Group; Late Cretaceous (ca. Coniacian-Campanian) of the Bauru Basin (Castro et al. 2018).

**Diagnosis (autapomorphies marked with *).** (Figure 3) Baurusuchidae with four premaxillary teeth and five maxillary teeth; depression on posterior portion of nasal bearing a longitudinal ridge*; contact of prefrontals restricted to midpoint of medial surface; absence of a longitudinal crest on frontal surface*; squamosal dorsal surface slightly convex; squamosal prongs verticalized in lateral view forming a right angle between the dorsal and occipital surfaces; lateral convexity of squamosal prongs leading to a more conspicuous participation on the lateral portion of the occipital wall*; bulged contact of squamosal prongs and paroccipital process; jugal infraorbital ridge (*sensu* Montefeltro et al., 2011) extending on the anterior margin of lacrimal*; jugal foramina restricted to the ventral portion of antorbital portion; dorsal surface of parietals reduced, displaced posteriorly to the posterior portion of supratemporal fenestrae, providing a crest-like morphology to supratemporal rim; notch on the quadratojugal-quadrate ventro-lateral contact; absence of well-marked depressions and ridges on the occipital

surface of supraoccipital; choanal septum wide and flattened ventrally; palatine "T" shaped providing a triangular shape for the suborbital fenestrae, crested suture on the contact of palatines; medial pharyngeal tube and pharyngotympanic tubes (*sensu* Duffeau & Witmer, 2015) of same size; presence of a thin and conspicuous groove at the posterodorsal base of pterygoid.

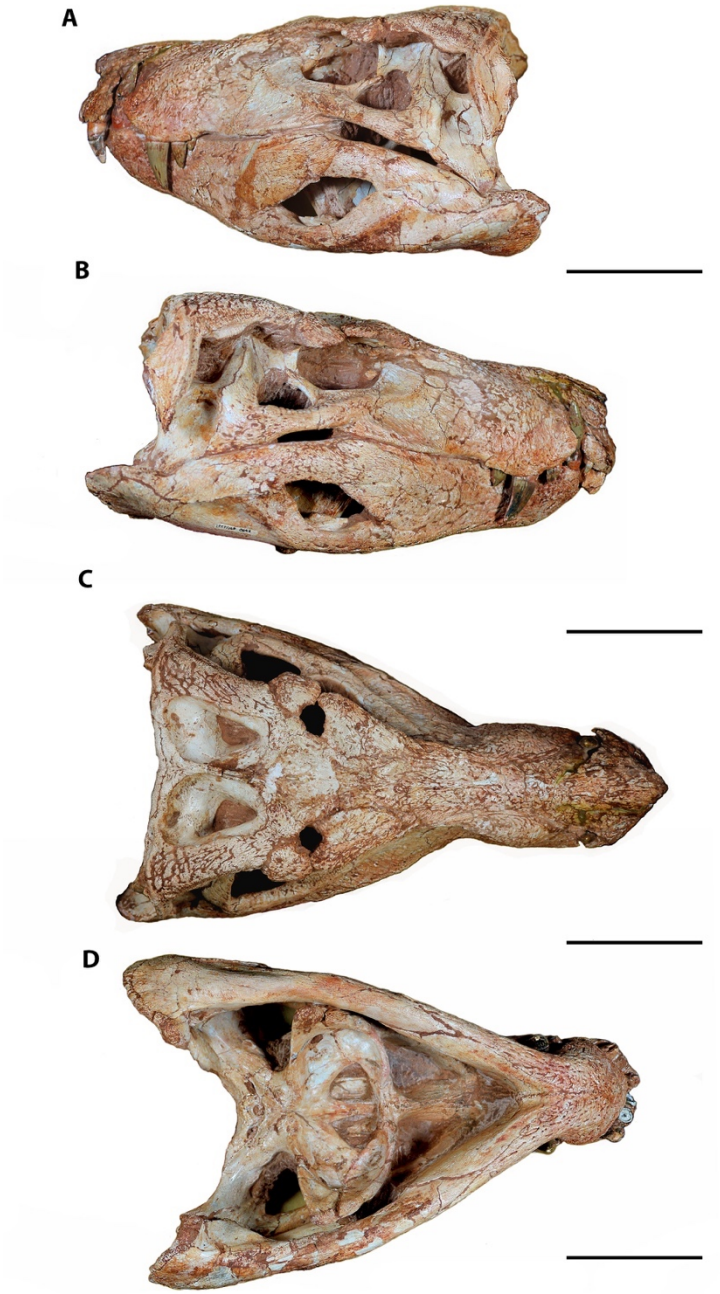


**Figure 3.** Skull of LPRP 0697 in (A) left lateral, (B) right lateral, (C) dorsal and (D) ventral views. Scale bar: 10 cm.

*4.2 Description*

4.2.1 General cranial morphology and skull openings

The skull of specimen LPRP/0697 is well-preserved, exposing the bones that compose the lateral, dorsal, and ventral surfaces of the skull (Figure 4, 5). The anterior end presents a small damage at anterior contact between premaxilla and the nasals, so that it is not possible to clearly assess the nostril anatomy. The specimen can be considered to have a short oreinirostral skull, comprising a deep rostrum with a convex upper margin and rostral length less than 55 percent of basal skull length (*sensu* Busbey, 1995). The skull in dorsal view is lateromedially compressed with a gradual lateral expansion posteriorly to the anterior portion of orbit. The most compressed part of the snout is localized right posterior to the last maxillary teeth. The mandible is also lateromedially compressed at the portion between the third to fifth maxillary teeth. In lateral view, the retroarticular process projects dorsally, just posteriorly to the quadrate-mandible articulation. The antorbital fenestrae are completely absent.

The outer surface of the skull shows some ornamentation. The dorsal surface is highly ornamented, specially the dorsal portion of the maxilla, bordering the lateral margin of the nasals, where conspicuous thin grooves are present. However, the predominant pattern is an irregular ornamentation along the entire surface, more evident in some bones, as the squamosals, nasals, premaxillae, maxillae, as well as in the mandible, and less in others, as the parietal, supraoccipital, quadrates and quadratojugals.

**Orbit.** The orbit is ovoid in lateral view, with the anterior portion slightly compressed dorsoventrally than the posterior portion, and anteromedially to posterolaterally inclined. The ventral border of the orbit is more laterally positioned than the dorsal, so that this opening faces dorsolaterally. In dorsal view it is possible to observe the lateral convexity of ventral border of orbit, as well as its anteromedial directed portion. The orbit is dorsally covered by the anterior and posterior palpebrals, except for its lateralmost border and the circular supraorbital fenestra formed between the contact of both palpebrals. The postorbital forms the dorsal portion of posterior margin of orbit, whereas its ventral portion is formed by the dorsal ramus of jugal. The jugal also forms the entire ventral border of orbit, sharing its anterior border with the lacrimal.

**Supraorbital fenestrae.** The skull roof is pierced by the supraorbital fenestrae, which is laterally enclosed by the posterolateral projection of anterior palpebral and the anteromedial portion of posterior palpebral. This contact arches laterally, leaving a semi-circular medial gap in between, slightly compressed anteroposteriorly. The medial margin of the supraorbital fenestrae is composed of two bones, a small lateral portion of the frontal and the anterolateral portion of the postorbital.

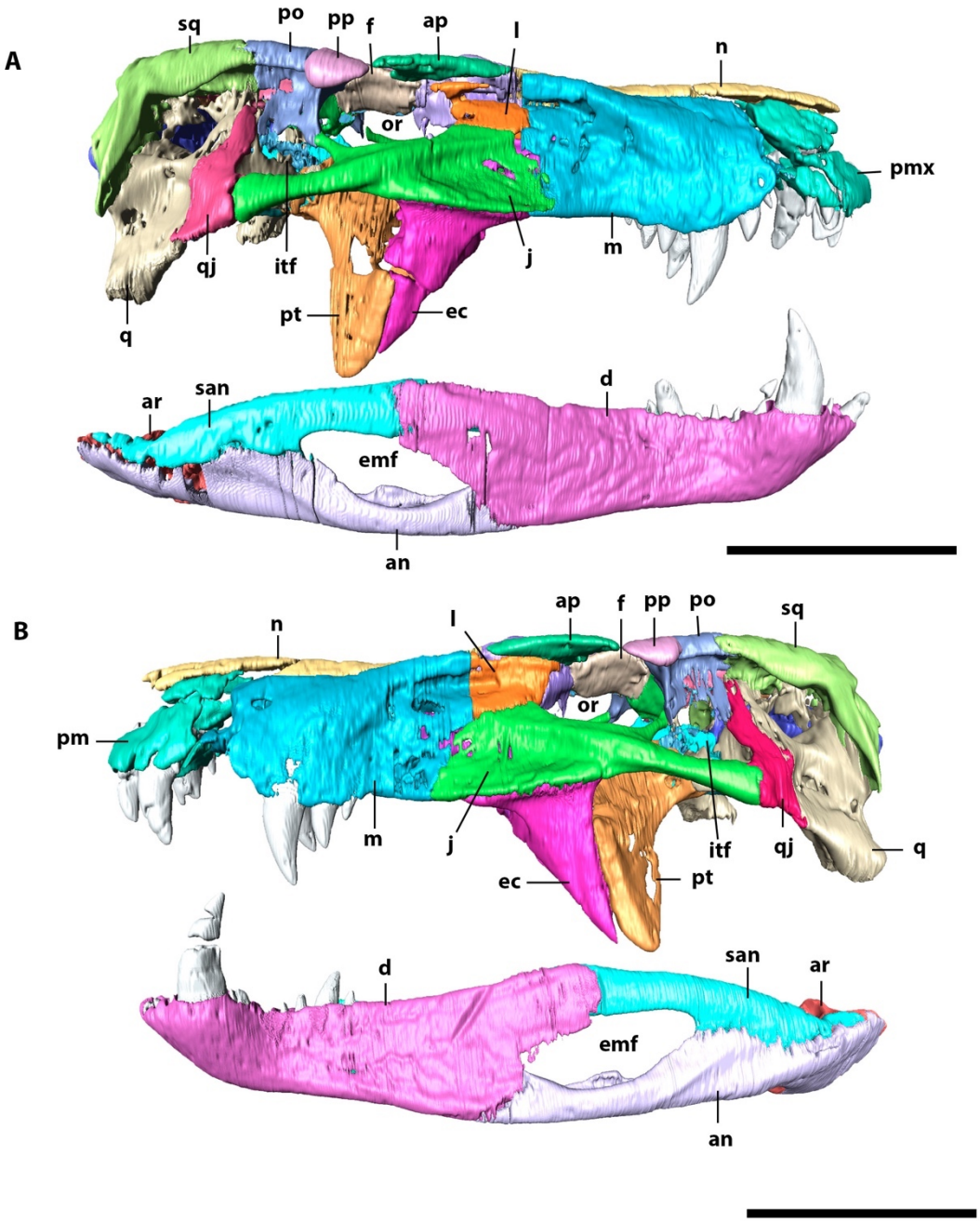


**Figure 4.** Digitally reconstructed skull and mandible of LPRP 0697 in (A) right lateral, and (B) left lateral views. Ap, anterior palpebral; an, angular; art, articular; d, dentary; ec, ectopterygoid;

emf, external mandibular fenestra; f, frontal; itf, infratemporal fenestra; j, jugal; l, lacrimal; mx, maxilla; n, nasal; or, orbit; pmx, premaxilla; po, postorbital; pp, posterior palpebral; pt, pterygoid; q, quadrate; qj, quadratojugal; san, surangular; sq, squamosal. Scale bar: 10 cm.

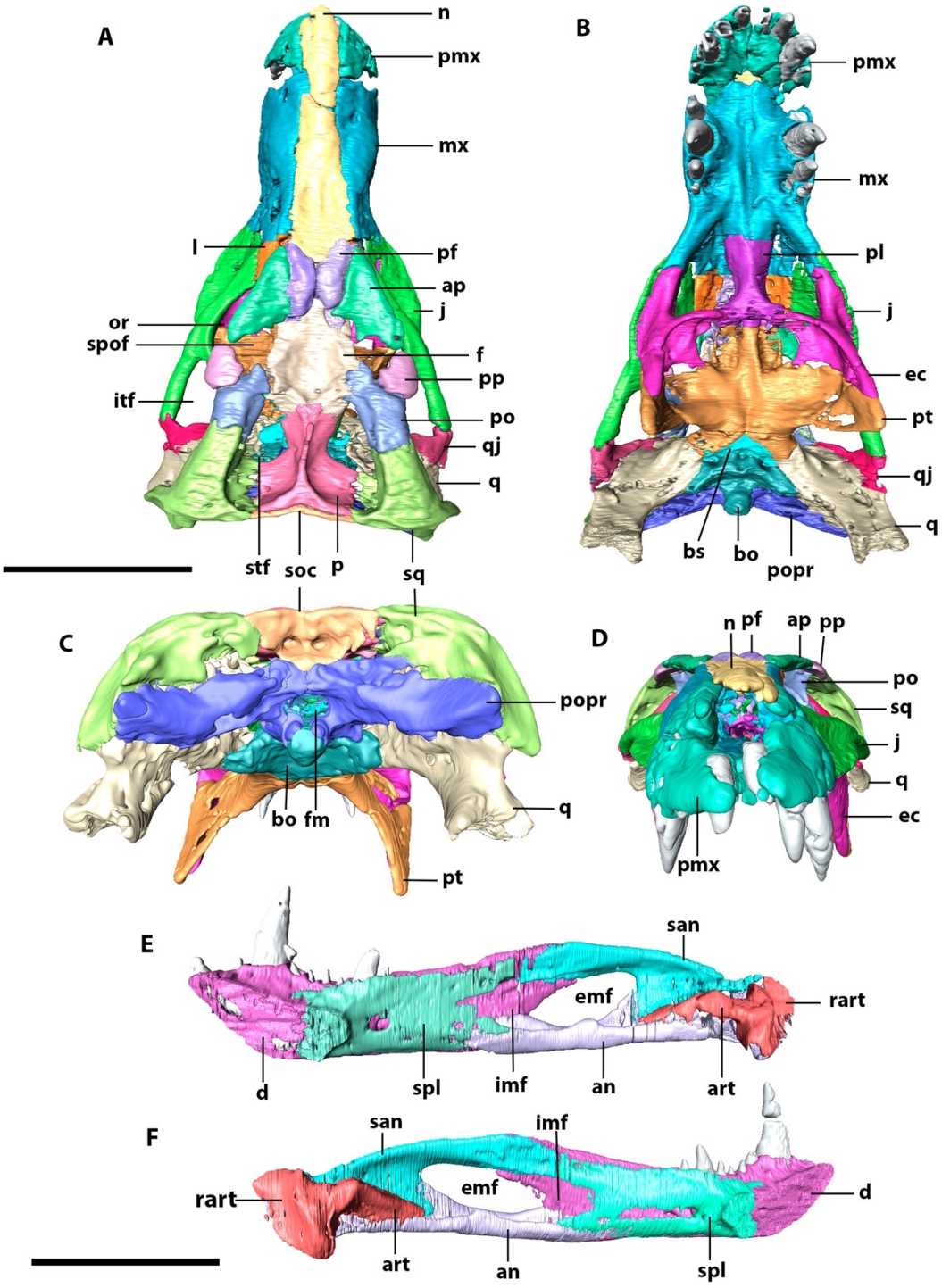


**Figure 5.** Digitally reconstructed skull and mandible of LPRP 0697. Skull in (A) dorsal, (B) medial, (C) posterior, and (D) anterior views, and (E) right and (F) left mandible in medial views. Ap, anterior palpebral; an, angular; art, articular; bo, basioccipital; bs, basisphenoid; d,

dentary; ec, ectopterygoid; emf, external mandibular fenestra; f, frontal; fm, foramen magnum; imf, internal mandibular fenestra; itf, infratemporal fenestra; j, jugal; l, lacrimal; mx, maxilla; n, nasal; or, orbit; p, parietal; pf, prefrontal; pl, palatine; pmx, premaxilla; po, postorbital; popr, paroccipital process; pp, posterior palpebral; pt, pterygoid; q, quadrate; qj, quadratojugal; rart, retroarticular; san, surangular; soc, supraoccipital; spl, splenial; spof, supraorbital fenestra; sq, squamosal; stf, supratemporal fenestra. Scale bar: 10 cm.

**Supratemporal fenestrae.** The supratemporal fenestra is composed by squamosal, parietal, postorbital and frontal. The external supratemporal fenestra is subtriangular, longer anteroposteriorly than lateromedially, compressed lateromedially anteriorly and presenting elevated rims, except for the anterior region, which is at the same level as the frontal. Anteriorly, the posterior portion of the frontal participates in a short portion of the supratemporal fenestrae. The postorbital comprises the anterolateral margin of the supratemporal fenestrae, whereas the squamosal delimits the posterolateral margin. The fused parietal borders the fenestra on the posteromedial margin and along the medial margin, separating the pair of supratemporal fenestrae by a thin crest (see Parietal). The internal supratemporal is formed by the same bones, however it is triangular and smaller than the external.

The supratemporal fossae comprises the unornamented surface of the bones that composes the external fenestrae and also the region between the external and internal supratemporal fenestrae. The fossa presents two main surfaces: one comprising a more dorsally exposed surface and one ventrally, with a more verticalized orientation. The dorsal surface of the supratemporal fossae is anteroposteriorlly constricted, whereas the lateral and medial surfaces are mediolaterally wider. The anterolateral surface of the fossae, formed by the medial surface of the postorbital is markedly convex, gradually turning concave posteriorly along the medial surface of squamosal. The posterior portion of the fossae, comprised by the squamosal and parietal is concave, presenting few muscle scars and a conspicuous cylindrical orbitotemporal foramen. This foramen is short dorsoventrally and more elongated mediolaterally located at the squamosal-parietal suture. The medial portion of supratemporal fossae is composed by the flattened surface of parietal. All these margins converge ventromedially, where they suffer a ventral inflexion and turns more verticalized and presents a smoother surface, lacking elevations and depressions.

**Infratemporal fenestrae.** The infratemporal fenestra is triangular shaped, smaller than the orbit, dorsomedial and lateroventral inclined, presenting all tips rounded. In lateral view, the fenestra extends from the level of approximately half-length of the posterior palpebral to slightly posterior to the postorbital-squamosal lateral suture. The anterodorsal margin of the fenestra is mostly formed by the dorsal ramus of the jugal, with its dorsalmost part formed a small anteroventral portion of postorbital. The posterodorsal border is formed by the ventral margin of the postorbital anteriorly, and posteriorly by the quadratojugal, which also forms the posterior end of the ventral margin of the fenestra. Finally, the fenestra is mostly bordered ventrally by the infratemporal process (or posterior ramus, see Jugal) of the jugal.

**External and internal mandibular fenestrae.** The external mandibular is relatively large, representing the largest (anteroposterior length) external fenestra of the cranium, with 74.4 mm. Its dorsal border is formed by the dentary anteriorly and the surangular posteriorly. The dentary border faces anterodorsally, whereas the surangular margin is horizontally straight, with a conspicuous ventral inflexion on its posterior end, near the ventral contact with angular. The ventral border of the fenestra is sigmoidal and entirely composed by the angular, except for a small portion at the anterior tip of the fenestra, which is composed by the dentary. This anterior corner is conspicuously pintched dorsoventrally, whereas the posterior tip is more rounded due to the curvature of the surangular. The anterior tip is more ventrally positioned than the posterior.

The internal mandibular fenestra is ovoidal, larger than the external, dorsoventrally compressed, mainly on its anterior corner, and anteroposteriorly elongated. It is formed ventrally mostly by the angular, which also comprises its posterior portion more medially. The anterior corner is formed exclusively by the splenial, which forms a rounded and dorsoventrally compressed corner. Dorsoposterior to that portion, the dentary and the surangular form the dorsal surface of the internal mandibular fenestra, which its posteriormost portion is more laterally positioned in relation to the angular, not presenting a clear posterior limit for the fenestra.

**Choana.** The choanal outline is ovoid, anteroposteriorly compressed and mediolaterally elongated. It is divided sagittally by the large choanal septum (see pterygoid), which comprises the medial margin and gives a subtriangular shape for those apertures. The anterior margin of the choanal apertures is composed by the palatine medially and the ectoperygoid laterally, which the last also forms the anterior portion of the lateral margin. The remaining lateral margin

is formed by the pterygoid. There are two flat bony segments displaced parasagitally to the septum along the entire anteroposterior medial margin of choana, that represents an anterior projection of the dorsal surface of pterygoid. The area between these bony structures and the septum choanal forms the choanal grooves. Furthermore, those parasagittal bony structures are continuous anteriorly with the posterolateral portion of palatine, forming a lateral subtriangular gap at the lateralmost portions of the choana, called parachoanal fenestra.

4.2.2 Cranial elements

**Premaxillae.** The premaxilla is subtriangular in lateral view, bordered posteriorly by the maxilla and dorsally by the nasal. Anteriorly, the premaxillae process, that would form the internarial bar, is broken. Ornamentation on the premaxilla is concentrated in the posterodorsal part of the bone, composed dorsally by irregular ridges and thin grooves posteroventrally oriented. The posteroventral margin of premaxilla is projected posteriorly, forming the anterolateral margin of the semi-circular premaxilla-maxilla notch for the reception of the caniniform (D4). There is a small concavity dorsally to the notch, in which an elongated groove extends anteroventrally, ending in a set of foramina slightly above the third premaxillary tooth. The perinarial fossa excavates the premaxilla posterolaterally to the external naris in the form of a smooth round concavity displaced anterodorsally and laterally to the premaxillae (Fig. 6). This is the region where it would be the nostrils originally. Due the preservation of these bones, it is not possible to reconstruct the entire set of premaxillary foramina.

The suture with the maxilla is internalized in anteroventrally to posterodorsally oriented notch. CT digital reconstructions of this area show the presence of a foramen at the premaxilla-maxilla lateral suture. Its exact shape is not clear due to the preservation deficiencies of the bone. In the ventral view, a rounded foramen incisivum is present on the midline contact between the premaxillae and maxillae (Fig. 10). Furthermore, also on the ventral surface, the premaxilla has a small pit between the posterior margin of the first and second premaxillary teeth for the first dentary teeth (Fig. 7).

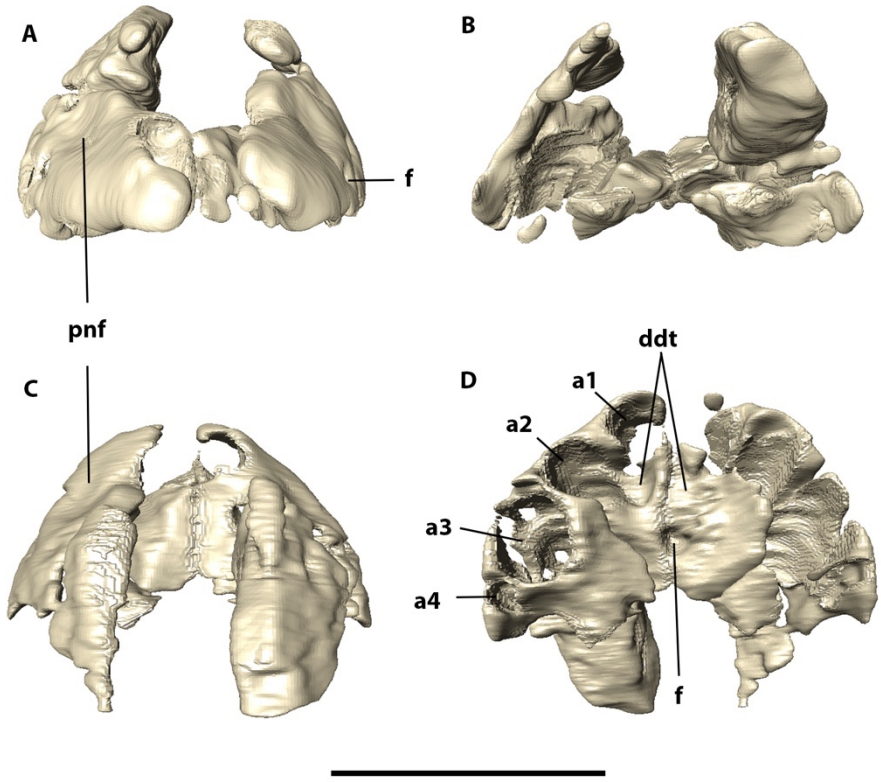


**Figure 6.** Digital reconstruction of articulated premaxillae of LPRP 0697. (A) anterior view. (B) posterior view. (C) dorsal view. (D). Ventral view. Al1-4, alveoli; ddt, depressions for the insertion of the first dentary teeth; f, foramen; pnf, perinarial fossa. Scale bar: 5 cm.

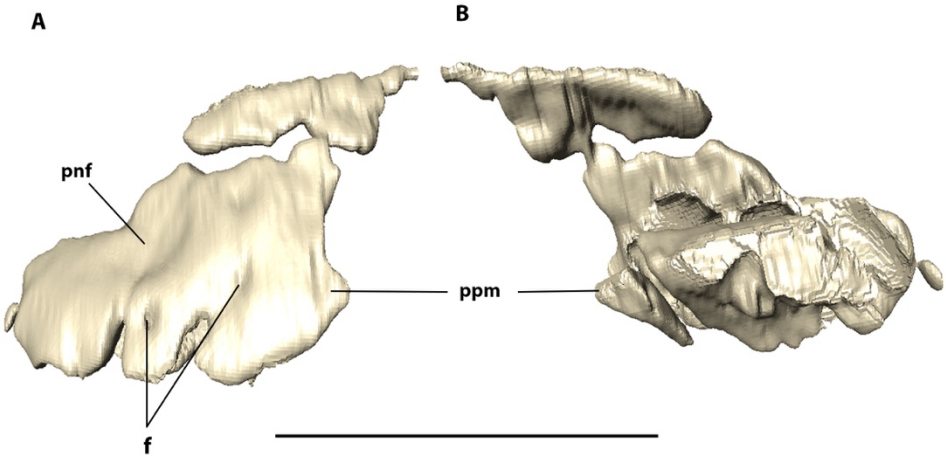


**Figure 7.** Digital reconstructed left premaxilla of LPRP 0697 in (A) lateral and (B) medial views. F, foramen; pnf, perinarial fossa; ppm, posterior projection. Scale bar: 5 cm.

**Maxilla.** The maxilla is a verticalized bone that forms most of the lateral surface of the rostrum (Figs. 8 and 9). It is sub-rectangular in lateral view, bordered by the jugal and lacrimal posteriorly, by the nasal for mostly of its dorsal margin, and by the premaxillae anteriorly and anterodorsally. The ornamentation of the maxilla is composed of roughly vertical ridges, which extend dorsally from the small foramina near the alveolar margin. At the depressed posterior portion of the bone, the ridges are less conspicuous and more horizontally oriented, turning ventrally at their anterior ends. The maxilla-jugal suture is slightly inclined posterodorsally, turning posteriorly on its ventral end. The anterior portion of the maxilla is projected, forming the posteroventral portion of the notch for the reception of the dentary caniniform. Posteriorly to this portion, the maxillae present a bulged lateral surface that extends posterodorsally from the third maxillary tooth, related to its alveolus due the large root of third maxillary tooth (m3). This bulged lateral surface extends onto the dorsal surface of the rostrum. The alveolar margin possesses seven neurovascular foramina laterally forming a continuous line. Slightly posterior to the posteriormost maxillary tooth, the maxilla is laterally compressed, forming the depressed smooth surface continuous to the jugal infraorbital depression (*sensu* Montefeltro et al., 2011).

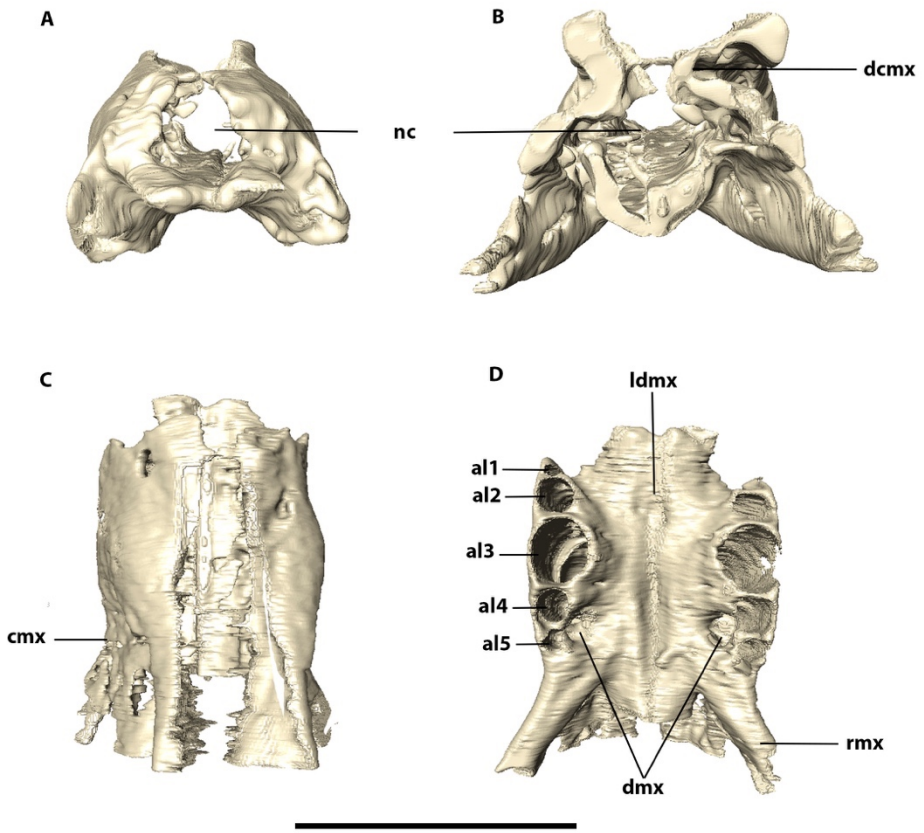


**Figure 8**. Digital reconstruction of articulated maxillae of LPRP 0697 in (A) anterior, (B) posterior, (C) dorsal, and (D) ventral views. Al, alveoli; cmx, mediolateral maxillary

constriction; dcmax, dorsal mediolateral maxillary constriction; dmx, depression for the insertion of dentary teeth; ldmx, midline longitudinal depression of maxillae; nc, nasal cavity; rmx, posterior ramus of maxilla. Scale bar: 10 cm

The ventral surface of maxillae has an alveolar portion more lateromedially expanded. It presents a conspicuous midline longitudinal depression along the palatal contact with its antimere, extending posteriorly to the contact with the palatines. Furthermore, medially to the alveolar margin of the fourth and fifth maxillary teeth, there is a set of small circular pits for the insertion of the dentary teeth. The CT scans show that the internal structure of the bone is highly pneumatic posterior to the fifth maxillary teeth.

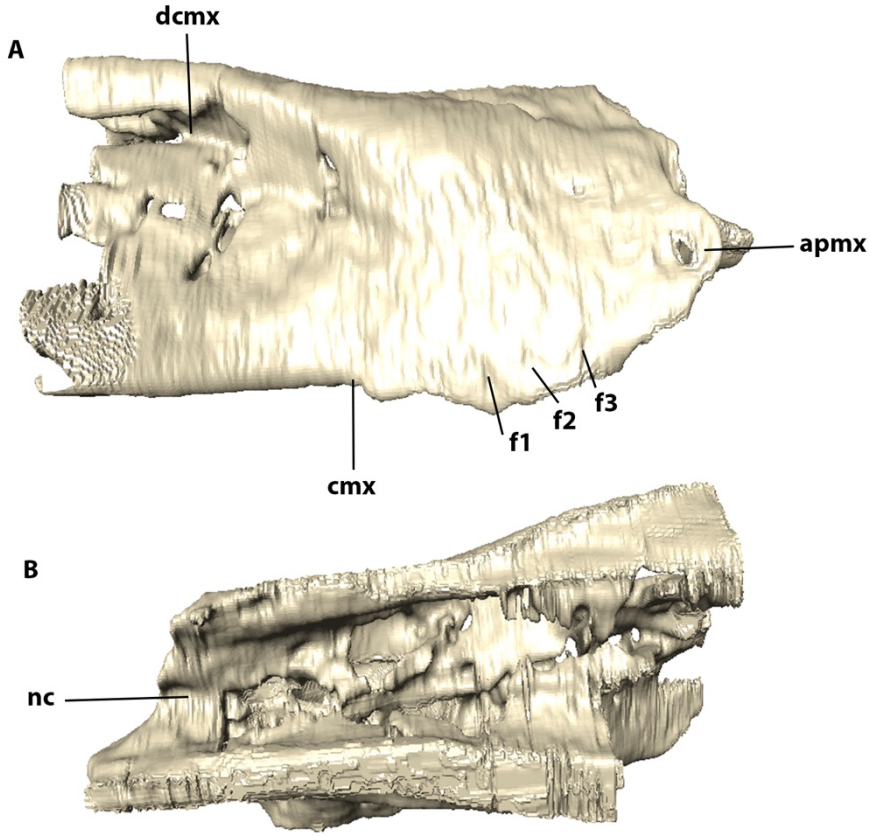


**Figure 9**. Digitally reconstructed right maxilla in (A) lateral, and (B) medial views. Apmx, anterior projection of maxilla; cmx, mediolateral maxillary constriction; dcmx, dorsal mediolateral maxillary constriction; f, foramen. Scale bar: 10 cm.

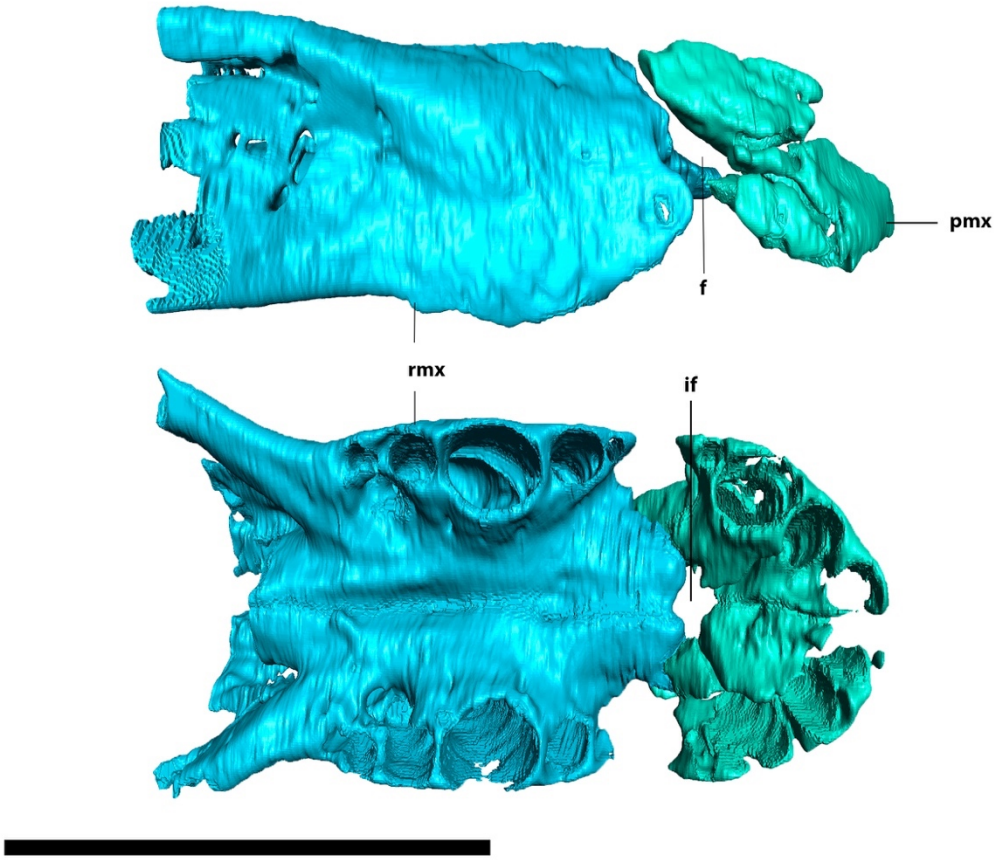


**Figure 10.** Digitally reconstructed articulation of the premaxillae and maxillae of LPRP 0697 in (A) lateral and (B) ventral views. F, foramen; if, foramen incisivum; pmx, premaxilla; rmx, posterior ramus of maxilla. Scale bar: 10 cm.

**Nasal.** The nasals are co-ossified, with no sign of suture between the paired bones (Fig. 11). The pair forms a narrow and anteroposteriorly elongated element. Its lateral margins are predominately straight and its anterior tips is broken, but certainly forming, together with the premaxillae, the posterodorsal margin of the external nares. The nasal contacts the premaxillae, maxillae, anterior palpebrals, lacrimals and prefrontals. Posteriorly, it is limited by the prefrontal pair, forming a small wedge between those bones. The sutures of the nasal with the prefrontals and frontal are obscured by the heavy ornamentation of the skull roof, but it is possible to see that the medial contact of the prefrontals prevents the contact between the nasals and the frontal. In dorsal view, the anterior portion of the nasal is thinner than the posterior, which gets wider posteriorly.

The ornamentation of the nasal changes along its dorsal surface. Paralleled and anteroposteriorly directed thin grooves are present on its anterior portion, whereas irregular grooves are seen posteriorly. However, at the posteriormost portion of the bone, close to the limit with the pre frontals, the grooves converge to the midline area of the bone. This area is traversed by a short, elongated, and anteroposteriorly directed ridge, (i.e. medial crest of nasal). Both sides of the medial nasal crest are marked by an elongated concavity.

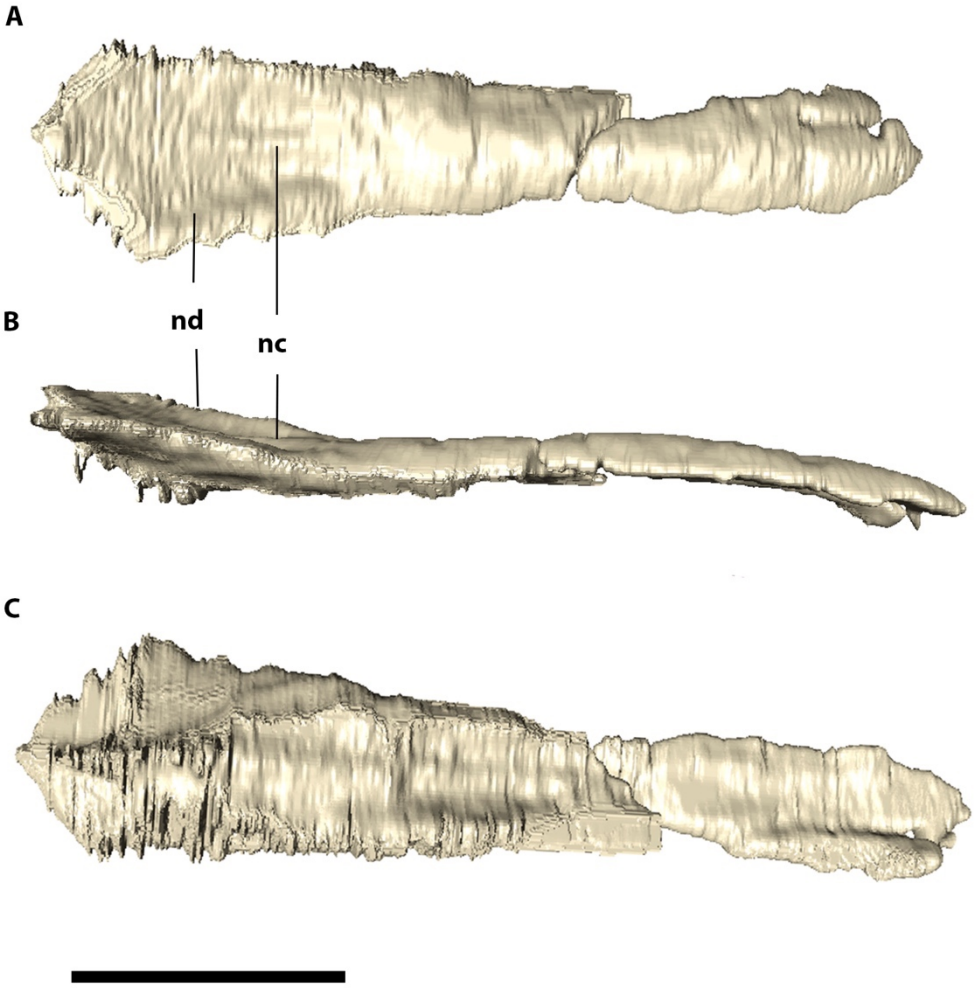


**Figure 11.** Digital reconstruction of fused nasal of LPRP 0697 in (A) dorsal, (B) lateral, and (C) ventral views. Nc, nasal crest; nd, nasal depression. Scale bar: 5cm.

The nasal is also exposed in lateral view, where the dorsal margin of the anterior portion is straight to slightly convex. This is followed by a depression approximately at the level

immediately posterior to the last maxillary teeth. In lateral view, at the posterior end of the depression, near the contact with the prefrontals, the dorsal outline of the skull directs dorsally in a gradual fashion. This region is one of the highest portions of the skull roof, together with the anterior portion of the nasal and the sagittal crest formed by the parietals.

**Anterior palpebral.** The anterior palpebral is dorsoventrally flattened, almost triangular in dorsal view, with its lateral expanding margins, covering most of the orbit dorsally (Fig. 12). The bone rests over the lacrimal and prefrontal, and possesses a lateromedial thin anterior portion that contacts the posterolateral corner of the nasal. The medial margin of the anterior palpebral is rounded, covering the lateral platform for the reception of the anterior palpebral formed by the lateral expansion the prefrontal and the anterolateral margins of the frontal. Its posterior margin is slightly concave forming the anterior border of the supraorbital fenestra, with its lateralmost rounded tip contacting the anteriomost portion of the posterior palpebral.

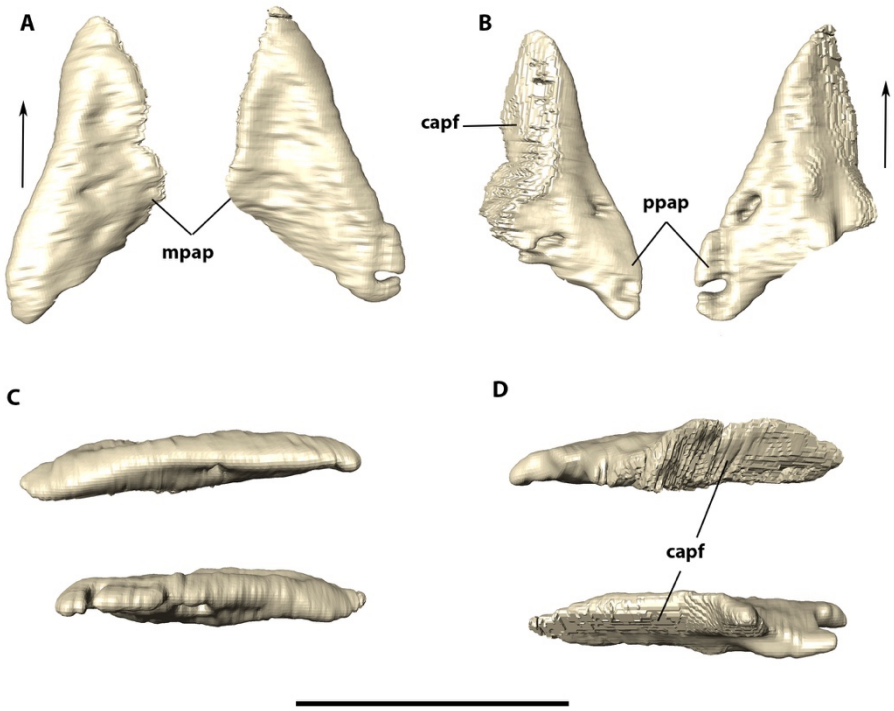


**Figure 12**. Digital reconstruction of left and right anterior palpebrals of LPRP 0697 in (A) dorsal, (B) ventral, (C) lateral, and (D) medial views. Arrows indicate anterior portion. Capf, contact area with prefrontal; mpap, medial projection of anterior palpebral; ppap, posterior projection of anterior palpebral. Scale bar: 5 cm.

The medial surface of anterior palpebral is slightly depressed along its anteroposterior margin in dorsal view. The ornamentation of the bone is restricted to its dorsal and lateral surfaces, whereas the medial portion bears lateromedially directed small grooves, forming smooth grooves. The CT scans showed some small excavations canals along the entire palpebral surface, except on the margin contacting the lacrimal. The overall bone inner structure is solid.

**Posterior palpebral.** The posterior palpebral is smaller than the anterior one. It forms the posterolateral margin of the supraorbital fenestra. The bone is rounded in dorsal view, covering the posterior portion of the orbit. Its lateral portion is anteroposteriorly expanded, than its medial portion and is also slightly inclined ventrally (Fig. 13). Posteriorly, the posterior palpebral contacts the postorbital by fitting into the concave anterolateral surface of that bone. The ornamentation on this bone consists of irregular grooves on the dorsal and lateral surface. As in anterior palpebral, the CT scan shows the posterior palpebral as a solid bone, presenting four major internal canals, which two of them are close to one another, whereas the remaining two are positioned at the lateral surface of the bone.

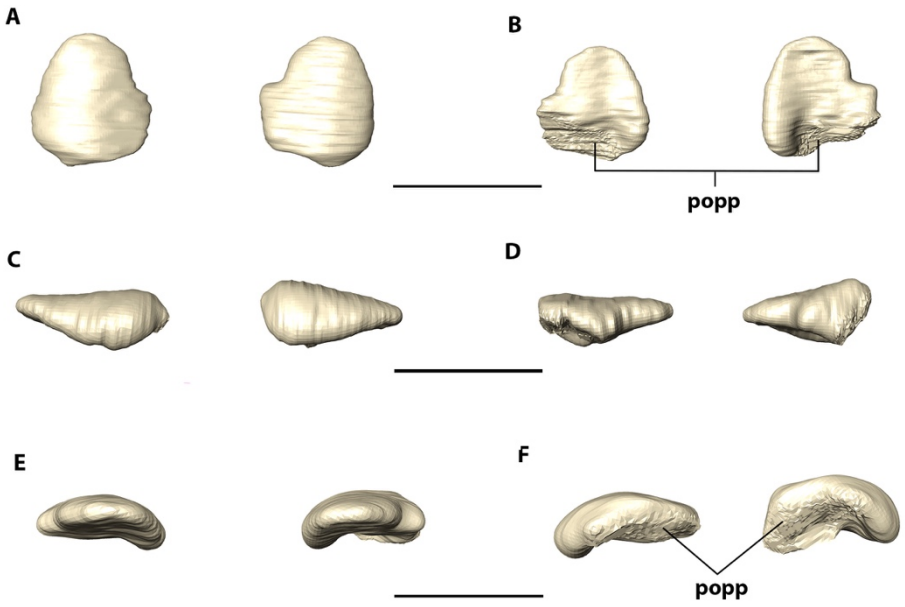


**Figure 13.** Digital reconstruction of left and right posterior palpebral of LPRP 0697 in (A) dorsal, (B) ventral, (C) lateral, (D) medial, (E) anterior, and (F) posterior views. Popp, postorbital contact area with posterior palpebral. Scale bar: 3 cm

**Prefrontal.** The prefrontal is roughly triangular and its dorsal surface is convex, forming one of the highest portions of the skull roof, reaching the same level of the sagittal crest of parietal. Its posterior portion is lateromedially compressed, forming a pointed tip (Fig. 14). The medial margins of the prefrontal converge to its antimere, touching one another and preventing the frontal/nasal contact at midline. The prefrontal extends laterally forming most of the platform that supports the anterior palpebral together with the lacrimal lateroventrally. On its entire dorsal surface, the prefrontal is highly ornamented by irregular grooves.

CT images allow the visualization of the prefrontal pillar. This element contacts the lacrimal dorsolaterally and the dorsal surface of pterygoids ventrally. However, its lateral surface does not touch the medial surface of lacrimal, leaving a gap in between those bones.

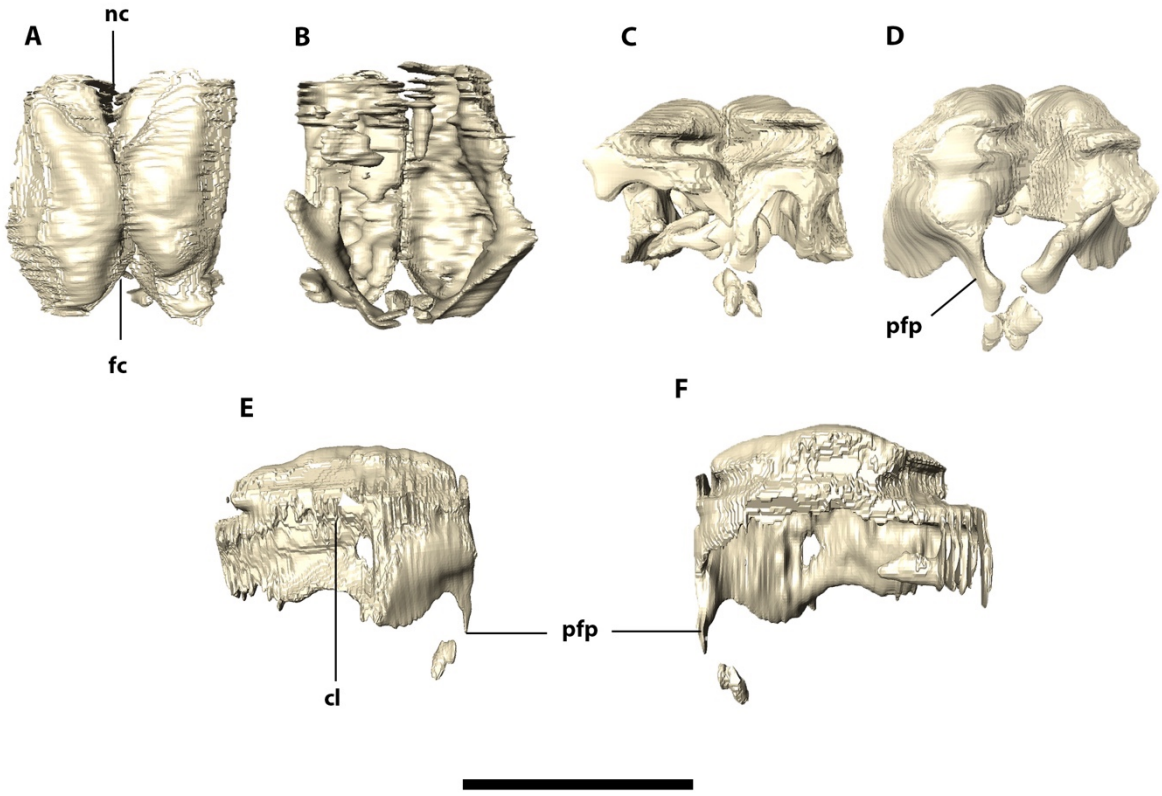


**Figure 14.** Digital reconstruction of left and right prefrontal of LPRP 0697 in (A) dorsal, (B) vental, (C) anterior, (D) posterior, (E) left lateral, and (F) left medial views. Cl, contact with lacrimal; fc, area of contact with frontal; nc, area of contact with nasal; pfp, prefrontal pillar. Scale bar: 5cm.

**Lacrimal.** The lacrimal is rectangular shape in lateral view, with smooth ornamentations mainly covering its posterodorsal portion. The lacrimal fits to the anterior portion of the anterior process of the jugal, forming the anterior and anterodorsal borders of the orbit. It contacts the maxilla anteriorly, via an almost straight and interdigited suture. This suture is inclined posteriorly at its dorsalmost portion. Dorsally, the lacrimal forms the lateral portion of the platform for the support of the anterior palpebral (Fig. 15). The anterior margin of lacrimal is raised laterally, following the crested portion of jugal. The posterior margin of the lacrimal forms the inner anterior margin of the orbit. The CT scans shows a small and circular lacrimal duct positioned just above the posteroventral suture with the jugal. Furthermore, they also show a medial contact between the lacrimal and the laterodorsal portion of the prefrontal pillar.

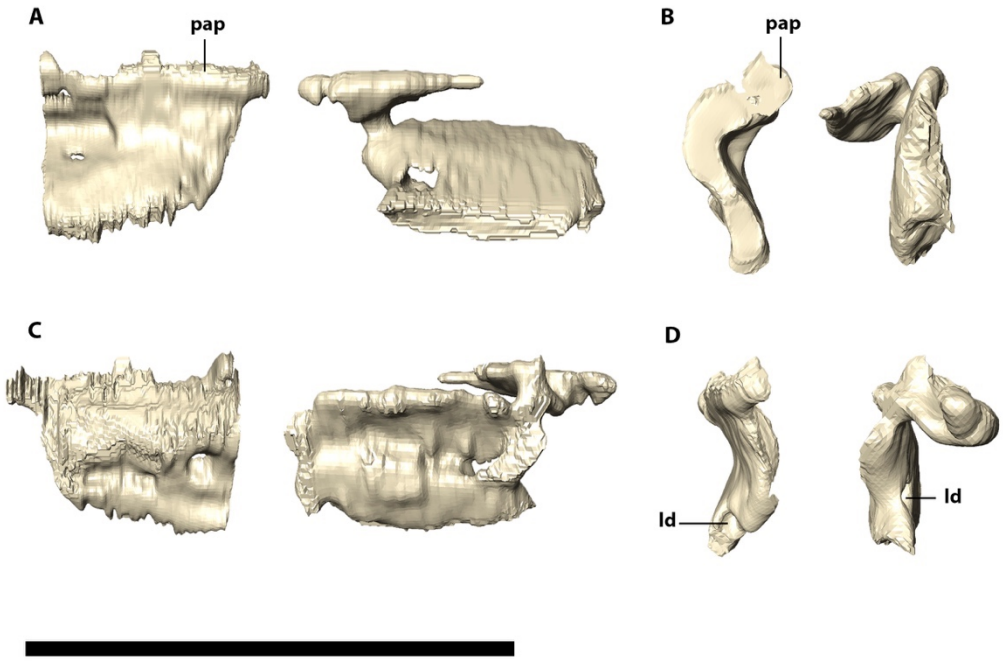


**Figure 15.** Digital reconstruction of left and right lacrimal of LPRP 0697 in (A) lateral, (B) anterior, (C) medial, and (D) posterior views. Ld, lacrimal duct; pap, platform for the anterior palpebral. Scale bar: 5 cm.

**Jugal.** The jugal is a triradiated and heavily ornamented bone, taking part in the borders of the orbit and infratemporal fenestrae. In dorsal view, the lateral outline jugal is convex, with the posterior portion more laterally positioned (Fig. 16).

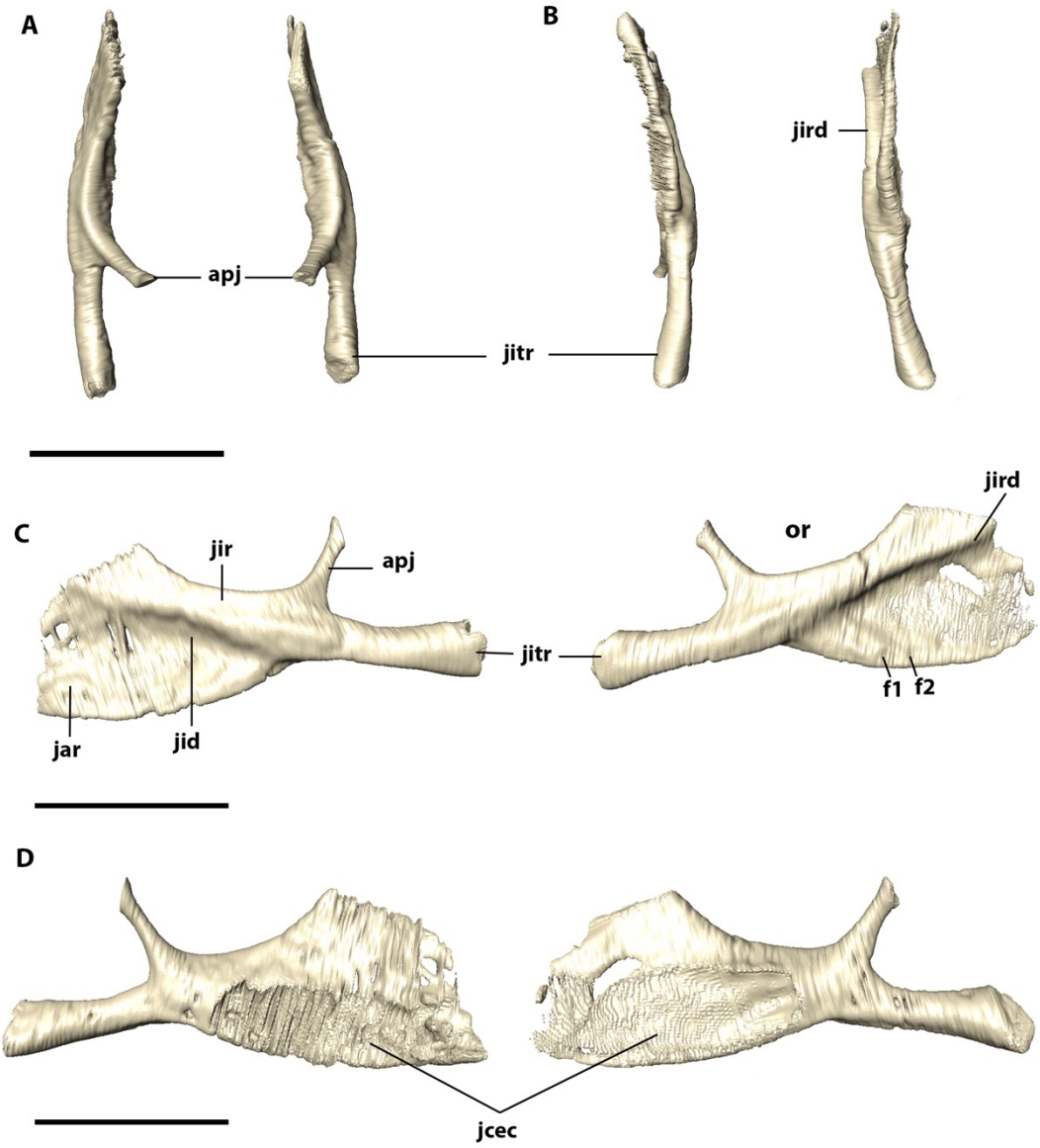


**Figure 16.** Digital reconstruction of left and right jugal of LPRP 0697 in (A) dorsal, (B) ventral, (C) lateral, and (D) medial views. Apj: ascending process of jugal; f, foramen; jar, jugal antorbital ramus; jcec, jugal medial contact with ectopterygoid; jid: jugal infraorbital depression; jir, jugal infraorbital ramus; jird, jugal infraorbital ridge; jitr: jugal infratemporal ramus; or, orbit. Scale bar: 5cm.

The anterior ramus of the jugal (infraorbital) forms the ventral margin of the orbit and contacts the posterior margin of the maxilla forming a notably convex suture, in the ventral portion of which the jugal briefly overlaps the maxilla. Dorsal to that, there is a triple contact between jugal, lacrimal, and maxilla. The infraorbital ramus of the jugal gradually expands dorsoventrally as it extends anteriorly, so that the antorbital portion is twice the depth of the posterior ramus (infratemporal). A longitudinal jugal infraorbital ridge extends posteroventrally from the lacrimal suture anteriorly along the lateral surface of the infraorbital ramus of the jugal, separating a dorsal and a ventral portion of the body of the jugal. The dorsal portion is lateromedially flattened portion and somewhat continuous to the infratemporal portion of the bone. Dorsal to the jugal infraorbital ridge, there is a well-marked jugal infraorbital depression (Montefeltro et al., 2011). The ventral portion of the infraorbital ramus of the jugal is the most lateromedially flattened portion of the bone. It is slightly concave dorsoventrally and bears elongated ventromedially directed grooves along its surface. These grooves tend to become shorter and closer to one another posteriorly. The ventralmost surface of the ventral portion of the infraorbital ramus of jugal, bears a series of foramina, varying from small circular foramina to oval and to anteroposteriorly elongated foramina.

The ascending process of the jugal is cylindrical, expanding dorsomedially from the main body of the bone and slightly turning posteriorly at is dorsalmost portion. It lacks any kind of ornamentation and connects with the ventral process of the postorbital forming the postorbital bar, which separates the orbit from infratemporal fenestra. The infratemporal ramus of the jugal contacts the quadratojugal and forms the ventral margin of the infratemporal fenestra. The foramen for the entrance of the maxillary ramus of the cranial trigeminal nerve pierces the posteroventral portion of the ascending process of the jugal.

The infratemporal ramus, of the jugal is cylindrical, composing almost the entire ventral border of infratemporal fenestra and posteriorly articulating with the quadratojugal via a verticalized, interdigitated suture. Its dorsal surface bears large, transversally elongated grooves. The shape of this ramus is somehow maintained forward, along dorsal portion of the anterior ramus of the bone, reaching the lacrimal suture anteriorly. The transition of the ventral margin of the anterior ramus to the posterior ramus of jugal is marked by an inflexion. CT scans images shows the medial contact with the ectopterygoid, which occurs along the entire medial antorbital surface of the jugal, forming a slightly upper lifted ventrolateral border. Furthermore, it is possible to observe a series of foramina along the entire internal surface of jugal, except on its antorbital portion, especially on the cylindrical portion or the posterior ramus.

**Frontal.** The frontals are fused into a single and overall dorsally concave element, located anteriorly to the parietal. This bone anteriorly contacts the posterior portions of the prefrontals and the anterior palpebrals medially, posteriorly to which it enters the external supraorbital fenestrae and fossa. The frontal contacts the anteromedial margin of the postorbitals posterolaterally and its posterior margin contacts the parietal. The anterior part of the dorsal surface, near the contact with the prefrontals and anterior palpebrals, is elevated in relation to the posterior portion and is convex. Also, this anterior portion is slender lateromedially and, in dorsal view, the bone gradually widens posteriorly, reaching its maximum width at the anteriormost contact with postorbital. At its posteriormost contact with the postorbital, the frontal forms a posterior wedge, which enters the anteromedial supratemporal fossae. Along its sagittal line, the dorsal surface of the frontal lacks a continuous crest, only presenting small, inconspicuous and scattered elevations (Fig. 17).

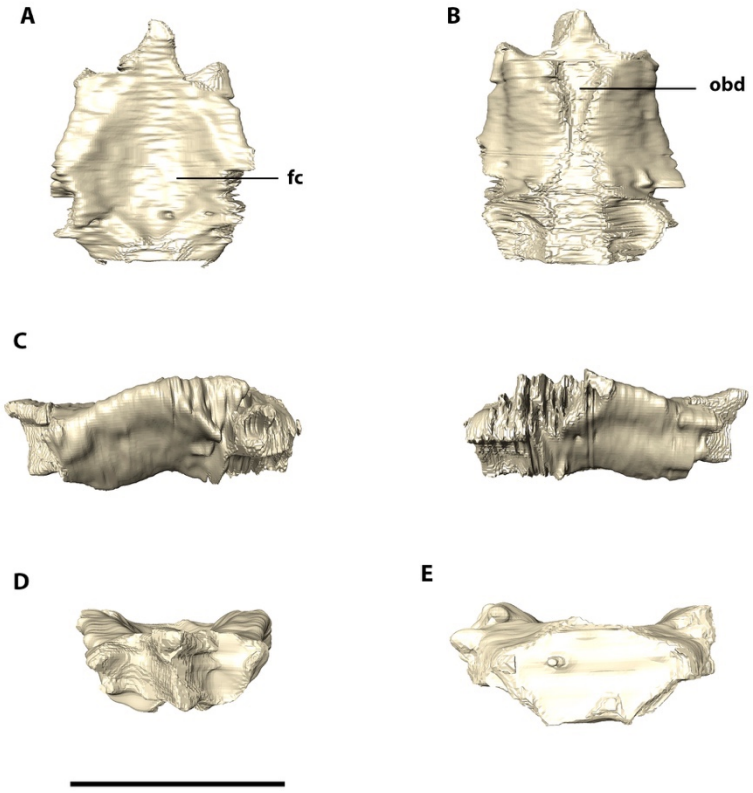


**Figure 17.** Digital reconstruction of the fused frontals of LPRP 0697 in (A) dorsal, (B) ventral, (C) left and right lateral, (D) anterior, and (E) posterior views. Fc, frontal concavity; obd, olfactory bulb depression. Scale bar: 5cm.

The borders of the frontal are elevated in relation to its central portion and the ornamentation of its dorsal surface is not as conspicuous as that of the remaining bones of the skull roof. However, irregular grooves are present on the elevated portions of the bone bordering the central portion. The CT scan images reveal that the ventral surface of the frontal has a sagittal depression traversing the bone, which is inferred to represent the depression for the olfactory bulbs.

**Postorbital.** The postorbital is anteroposteriorly elongated in dorsal view, participating on the anterolateral border of supratemporal fossa and fenestrae. The bone is composed of two distinct portions: a rugose dorsal part forming anterolateral corner of the skull roof, and a smooth ventral ramus forms participates on the meatal chamber (Fig. 18). The dorsal surface of the former is slightly convex, highly ornamented, following the pattern of grooves and ridges seen in the squamosal and gradually changing the pattern for smooth ornamentation more anteriorly. This portion is also ventrally curved at its lateral margin, forming a conspicuously concave ventral surface, which is continuous to the quadrate portion of the meatal chamber. Posteriorly, the postorbital-squamosal suture is slightly curved anteriorly, and both bones form the posterolateral margin of the skull roof. Anterolaterally, the postorbital is slightly concave to fit the posterior palpebral. Anteromedially the postorbital is connected with the frontal by an interdigitated dorsal suture at the anterior border of supratemporal fenestra. Also, a small portion of the supraorbital fenestra margin is formed by an anterolateral extension of the postorbital. In contrast, in lateral view, the ventral ramus of the postorbital extends ventrally and bifurcates, where its anterior ramus contacts the ascending process of the jugal, forming the postorbital bar between the orbit and the infratemporal fenestra. The posterior part of the bifurcation meets the quadratojugal, forming the posterior border of the infratemporal fenestra. The contact with the quadratojugal extends along all the posterior margin of the ventral ramus of the postorbital. CT scan images reveal that the postorbital seems to be an important bone for the passage of possible nerves and blood vessels due its conspicuous number of lateromedially aligned canals along the bone, which some are connected with the surrounding bones, such the squamosal and the frontal.

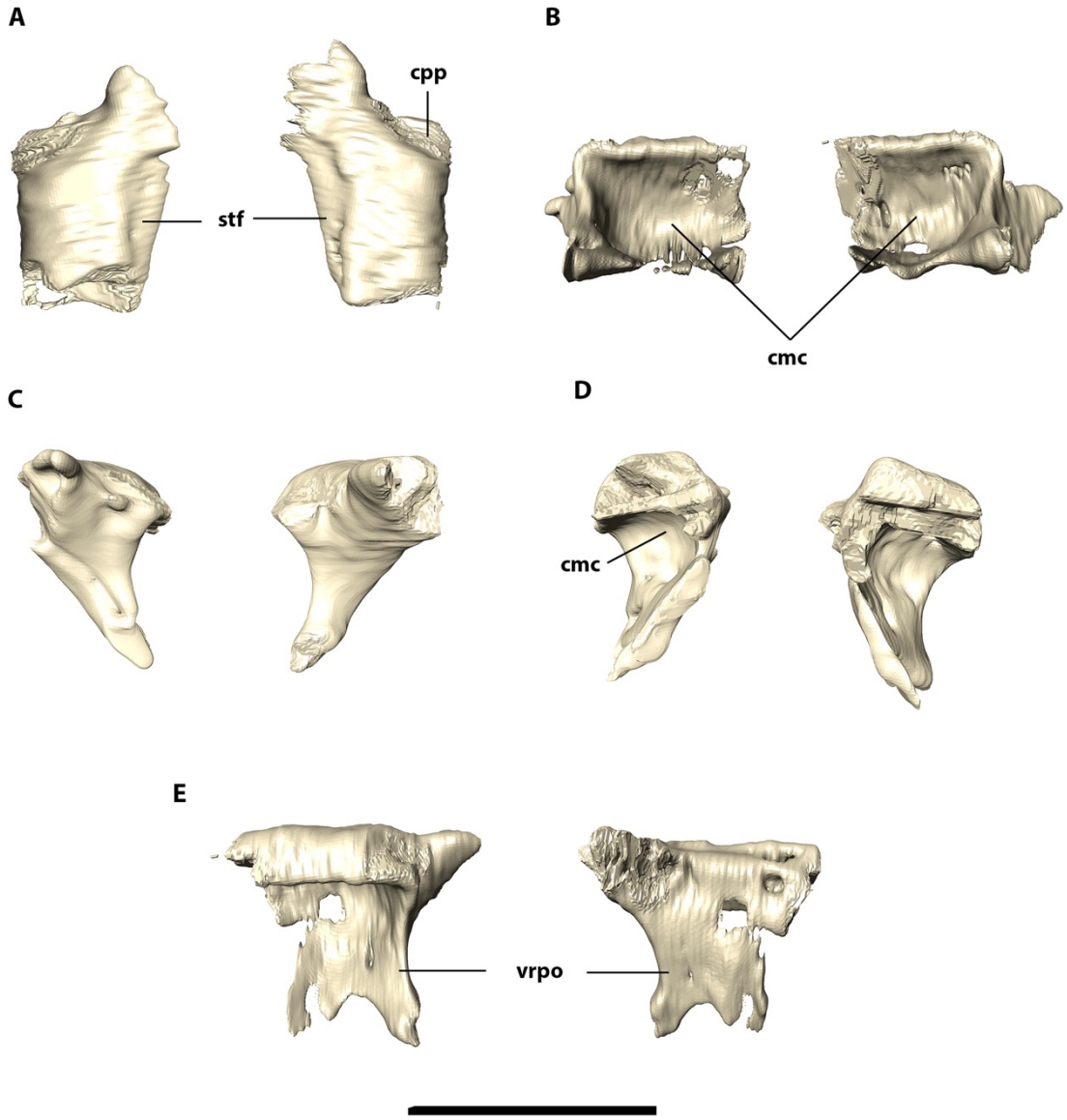


**Figure 18.** Digital reconstruction of left and right postorbital of LPRP 0697 in (A) dorsal, (B) ventral, (C) anterior, (D) posterior, and (E) right postorbital in lateral and medial views. Cmc, ventral concavity of postorbital composing the meatal chamber; cpp, contact area with posterior palpebral; stf, supratemporal fenestra; vrpo, ventral ramus of postorbital. Scale bar: 5 cm.

**Quadratojugal.** The quadratojugal forms the posterolateral surface of the skull, positioned posteriorly to the infraorbital fenestra and partially covered dorsally by the laterodorsal expansions of the postorbital and squamosal. The main body of the quadratojugal is ventrolaterally to dorsomedially inclined, shorter anteroposteriorly than dorsoventrally (Fig.

19). The ornamentation is restricted to the most lateralized portion of the bone, mainly near the contact with the posterior process of the jugal, where it is sub horizontal, elongated and thin grooves are present. The grooves gradually curve dorsally at the posterior margin of the infratemporal fenestra. The suture with jugal is interdigitated and verticalized, whereas the suture with quadrate is irregular but verticalized, extending dorsally until the ventral contact at the postorbital/squamosal suture. The anterodorsal suture with the ventral ramus of the postorbital is convex posteriorly, reaching the infratemporal fenestrae ventrally, posteriorly to its dorsal tip of the fenestra.

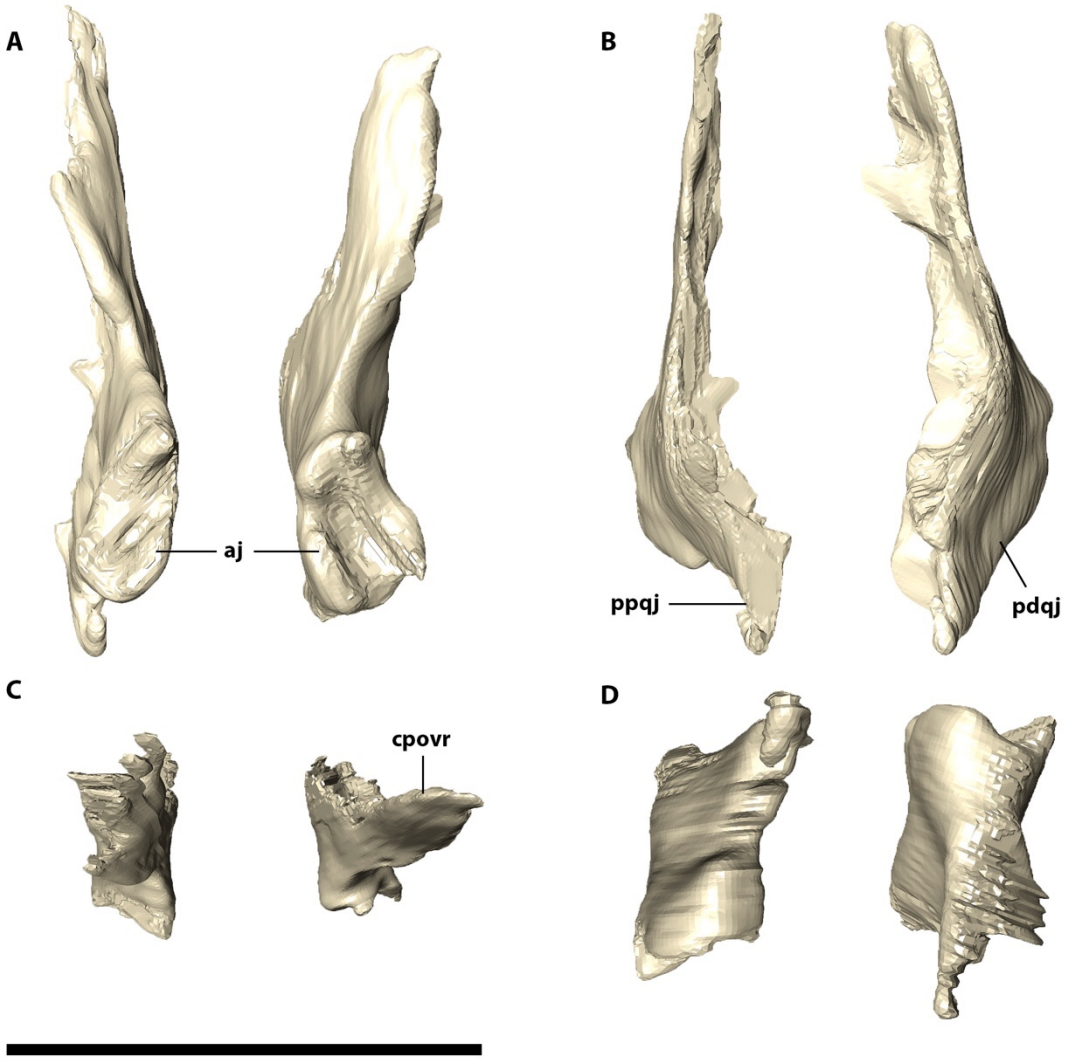


**Figure 19.** Digital reconstruction of left and right quadratojugal of LPRP 0697 in (A) anterior, (B) posterior, (C) dorsal, and (D) ventral views. Aj, articulation area with jugal; cpovr, contact with ventral ramus of postorbital; ppqj, posteroventral pointed tip of quadratojugal; pdqj, posteroventral depression of quadratojugal. Scale bar: 5 cm

The ventral portion of quadratojugal is posteriorly expanded. The posteroventral corner of the bone is pointed, not composing a continuous ventral margin with quadrate. Instead, a notch is seen at the contact between the quadrate and quadratojugal. The lateral surface of the base of the quadratojugal bears an anteroventral extension of the quadrate depression (Fig. 20). Right above this smooth concavity, the quadratojugal becomes convex on its lateral ornamented surface. The ornamentation of this area could be related to the insertion of *m. leavator bulbi* (Larsson & Sues, 2007, Montefeltro et al., 2011). Dorsal to this area, the anterior part of the bone turns medially, where it forms part of the posterior margin of the infratemporal fenestra, contacts the postorbital ventral ramus and enters the meatal chamber. Also, this area becomes flatter and the ornamentation is less conspicuous. The quadratojugal also forms the posteroventral corner of the infratemporal fenestra.

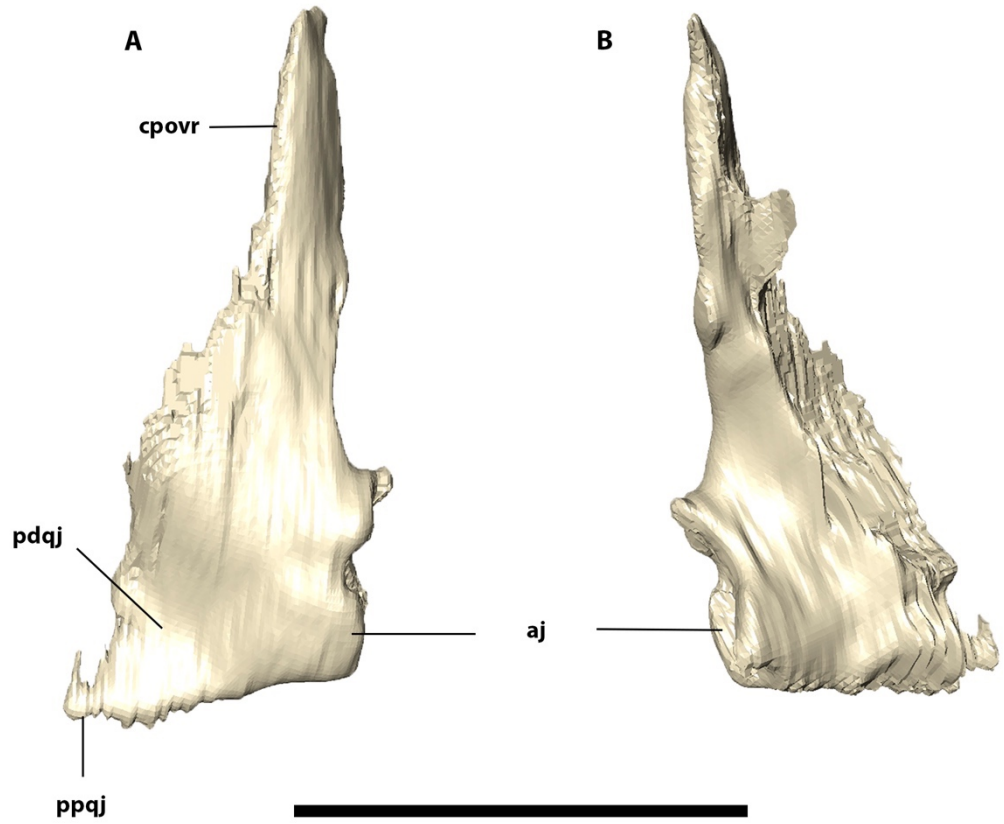


**Figure 20.** Digitally reconstructed right quadratojugal of LPRP 0697 in (A) lateral, and (B) medial view. Aj, articulation area with jugal; cpovr, contact with ventral ramus of postorbital; ppqj, posteroventral pointed tip of quadratojugal; pdqj, posteroventral depression of quadratojugal. Scale bar: 5 cm.

The CT scan images reveal a pneumatic bone, bearing three conspicuous canals located ventrally: the largest one, at the ventralmost margin of the bone, and two smaller at the ventrolateral margin. The largest canal seems to be continuous from the quadrate, whereas for the smaller two, it is possible to see the canal from the surface of the quadratojugal, possibly indicating an origin of those foramina at the bone. Furthermore, it is possible to notice a solid (not pneumatic) and laminar (mediolaterally thin) condition of the descending portion of quadratojugal.

**Quadrate.** The quadrate is verticalized, longer dorsoventrally than anteroposteriorly, slightly inclined medially at the dorsal portion, composing the posterolateral margin of the skull. It participates on the jaw joint, contacting the articular ventrally via two articular condyles. In posterior view, the lateral condyle is more expanded ventrally, and the surface between the two condyles is concave, dorsal to which the quadrate forms the pillar that extends until the point of contact with the squamosal and paroccipital process. The contact with the squamosal can be seen laterally; it is anterodorsally to posteroventrally oriented along the entire posterodorsal margin of quadrate. The ventral margin of quadrate in lateral view is also anterodorsally to posterovenrally oriented, forming an anterior notch at the contact with posteroventral portion of quadratojugal, which was only preserved on the left side of the cranium (Figs. 3 and 4).

Laterally the quadrate lacks ornamentation along its surface. The quadrate depression (sensu Montefeltro et al., 2011) occupies most of its ventral portion and expands forward as an anteroposteriorly elongated depression to the suture with the quadratojugal. Dorsally, the lateral surface of the quadrate bears the ovate and slightly posteriorly displaced otic incisure (sensu Montefeltro et al., 2016). Anteriorly to that, the lateral surface of the bone is at the same level of lateral exposure as that of the quadratojugal. This surface narrows anteroposteriorly as it extends dorsally. Posterior to that narrower portion, the bone surface slightly turns medially, forming a very reduced the anterior margin of otic incisure, or periotic fossa. This surface is pierced by a small and elliptical subtympanic foramen, anterodorsally to the otic incisure (Fig. 21).

The ventral portion of the quadrate composes the posterolateral part of the basicranium and contacts the paroccipital process, basioccipital, basisphenoid, and pterygoids via interdigited sutures, and this area represents surfaces of origin and insertion of mandibular adductor muscles (Iordansky, 1973). The contact with the paroccipital process is not marked by a crest as in the holotype of *B. salgadoensis* (MPMA 62-0001-02), whereas the basioccipital

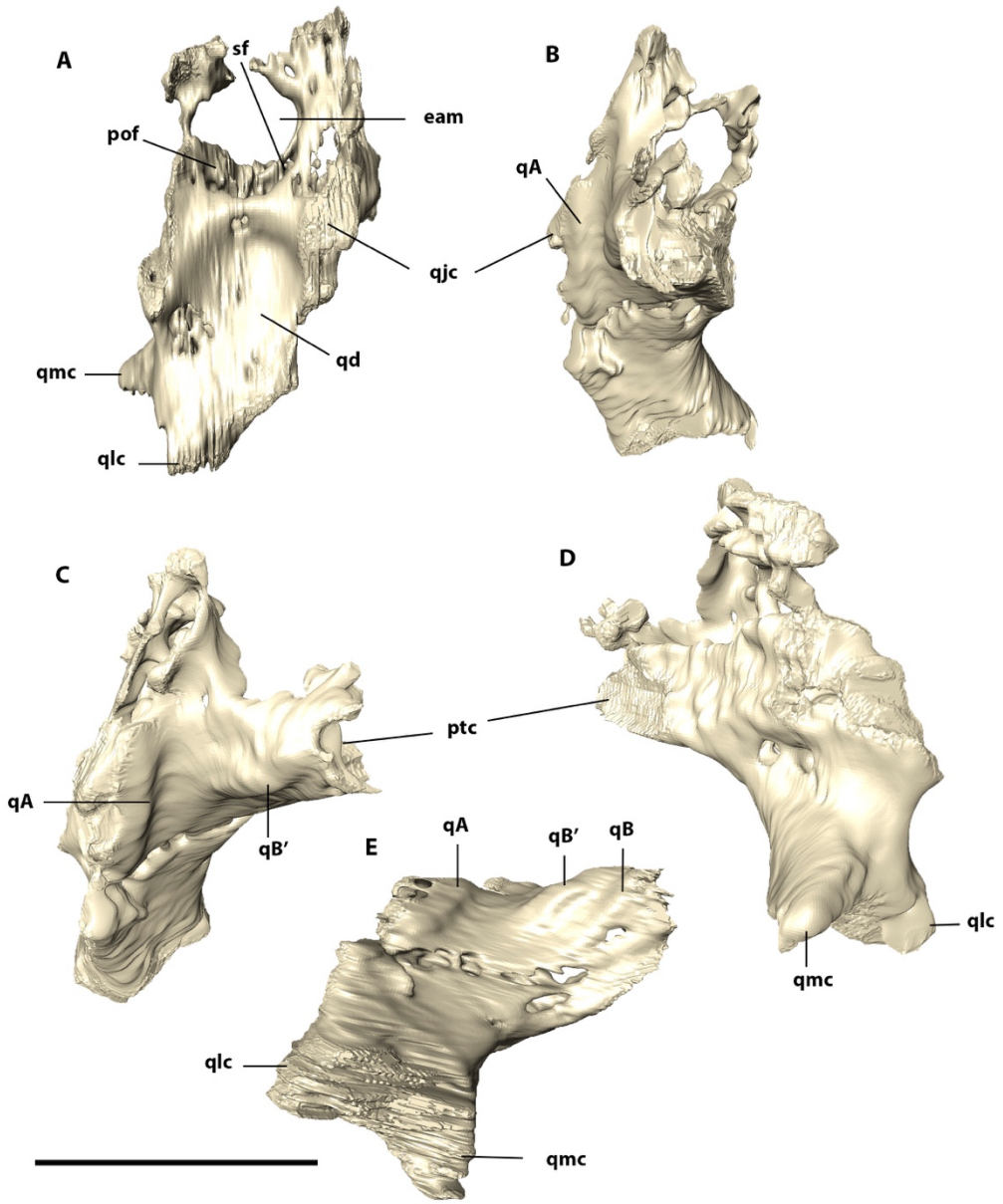


**Figure 21.** Digitally reconstructed right quadrate of LPRP 0697 in (A) lateral, (B) medial, (C) anterior, (D) posterior, and (E) ventral views. eam, external auditory meatus; pof, periotic fossa; ptc, pterygoid contact; qA, ventral quadrate crest for the insertion of M. adductor mandibula externus superficialis; qB, ventral quadrate crest for the insertion of M. ad. mand. ext. medialis; qB', ventral quadrate crest for the insertion of M. ad. mand. posterior; qd, quadrate depression; qjc, quadratojugal contact; qlc, quadrate lateral condyle; qmc, quadrate medial condyle. Scale bar: 5 cm

suture is marked by an elevated crest. This crest is restricted to the suture between those bones, not continuing ventrally along the medial surface of quadrate. Other crests described by Iordansky (1973) are recognized in the quadrate of LPRP/USP 0697. Crest 'A' corresponds to an elongated straight crest that extends along the anteromedial surface of quadrate, parallel and slightly posterior to the quadratojugal suture, associated to the insertion of the M. adductor mandibulae externus superficialis. Two other almost parallel crests are seen on the anterolateral contact of the quadrate with the pterygoid: crest 'B' is more marked medially and merges gradually with the remaining surface of the quadrate laterally, possible insertion for M. adductor externus medialis; and crest 'B'' is more conspicuous and extends dorsally to the most lateral portion of 'crest B', possible related to the insertion of M. adductor mandibulae posterior.

CT scan images show that the internal surface of quadrate as highly pneumatic, except for the more massive condylar portion of the bone. Furthermore, they reveal portions originally covered by rock matrix of the otic aperture, such as the visualization of the internalized subtympanic foramina, displaced more ventrally and structures of the meatal chamber, as the anteroposteriorly reduced dorsal otic incisure and a bony otic aperture suturing very closely the squamosal.

**Squamosal.** The squamosal is an "L-shaped" bone that occupies the posterodorsal portion of lateral surface of skull and the laterodorsal portion of the occipital wall. In dorsal view, the posterior portion of the squamosal is more expanded mediolaterally. In lateral view, this enlargement gives a sigmoid outline for the ventral surface of this part of the bone. The dorsal margin of the squamosal is slightly convex, as in most baurusuchids except for the strongly convex condition seen in *B. salgadoensis*. Anteriorly, the squamosal contacts the posterior portion of the postorbital via a slightly anteriorly convex suture in lateral view. The dorsomedial portion of the squamosal forms the posterolateral wall of the supratemporal fenestrae, contacting parietal medially, at the external border of the fenestra, via a sigmoid suture that gets more verticalized dorsally (Fig. 22). At the posterodorsally portion of the external supratemporal fenestra, there is the tempororbital foramen being relatively deep and compressed anterodorsally, providing a more elongated lateromedial length and an oval shape, positioned at the squamosal-parietal medial suture. In dorsal view, posterior to the supratemporal fossa, the squamosal-parietal suture is anteromedial to posterolaterally oriented. The ventral margin of the anterior ramus of the squamosal is sigmoid anteroposteriorly, dorsally enclosing the otic recess. At the posterior portion, the squamosal has a marked ventral inflexion,

forming the squamosal prong. The inflexion of this element forms a right angle with the anterior ramus of the bone, forming the posterior margin of the skull in lateral view.

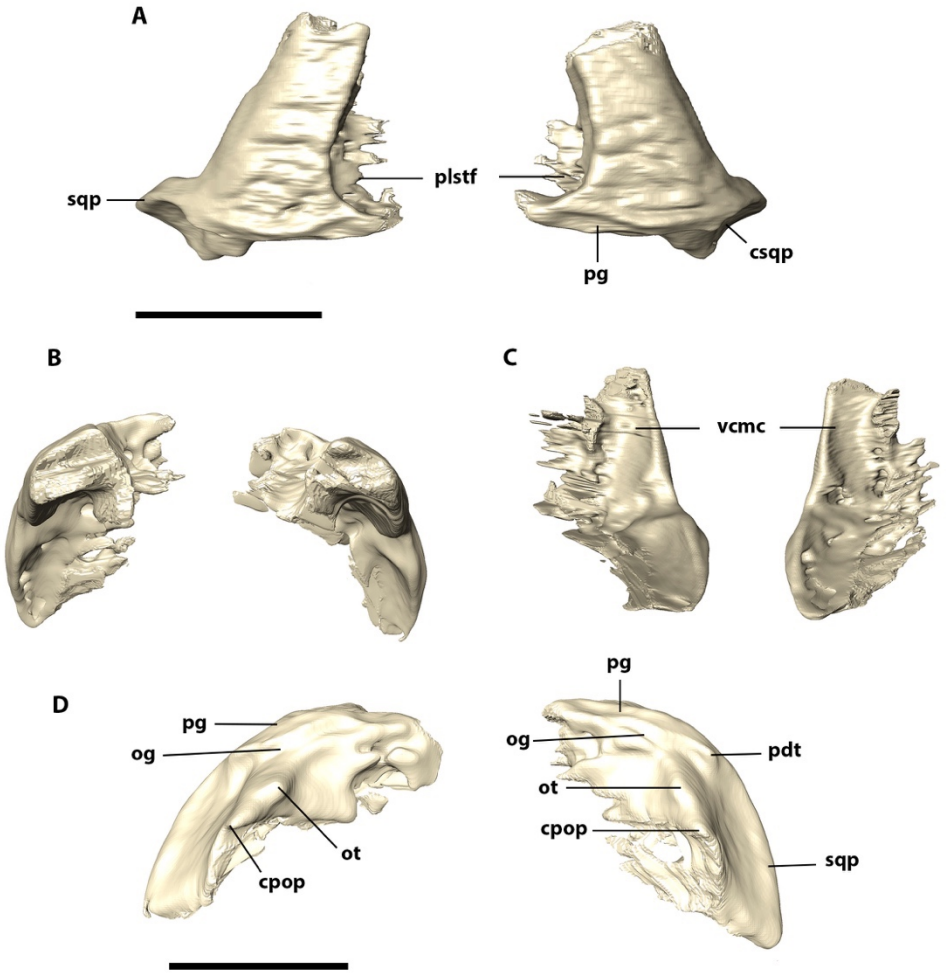


**Figure 22.** Digital reconstruction of left and right squamosal of LPRP 0697 in (A) dorsal, (B) anterior, (C) ventral, and (D) posterior views. Cpop, contact with paroccipital process; csqp, posterior concavity of squamosal prong; og, occipital groove; ot, occipital tuber; pdt, posterodorsal tuber; pg, posterodorsal groove; plstf, posterolateral wall of supratemporal fenestra; sqp, squamosal prong. Scale bar: 5cm.

The posterior surface of the squamosal forms most of the lateral portions of the occipital wall, due to the lateromedial (rather than anterolateral to posteromedial) orientation of the prong, which forms an almost right angle to the anterior ramus of the bone in lateral view (Fig.

23). The posterior surface of the prong is somewhat concave and its ventralmost portion expands laterally and overcoming the lateral extension of the dorsal portion. In posterior view, the medial suture of the prong with the supraoccipital and the paroccpital process is mostly sigmoidal. The suture is sub horizontal following the lateral half of the dorsal margin of the supraoccipital, extending ventrally in a sigmoidal shape until the ventral triple contact between squamosal, supraoccipital, and paroccipital process. Lateral to this point, the suture extends as a nearly straight line to the pointed and conspicuous bulged area at the dorsolateral corner of the paroccipital process. From this bulged area, the suture extends ventrally until reaching the contact with quadrate.

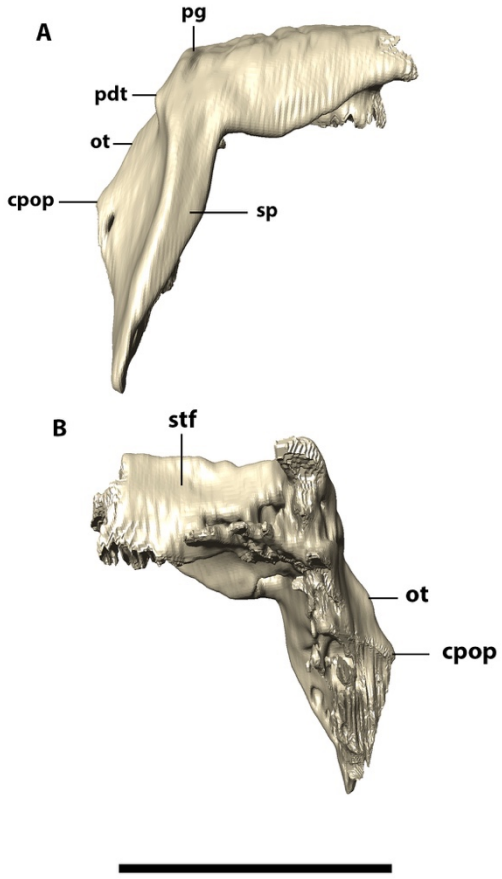


**Figure 23.** Digital reconstruction of right squamosal of LPRP 0697 in (A) lateral, and (B) medial views. Cpop, contact with paroccipital process; ot, occipital tuber; pdt, posterodorsal tuber; pg, posterodorsal groove; sqp, squamosal prong. Scale bar: 5cm.

In the transition from the dorsal to posterior surface of the squamosal, there is a horizontal rugose groove with elevated borders, the posterodorsal groove, starting slightly laterally to the upper limit of the squamosal-supraoccipital suture. This groove is slightly convex posteriorly and it stops laterally forming a small, posteriorly pointed posterodorsal tuber. Another depression is present on the posterior surface of the squamosal prongs, the occipital groove. It is smoother and positioned right below the posterodorsal groove. In posterior view, the occipital groove arches dorsally, ending laterally in a conspicuous occipital tuber. The surface below the occipital groove is flattened, whereas lateral to that, the lateralmost portion of the posterior surface of the squamosal prongs is depressed, becoming gradually more convex ventrally (Fig. 22B). The lateral surface of the squamosal prong is dorsoventrally convex, gradually getting narrower ventrally.

CT scan shows the medial participation of the squamosal on the supratemporal fenestrae, extending ventrally until the contact with medial portion of the quadrate. There is a series of multiple foramina at the internal dorsal surface of the bone, right below a conspicuously more solid surface

**Parietal:** The parietals are fused, composing the posterior portion of the skull roof and forming the medial margin of the external and internal supratemporal fenestrae (interfenestral bar). The CT scan images show a solid bone lacking any internal foramina. On its entire posterior margin, the parietal contacts the supraoccipital along a nearly straight line, slightly convex anteriorly. Laterally, the parietal contacts the squamosal via an irregular suture that extends anteroposteriorly along the posterior part of the supratemporal fossa, where a dorsoventrally compressed and mediolaterally elongated tempororbital foramen (see Squamosal) is present. Anterolaterally, the parietal contacts the postorbital at the anteromedial surface of the supratemporal fossa. The dorsal surface of parietal is “T-shaped” with an ornamentation composed by small and inconspicuous grooves. The dorsal surface of the parietal is thin and crest-shaped along its entire anteroposterior extension, lacking a conspicuous sagittal sulcus (Fig. 24).

The lateral surface of the parietal that composes the supratemporal fossa is smooth, lacking ornamentations except for thin irregular ridges located below the interfenestral bar and towards the tempororbital foramen.

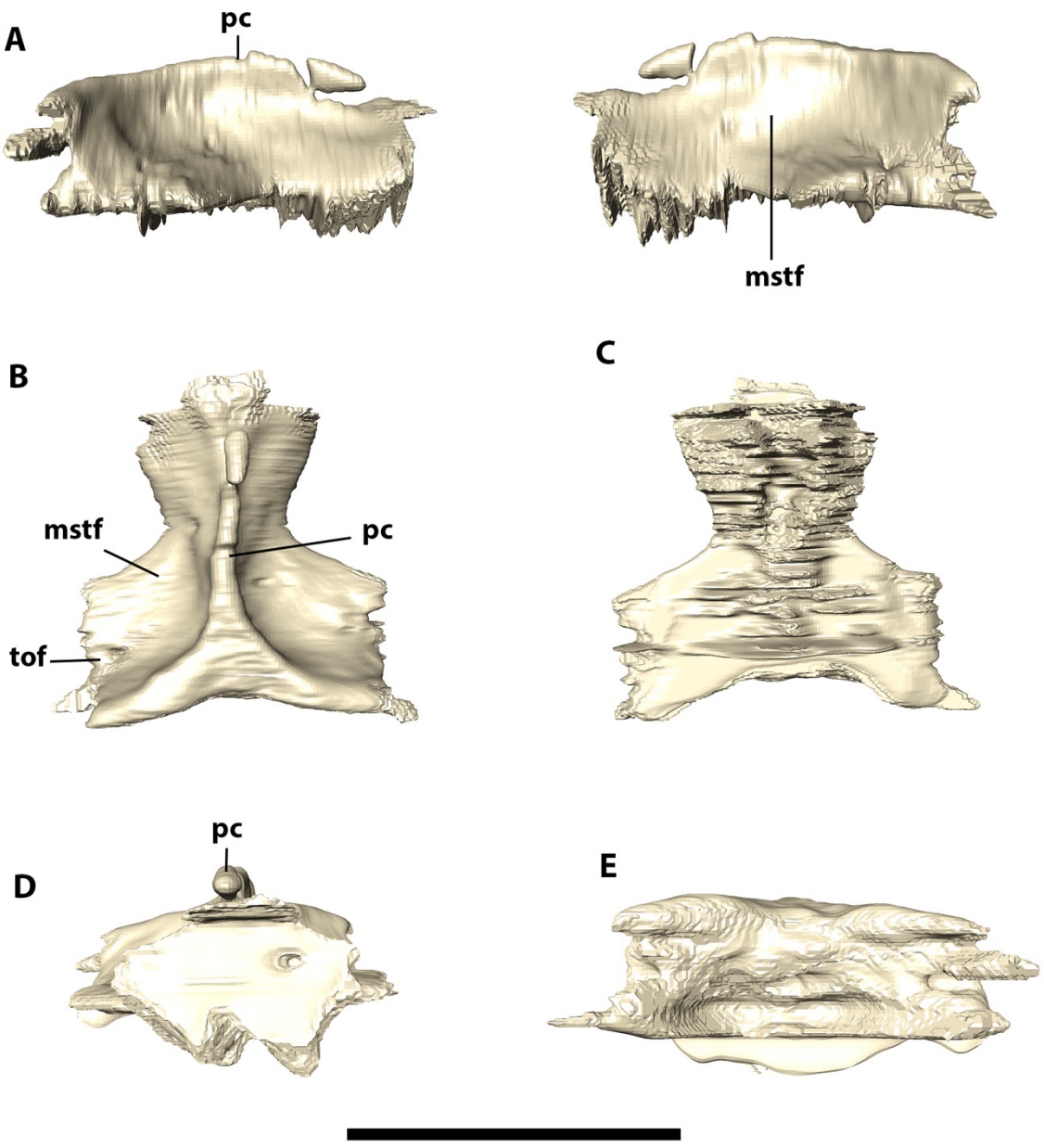


**Figure 24**. Digital reconstruction of fused parietal of LPRP 0697 in (A) right and left lateral, (B) dorsal, (C) ventral, (D) anterior, and (E) posterior views. Mstf, medial wall of the supratemporal fossa; pc, parietal crest; tof, temporoorbital foramen. Scale bar: 5cm.

**Laterosphenoid:** The laterosphenoid is a solid but relatively thin bone only observed via the CT scan images. It is located ventral to the frontal/parietal contact and also meets the dorsal portion of the pterygoid. The dorsal portion of the bone is relatively wider mediolaterally due its attachment to the ventrolateral portion of the frontal, whereas the ventral portion of the bone is more constricted posteriorly, providing a subtriangular shape in anterior view (Fig. 25). This ventral portion covers the posterior portion of the olfactory bulb. Also, the ventral constrict portion of the laterosphenoid contacts the dorsal surface of the basisphenoid.

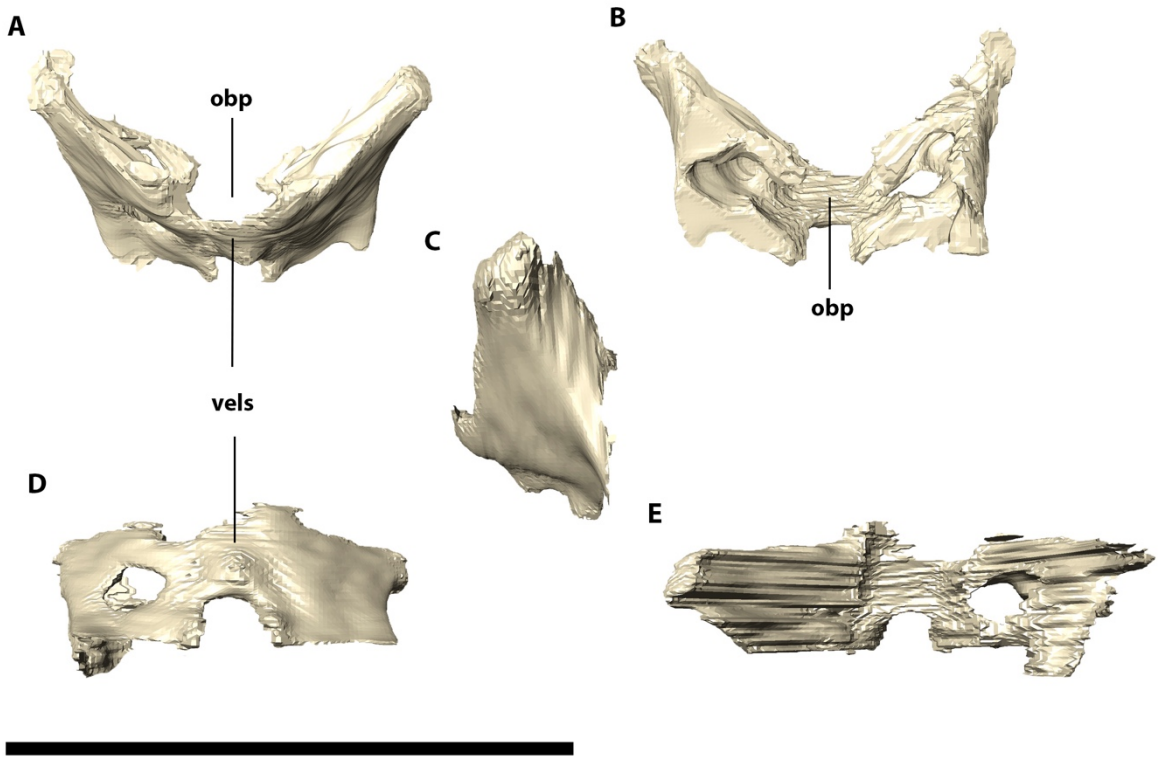


**Figure 25.** Digitally reconstructed laterosphenoid of LPRP 0697 in (A) anterior, (B) posterior, (C) left lateral, (D) ventral, and (E) dorsal views. Obp, olfactory bulb passage; vels, ventral enclosure of laterosphenoid. Scale bar: 5 cm.

**Supraoccipital:** The supraoccipital is an anteroposteriorly restricted bone, subtriangular in posterior view, where it forms the dorsomedial part of the occipital wall. The CT scan reveals two canals (left and right) that extend parasagittally inside the supraoccipital and gradually close towards the anterior contact with the parietal. The dorsal surface of the bone bears the same ornamentation of small pits seen in the posterior portion of the parietal. Its posterior

surface is covered of thin, dorsoventrally directed ridges and is almost flat lateromedially (Fig. 26), only presenting some irregular small ridges and grooves. The surface bears a sagittal inconspicuous crest that almost reaches the ventral margin of the bone.

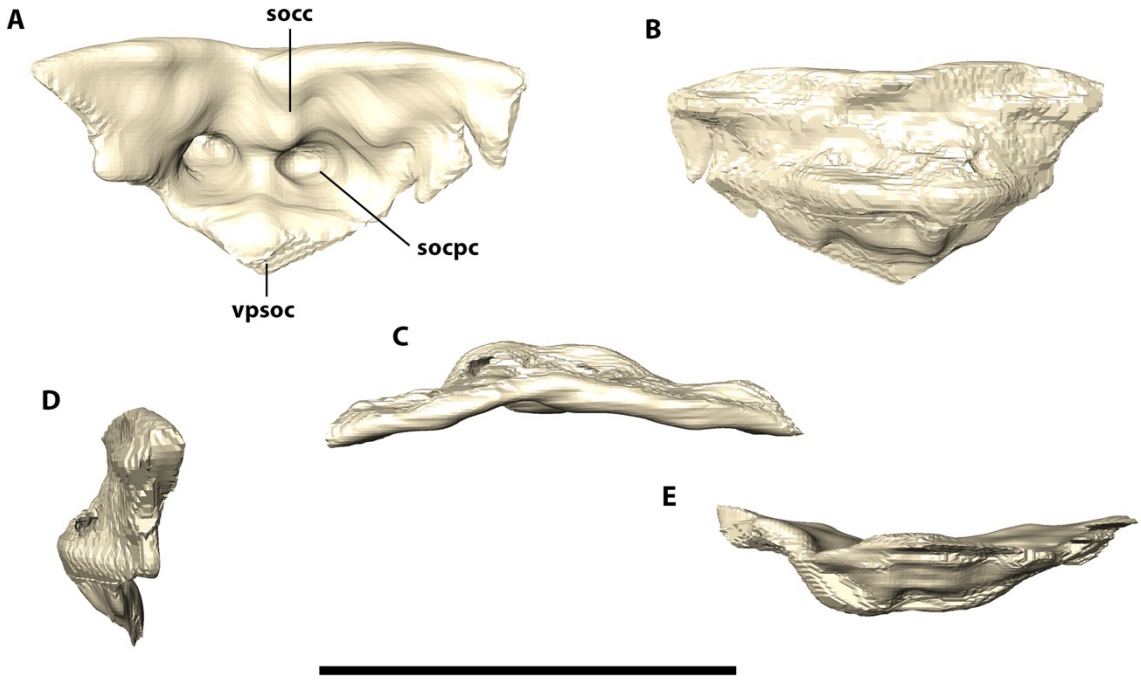


**Figure 26.** Digital reconstruction of supraoocipital of LPRP 0697 in (A) posterior, (B) anterior, (C) dorsal, (D) left lateral, and (E) ventral views. Socc, supraoccipital crest; socpc, supraoccipital paralle canals; vpsoc, ventral projected tip of supraoccipital. Scale bar: 5cm.

The supraoccipital contacts the parietal anteriorly via a slightly posteriorly concave suture. It contacts the squamosal posterolaterally via a suture that, as seen in posterior view, extends lateromedially at its medial portion and turns ventrally towards the triple contact between those bones and the paroccipital process. In occipital view, the supraoccipital is "V-shaped" ventrally, forming a thin pointed tip that contacts the dorsal portion of vertical suture that suparates both paroccipital process.

**Otoccipital and Paroccipital process:** The exoccipital and opisthotic are fused into the otoccipital, which forms a horizontally elongated portion of the occipital wall. They meet one another at the midpoint via a vertical suture and expands dorsolaterally from that suture,

bordering the ventral limit of the supraoccipital (Fig. 27). Lateral to the supraoccipital, each otoccipital forms a sub-triangular dorsal tip, lateral to which the bones remain sutured laterodorsally to the supraoccipital until they reach the squamosal. The CT scan images provide a clear view of the participation of the ottocipital in the dorsal margin of the foramen magnum and the occipital condyle. Internally, the ottocipital, including the paroccipital process, is highly pneumatic, presenting more compact bone at its posteriormost portion, forming the occipital wall.

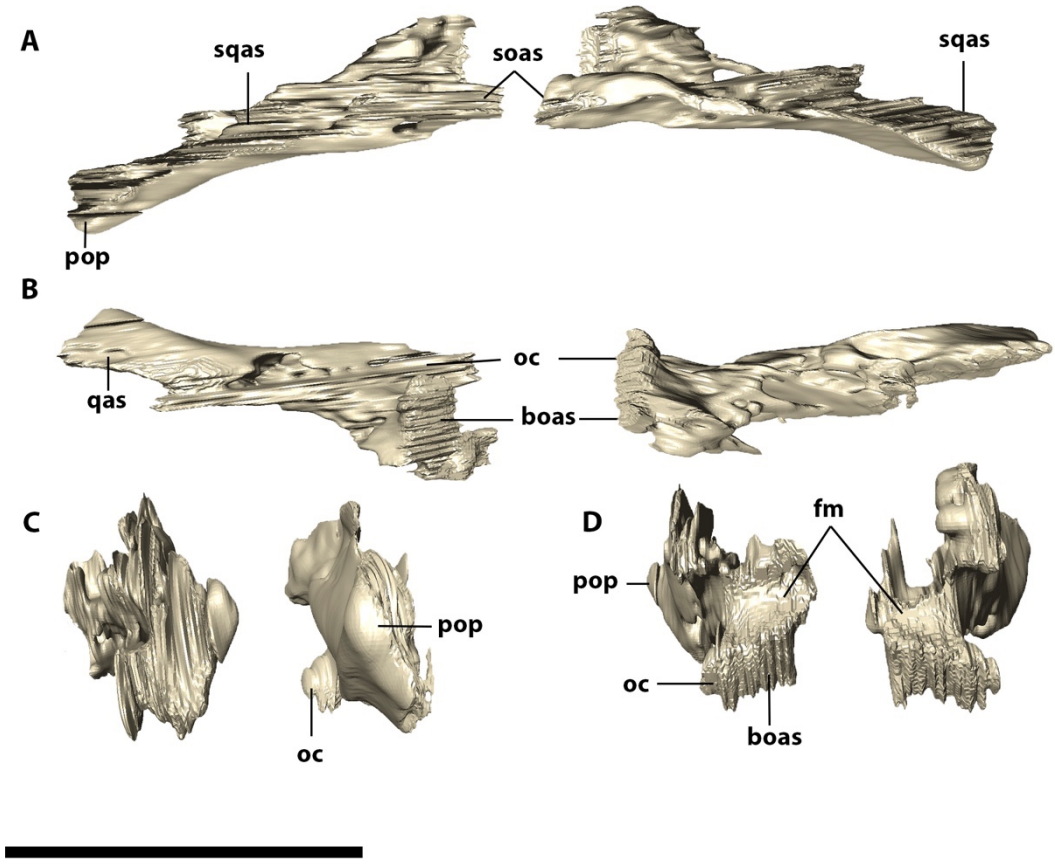


**Figure 27.** Digital reconstruction of left and right otoccipitals and paroccipital processes of LPRP 0697 in (A) dorsal, (B) ventral, (C) lateral, and (D) medial views. Boas, basioccipital articular surface; fm, foramen Magnum; oc, occipital condyle; pop, paroccipital process; qas, quadrate articular surface; soas, supraoccipital articular surface; sqar, squamosal articular surface. Scale bar: 5 cm.

The ottocipital extends laterally forming the paroccipital process, which contacts the quadrate and squamosal. The lateralmost contact with squamosal is given by the occipital tuber, ventral to which the contact between the two bones continues vertically until the quadrate contact. From that point on, the suture extends ventromedially, with the quadrate positioned ventrally, until it reaches the triple contact between both bones and the basioccipital. The contact with basioccipital is marked by a small protuberance, which slightly deflects the suture posteriorly. From this point on, the suture follows dorsomedially, where the bones participate in the dorsolateral surface of the occipital condyle (Fig. 28).

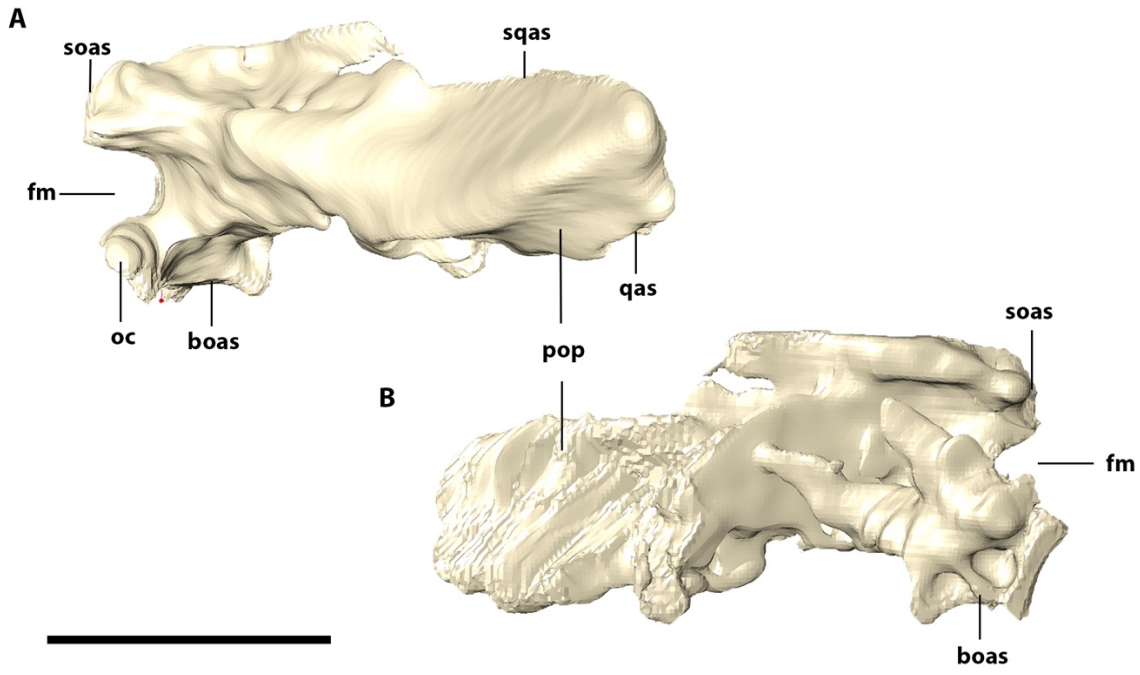


**Figure 28.** Digitally reconstructed right otoccipital and paroccipital process of LPRP 0697 in (A) lateral, and (B) medial views. Boas, basioccipital articular surface; fm, foramen Magnum; oc, occipital condyle; pop, paroccipital process; qas, quadrate articular surface; soas, supraoccipital articular surface; sqar, squamosal articular surface. Scale bar: 5 cm.

**Basioccipital:** The basioccipital is an anteroposteriory compressed and vertically oriented bone that forms the ventralmost portion of the occipital wall. Its dorsal portion forms the occipital condyle, the dorsal surface of which participates on the ventral margin of the foramen magnum. The ventral portion of the basioccipital contacts the basisphenoid where the bone arches anteroventrally. This posteroventrally inclined surface lacks strong ornamentation and comprises the posteromedial margins of the medial pharyngeal tube and the pharyngotympanic tubes (Fig. 29). Laterally, the basioccipital contacts the quadrates at occipital wall via an elevated suture. In the ventral contact between those bones, the basioccipital bears an elongated concavity extending along the suture. This concavity gradually becomes shallower and disappears posterolaterally, anterior to the point of maximal posterior inflexion of the basioccipital. The occipital surface of the basioccipital is subtriangular in posterior view, slightly concave medially, and presenting an inconspicuous sagittal elevation. It is bordered laterally by the otoccipital and ornamented only at its ventralmost surface.

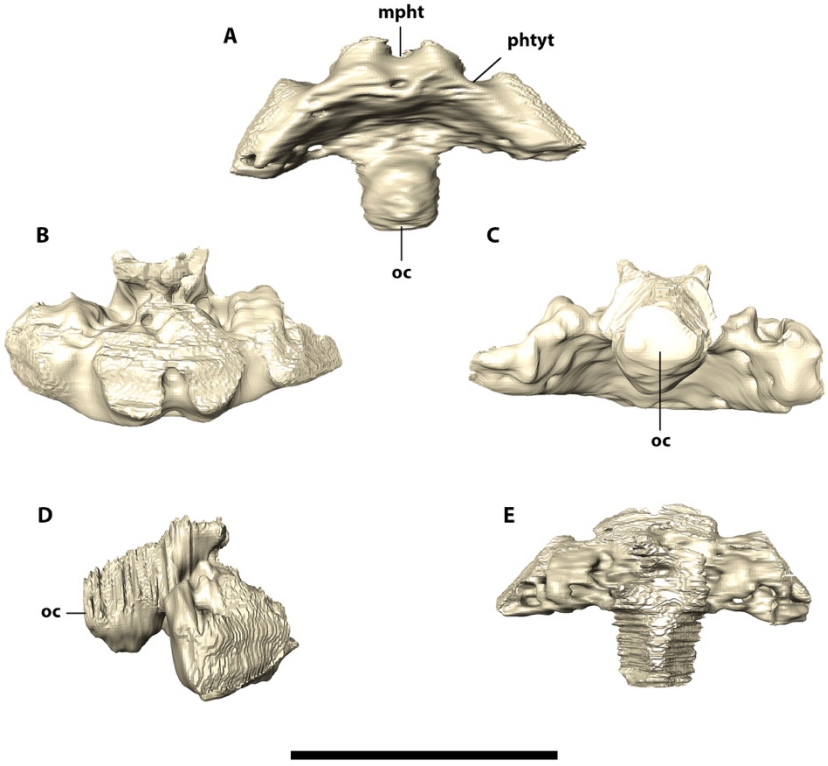


**Figure 29.** Digital reconstruction of basioccipital of LPRP 0697 in (A) ventral, (B) anterior, (C) posterior, (D) right lateral, and (E) dorsal views. Mpht, medial pharyngeal tube; oc, occipital condyle; phtyt, pharyngotympanic tube. Scale bar: 5 cm.

**Basisphenoid:** The basisphenoid is triangular shaped in ventral view, located at the posterior portion of the ventral surface of the skull. It contacts the basioccipital posteriorly, the quadrate and quadrate ramus of the pterygoid laterally, and pterygoid anteriorly. The surface where the basisphenoid is exposed, which also includes parts of the pterygoid and quadrate, is inclined anteroventrally to posterodorsally. The anterior contact with the pterygoid is given by a suture internalized into the narrow and conspicuous sagittal groove, which forms the medial edge of the posterior portion of the pterygoid wings. This contact is anteriorly pinched and from this point it diverges posterolaterally following the medial portion of the quadrate ramus of the pterygoid as a slightly elevated suture. At its most posterolateral and dorsal portion, the basisphenoid contacts the quadrate, and the entire posterior margin of the bone forms a transverse contact with the basioccipital. This latter suture is internalized into the medial pharyngeal tube and the pharyngotympanic tubes, but displaced anteriorly, showing that the basioccipital forms most of these apertures. The lateral foramina are displaced slightly posteriorly relative to the median, and all three are approximately of the same size, but with different shapes: the lateral foramina are elliptical, whereas the middle one is clearly more circular. The surface lodging the sutures between those foramina is elevated posteroventrally. The ventral surface of the basisphenoid has a pair of parasagittal crests, in which between them and the elevate suture of the quadrate ramus, forms elongated concavities. Those concavities extend anteromedially from the anterior margin of the pharyngotympanic tubes to the posterolateral triple contact of the basisphenoid, the quadrate and the quadrate ramus of the pterygoid. The anterior portion of these elongated concavities is more ornamented and a small circular foramen is seen at the sagittal line between then. Between the two parasagittal crests of the basisphenoid, there is a smooth transverse elevation that separates the medial pharyngeal tube from a marked longitudinal anterior groove.

The CT scans images reveal more about the morphology of basisphenoid and its contact with surrounding bones. Anteriorly the basisphenoid is more constricted lateromedially and dorsoventrally forming the cultriform process (Fig 30 and 31), which contacts dorsally the ventral portion of the laterosphenoid (Fig. 30). The inner portion of the process is only bordered by the bone, leaving a gap medially. This region is highly pneumatic, presenting the complex canals of the medial pharyngeal tube and the pharyngotympanic tubes that pierces the ventral surface of the bone.

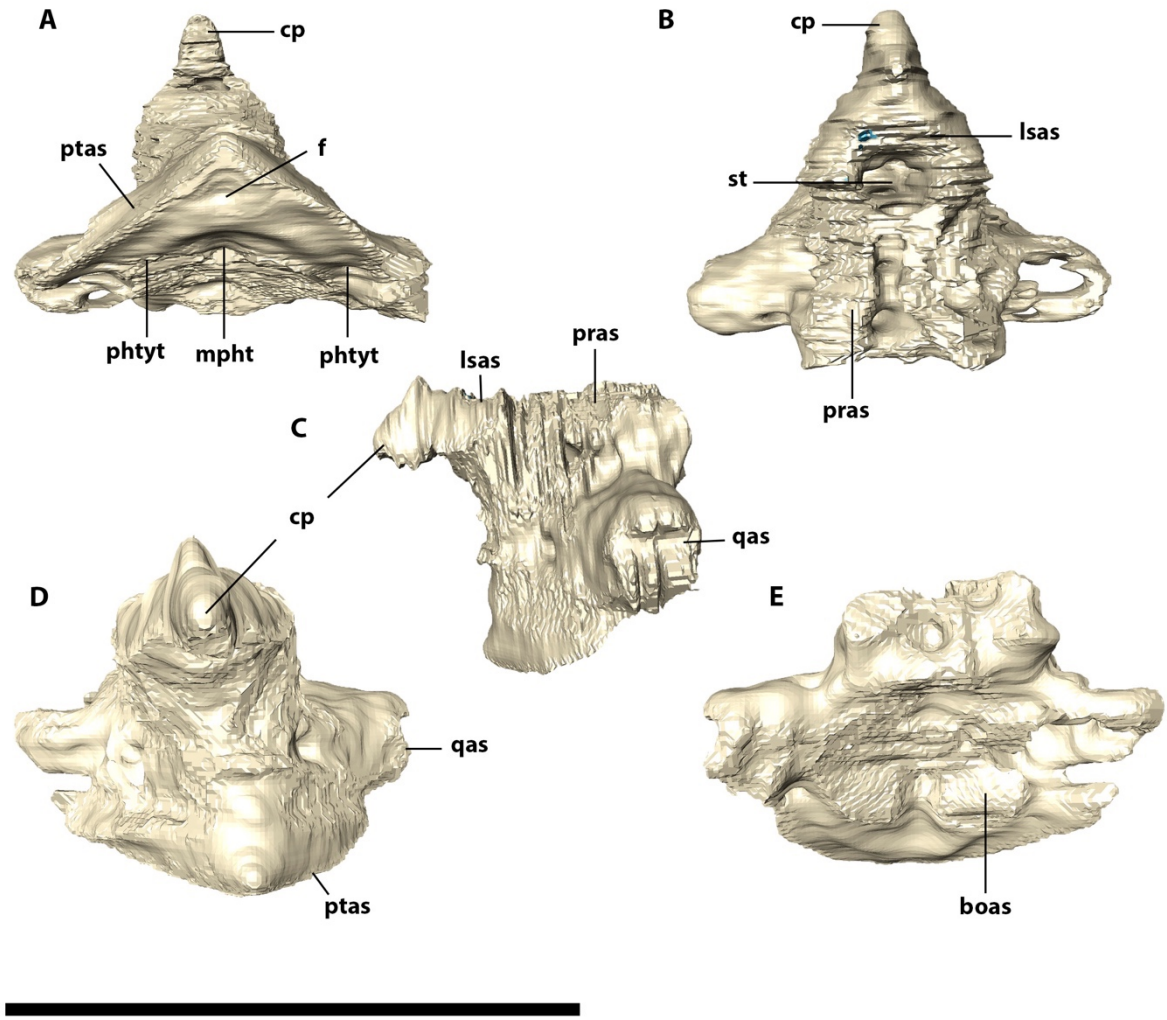


**Figure 30.** Digitally reconstructed basisphenoid of LPRP 0697 in (A) ventral, (B) dorsal, (C) lateral, (D) anterior, and (E) posterior views. Boas, basioccipital articular surface; cp, cultriform process; f, foramen; lsas, laterosphenoid articular surface; mpht, medial pharyngeal tube; phtyt, pharyngotympnic tube; pras, prootic articular surface; ptas, pterygoid articular surface; qas, quadrate articular surface; st, sella turcica. Scale bar: 5cm.

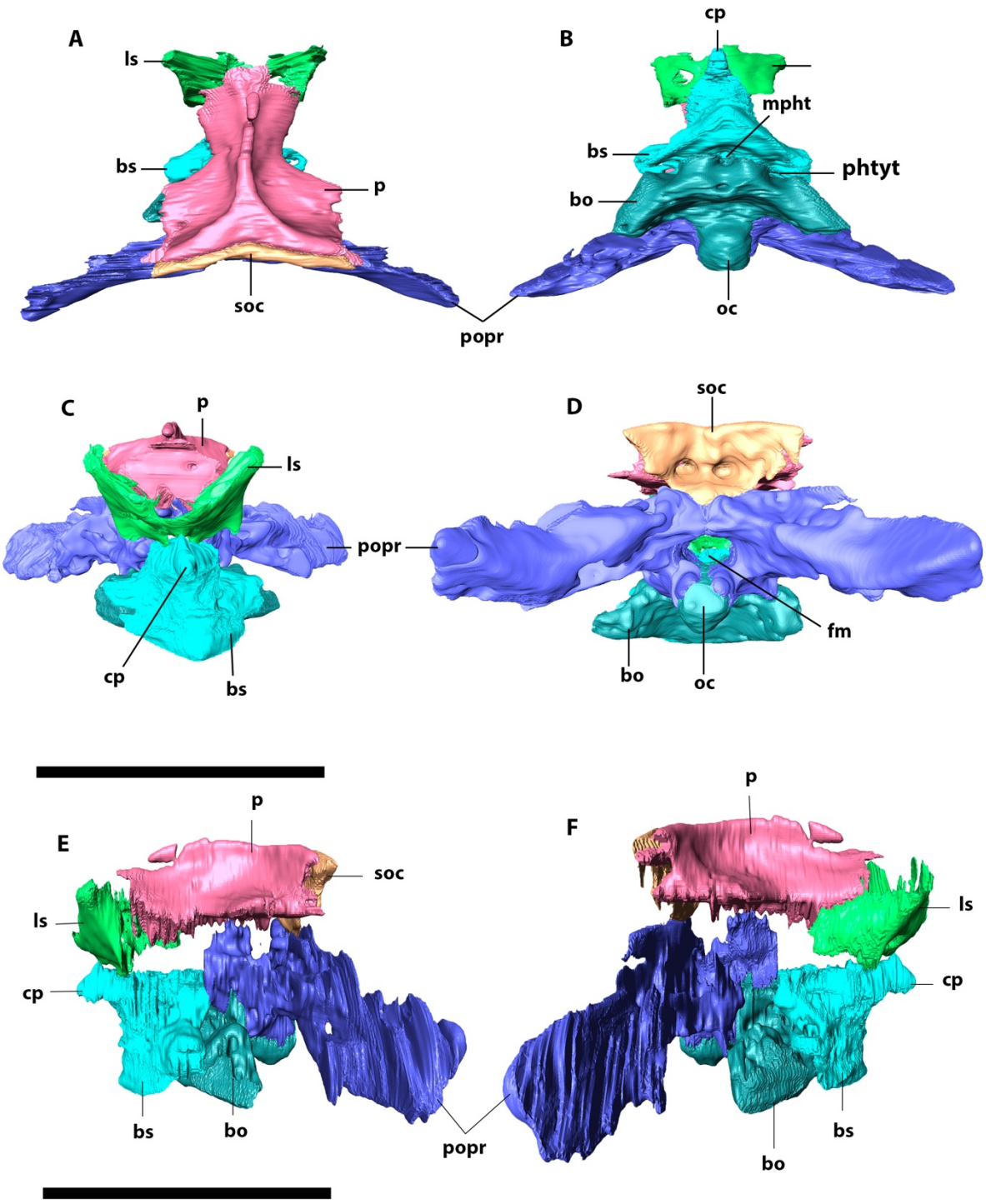


**Figure 31.** Digitally reconstructed braincase of LPRP 0697 (except for prootic). (A) dorsal, (B) ventral, (C) anterior, (D) posterior, (E) left, and (F) right lateral views. Bo, basioccipital; bs, basisphenoid; Cp, cultriform process; fm, foramen magnum; ls, laterosphenoid; mpht, medial pharyngeal tube; p, parietal; phtyt, pharyngotympnic tube; popr, paroccipital process; soc, supraoccipital. Scale bar: 5 cm.

**Pterygoid**: The pterygoids are a highly pneumatized bone, fused into a large and complex bone forming most of the posterior portion of the palatal surface. It contacts the ectopterygoids and palatines anteriorly, the basisphenoid posteriorly, and the quadrates lateroposteriorly (Fig 32). The pterygoids wings are ventrally projected, extending beyond the level of the ventral border of the lower jaw. Except for the pterygoid wings, the bony sheets structures laterally to the choanal septum corresponds to the most ventrally projected portions of the skull, whereas the choana, choanal septum and fenestrae are recessed and located in a dorsally arching part of the palate. There is a conspicuous ventral concavity in the center of each the pterygoid wing, almost continuous to a similar ventral depression in the ectopterygoid, but separated from it by the slightly elevated suture between both bones. The pterygoid wings border the choanal fenestrae lateroposteriorly. Their tips are slightly rounded and heavily ornamented, as in the adjacent portion of the ectopterygoid. The sagittal portion of the ventral surface of the pterygoids is smooth, with a longitudinal concavity that extends from the contact with the basisphenoid, to the posteriomost portion of the choanal septum. The septum is robust and ventrally flattened, possessing only small and inconspicuous ridges ornamenting its posterior portion. Laterally to the septum, two laterally expanded flattened sheet of bone are present, presenting the lateralmost borders projected ventrally and its ventral surface smooth. These pterygoids bony sheets border medially the choanal fenestrae and it presents a continuous smooth surface along its ventral surface. CT scans images shows that those bony sheets are converging medially on its dorsal portion, providing a subtriangular shaped structure forming the roof of the choanal aperture, at the same level of the choanal septum ventrally. Both portions, the bony sheets and the choanal septum are continuous anteriorly with the vomer and the palatine respectively. These bones seem to be fused dorsally, not being able to identify sutures. Along its medial surface, the pterygoid is more ventrally projected at its posterior portion, reaching the same level of the ventral surface of palatine. Lateral to the narrow sagittal grove at the posterior end of the pterygoid, the surface of pterygoid possesses a highly ornamentation that in continuous slightly laterally, into the base of the posterior margin of pterygoid wings. Posteriorly to this point, the pterygoids suffers a dorsal inflexion, extending posterolaterally to form the quadrate ramus of pterygoid and contact the eponymous bone. Each of these rami possesses a rounded and highly ornamented pterygoid tuberosities at its medial margin. This contacts laterally the anteroventral portion of basisphenoid. Following posterolaterally, and slightly dorsally, from the pterygoid tuberosity, the contact of the ramus with the basisphenoid is marked by an interdigitated suture that reaches the quadrate. The lateralmost portion of the quadrate ramus of the pterygoid bears a conspicuous muscle scar, termed here as “crest B” (Iordanski, 1973).

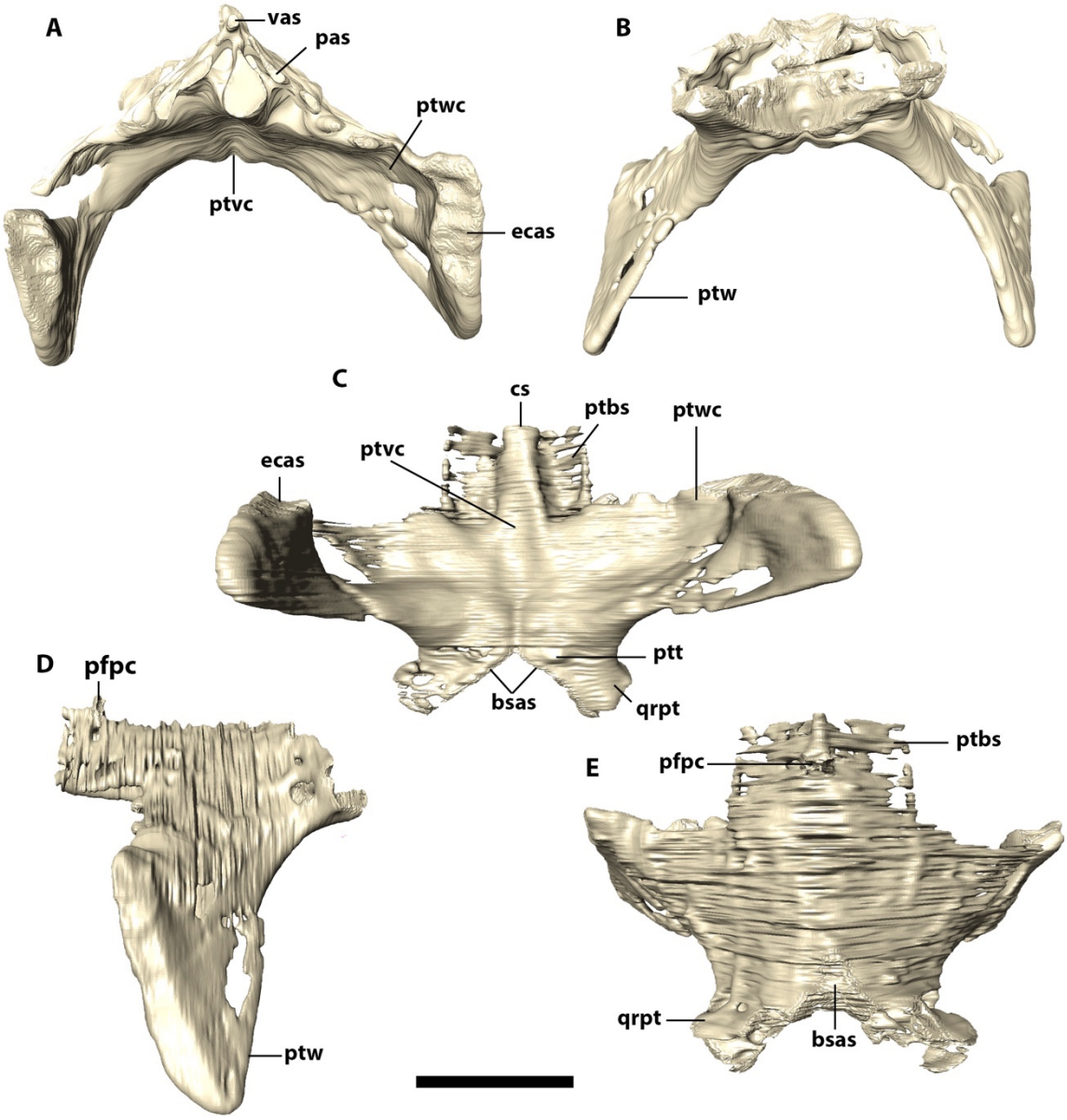


**Figure 32.** Digitally reconstructed fused pterygoids of LPRP 0697 in (A) anterior, (B) posterior, (C) ventral, (D) lateral, and (E) dorsal views. Bsas, basiphenoid articular surface; cs, choanal septum; ecas, ectopterygoid articular surface; pas, palatine articular surface; pfpc, prefrontal pillar contact; ptbs, pterygoid bony sheets; ptt, pterygoid tuberosity; ptvc, pterygoid longitudinal ventral concavity; ptw, pterygoid wing; ptwc, pterygoid wing concavity; qrpt, quadrate ramus of pterygoid; vas, vomer articular surface. Scale bar: 5 cm.

**Ectopterygoid**: The ectopterygoid is composed by two main parts: the dorsolateral process and the posteroventrally projected flanges, or ectopterygoid wings (Fig. 33). The CT scan images show a solid internal structure for the entire bone, differing of the condition observed in the pterygoid. The dorsolateral process contacts the medial surface of the jugal medially and the maxilla anteriorly. The ectopterygoid-maxilla suture is posteriorly directed. Also, the dorsolateral process forms the lateroposterior border of the suborbital fenestra. Its lateral surface can only be observed in the CT scan images, which show a smooth surface, lacking any foramina. The ectopterygoid wing is mediolaterally expanded, convex dorsolaterally and concave ventromedially. The concavity is well marked and is an extension of the same concavity present at the medial surface of the pterygoids (Fig. 34). The ectopterygoid concavity is divided by a medially positioned thin crest, forming a small concavity slightly lateral to the suture with palatine. Due this accentuated concavity, the morphology of the pterygoids and ectopterygoids wings are mostly verticalized ventrally.

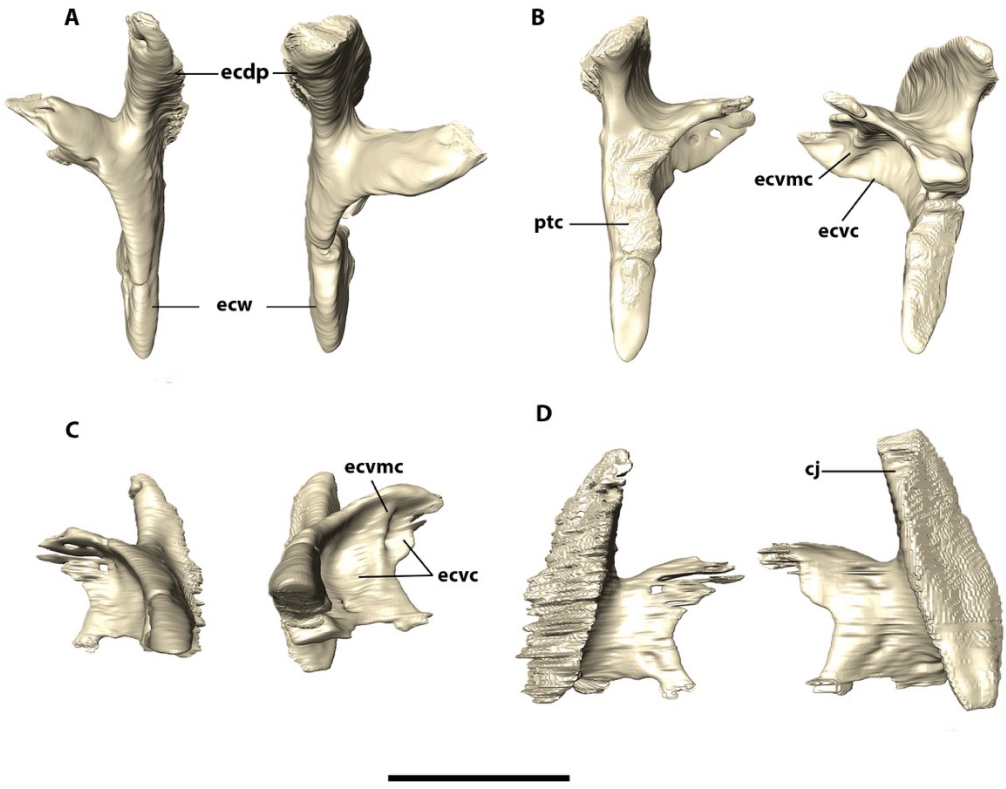


**Figure 33.** Digital reconstruction of left and right ectopterygoid of LPRP 0697 in (A) anterior, (B) posterior, (C) ventral, and (D) dorsal views. Cj, area of contact with jugal; ecdp,

ectopterygoid dorsal process; ecvc, ectopterygoid ventral concavity; ecvmc, ecpterygoid ventromedial crest; ecw, ectopterygoid wings; ptc, pterygoid contact. Scale bar: 5cm.

The medial portion of the ectopterygoid forms the anterolateral border of the parachoanal fenestrae posteriorly and anteriorly the entire posterior margin of the suborbital fenestrae, except for a short posteromedial participation of the palatine. Laterally to the suture with palatine, the base of ectopterygoid wing is ventrally convex, but laterally from this point it assumes a smoother and more concave pattern until the tip of the wing. The contact with pterygoid occurs along the entire posterior margin of the ectopterygoid and is verticalized at its lateral portion, where the tip of the ectopterygoid wing is subtriangular and ventrally projected, nearly reaching the tip of pterygoid wing. The tip of ectopterygoid wing is ornamented by small dots more ventrally and very thin grooves more dorsally, which can be related to the insertion of *m. pterygoideous anterior* (Schumacher, 1973).

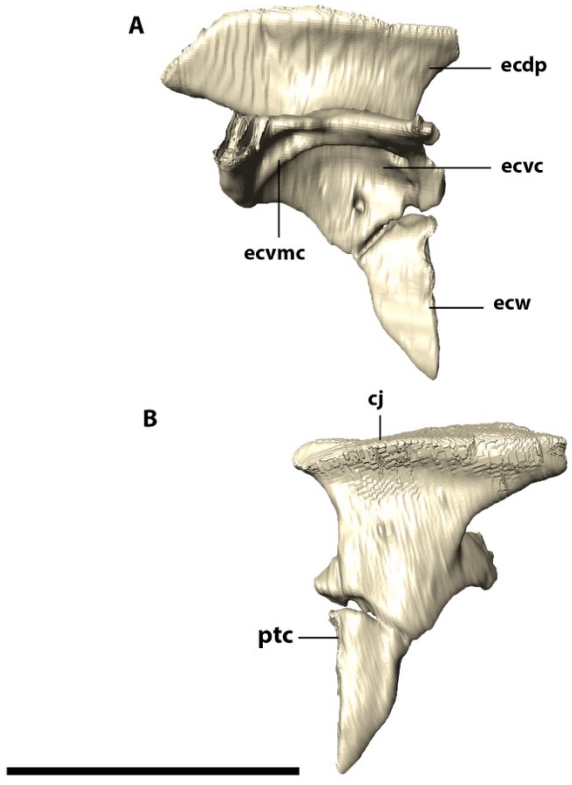


**Figure 34**. Digitally reconstructed right ectopterygoid of LPRP 0697 in (A) medial, and (B) lateral view. Cj, area of contact with jugal; ecdp, ectopterygoid dorsal process; ecvc,

ectopterygoid ventral concavity; ecvmc, ecpterygoid ventromedial crest; ecw, ectopterygoid wings; ptc, pterygoid contact. Scale bar: 5cm.

**Palatine:** The palatine pair forms a tubular anteromedially elongated structure. Each bone contacts the maxilla anteriorly via a transverse and anteriorly convex suture and expands laterally at the posterior limit (posterolateral ramus) contacting the anteromedial portion of ectopterygoid. The posterolateral ramus is aligned perpendicular to the sagittal line, providing a "T-shaped" to the palatine in ventral view (Fig. 35) and a triangular shape for the suborbital fenestra. The bone forms the anterior margin of the choana and of the medial border of the suborbital fenestra. The anterior extension of the palatine does not reach the level of the anterior margin of the suborbital fenestra. The ventral surface of palatine is not flattened, but inclined dorsolaterally from a sharp sagittal suture. Also, the ventral surface of the palatine is pierced only by a few foramina, concentrated in its posterior portion, right anterior to the posterolateral ramus. Such ramus has a slightly ornamented flattened ventral surface. The posterior surface of palatine, ventrally to the choanal septum of pterygoid, is completely verticalized, where a small foramen bordered ventrally by a small transverse crest on the point of inflexion of the bone is seen only on the right side.

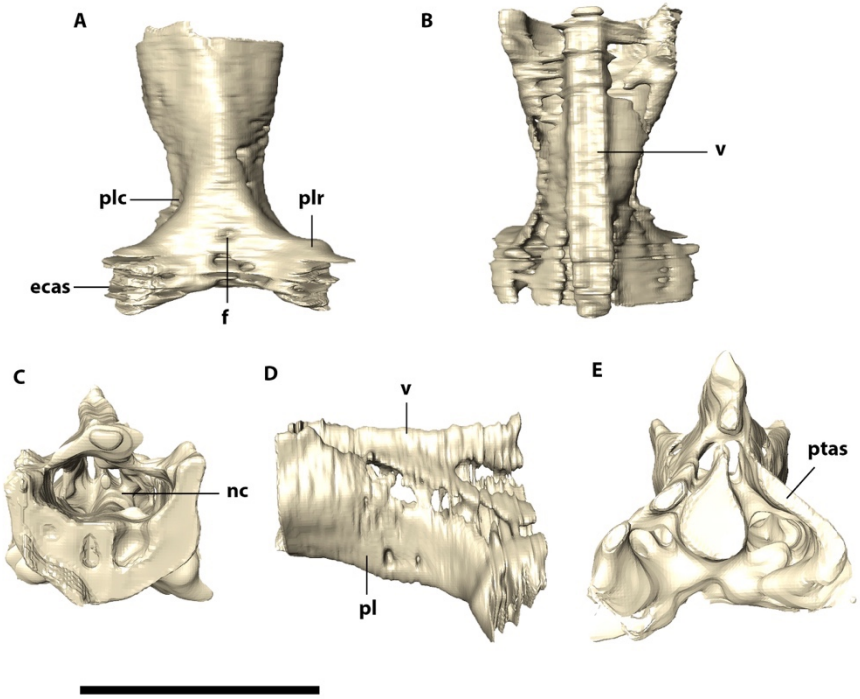

**Figure 35.** Digitally reconstructed fused palatine and vomer of LPRP 0697 in (A) ventral, (B) dorsal, (C) anterior, (D) lateral, and (E) posterior views. Ecas, ectopterygoid articular surface; f, foramen; nc, nasal cavity; pl, palatine; plc, palatine lateromedial constriction; plr, palatine posterolateral ramus; ptas, pterygoid articular surface; v, vomer. Scale bar: 5 cm

**Vomer:** The vomers can only be assessed in CT scan images. It is positioned dorsal to the palatine, but the sutures are not visible, which seems that those bones are probably fused to one another and fused with the palatine ventrally (Fig. 35 and 36). The vomer has a subtriangular

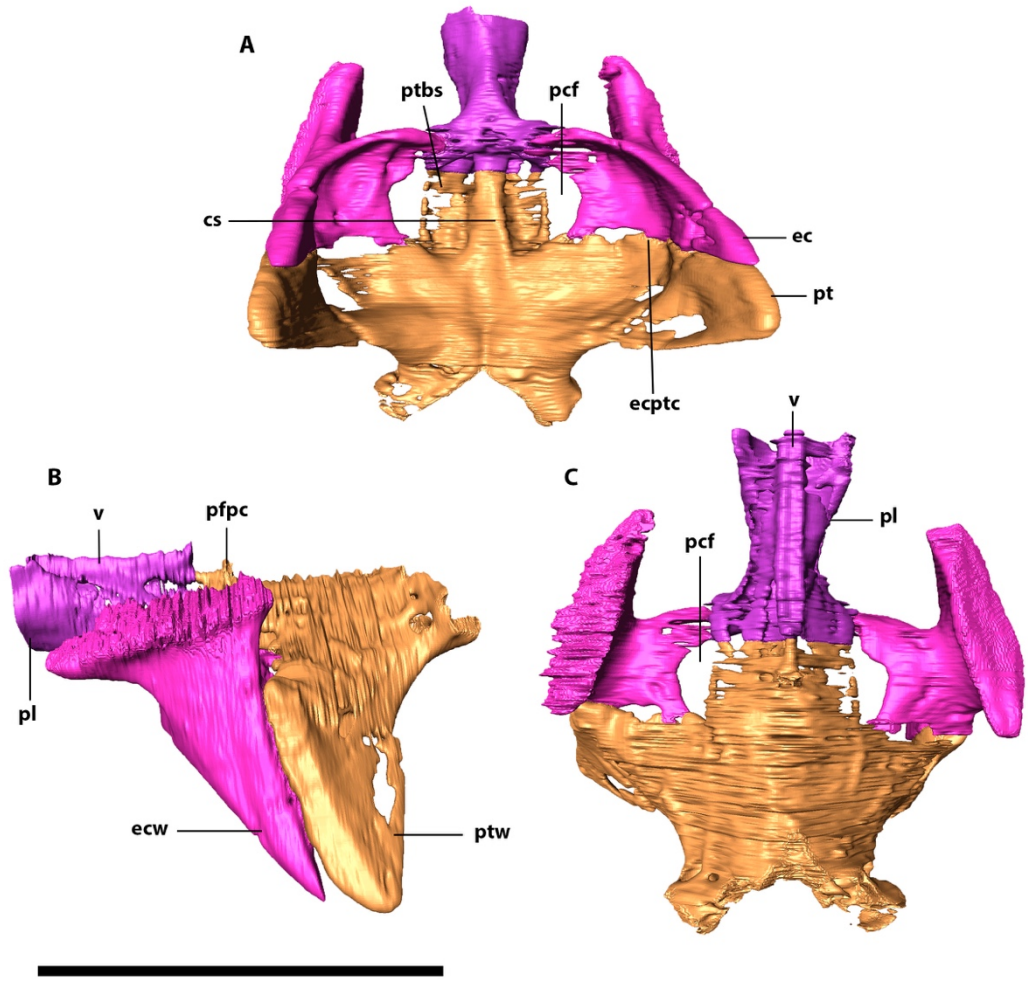


**Figure 36.** Digitally reconstructed bones from choanal region of LPRP 0697 in (A) ventral, (B) lateral, and (C) dorsa views. Cs, choanal septum; ec, ectopterygoid; ecptc, ectoperygoi-

pterygoid ventral concavity; ecw, ectopterygoid wing; pcf, parachoanal fenestra; pl, palatine; pt, pterygoid; ptbs, pterygoid bony sheets; ptw, pterygoid wing; v, vomer. Scale bar: 10 cm.

cross section, more mediolaterally constricted dorsally than ventrally. The vomer is separated from the dorsal surface of palatine by a gap that extends along its entire medial surface, forming a passage. This passage has dorsoventrally concave lateral borders which are continuous to the medial surface of maxilla. This canal corresponds to nasal cavity, whereas the vomer-palatine cavity can be related to the posterior portion of the air passage of the nasal cavity, where the air exits at the choanal region near to the anterior portion of the pterygoid. In addition, the choanal septum is continuous anteriorly in between the vomer and palatine.

### 4.2.3 Mandible

**Dentary:** The dentary is a heavily ornamented bone that comprises the anterolateral portion of mandible and forms the anterior dorsal and ventral border of the external mandibular fenestra. Its ornamentation is given by conspicuous irregular shaped ridges and grooves. In addition, there is a longitudinal, thin and deep sulcus that runs along the dorsolateral surface of the dentary, from the fourth dentary teeth to the dentary-surangular suture posteriorly (Fig. 37). Laterodorsally, the dentary contacts the surangular by a posteriorly convex suture at the level of the highest dorsoventrally extension of the external mandibular fenestrae, and ventrally it contacts the angular at the anteriormost portion of the ventral surface of the fenestra, by an anteroventral to posterodorsally inclined suture. The dentary is most lateromedially constricted at the level of the seventh dentary teeth. This constriction divides the bone into two portions: The mandibular symphysis and the mandibular rami (Fig. 38). The first is anteriorly positioned, rounded at the contour of the large fourth dentary teeth, becoming more constrict and slightly pointed at the anteriormost portion of the symphysis. CT scan shows that, at this point, the dorsal portion of the dentary is mediolaterally expanded, forming an expanded floor of the mandibular symphysis which is slightly ventrally concave. The mandibular symphysis is anterodorsally to posteroventrally inclined ventrally, forming a convex profile in lateral view; In the other hand, the mandibular rami are diverging lateroposteriorly from the symphysis, providing a “v” shape to the mandible, and also, the CT scan images show that this portion is considerably mediolaterally thinner than the anterior portion.

The dentary bears ten teeth (d1-d10) of different sizes but similar in shape. Due the articulation between the mandible and the skull, only the fourth mandibular tooth is exposed. This is the largest of the dentary teeth, which fits dorsally at the notch of the premaxilla-maxilla suture.

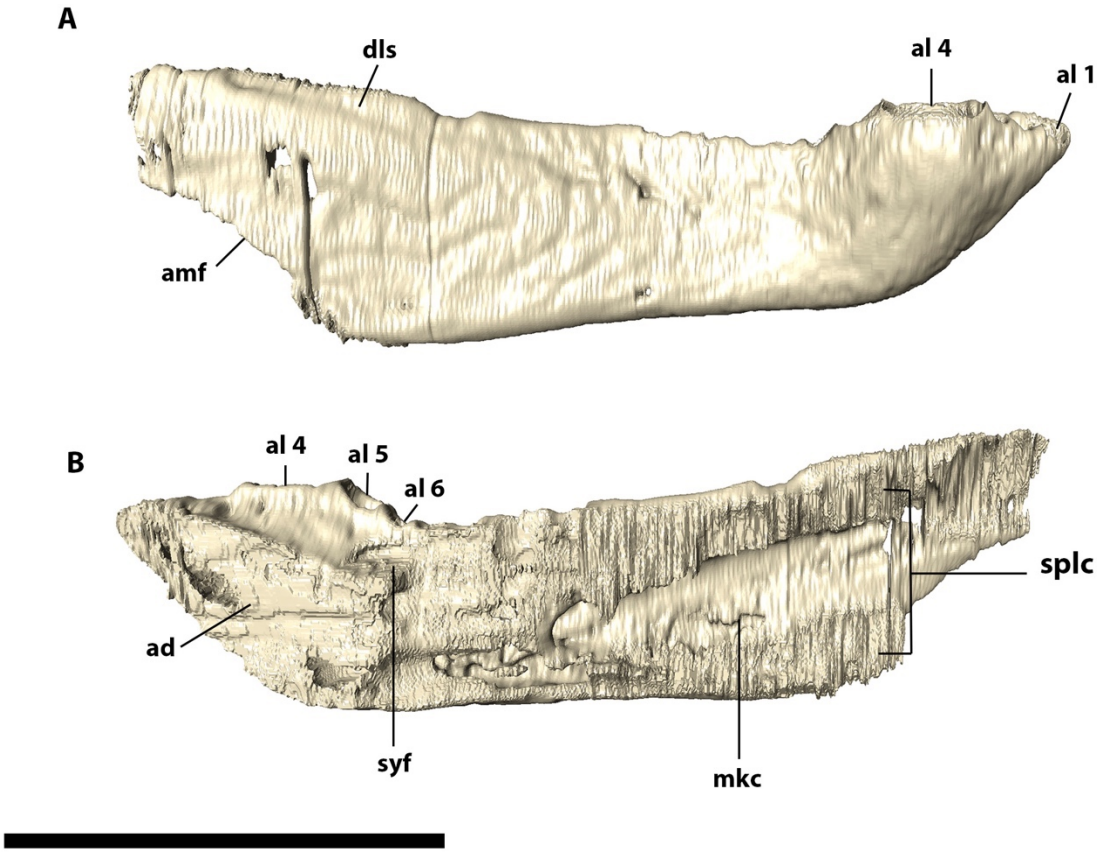


**Figure 37.** Digitally reconstructed right dentary in (A) lateral, and (B) medial views. Al, alveoli 1-6; ad, articulation area with left dentary; amf, anterior margin of mandibular fenestra; dls, dorsal longitudinal sulcus of dentary; mkc, Meckelian cavity; splc, splenial contact area; syf, symphyseal fossa. Scale bar: 10 cm.

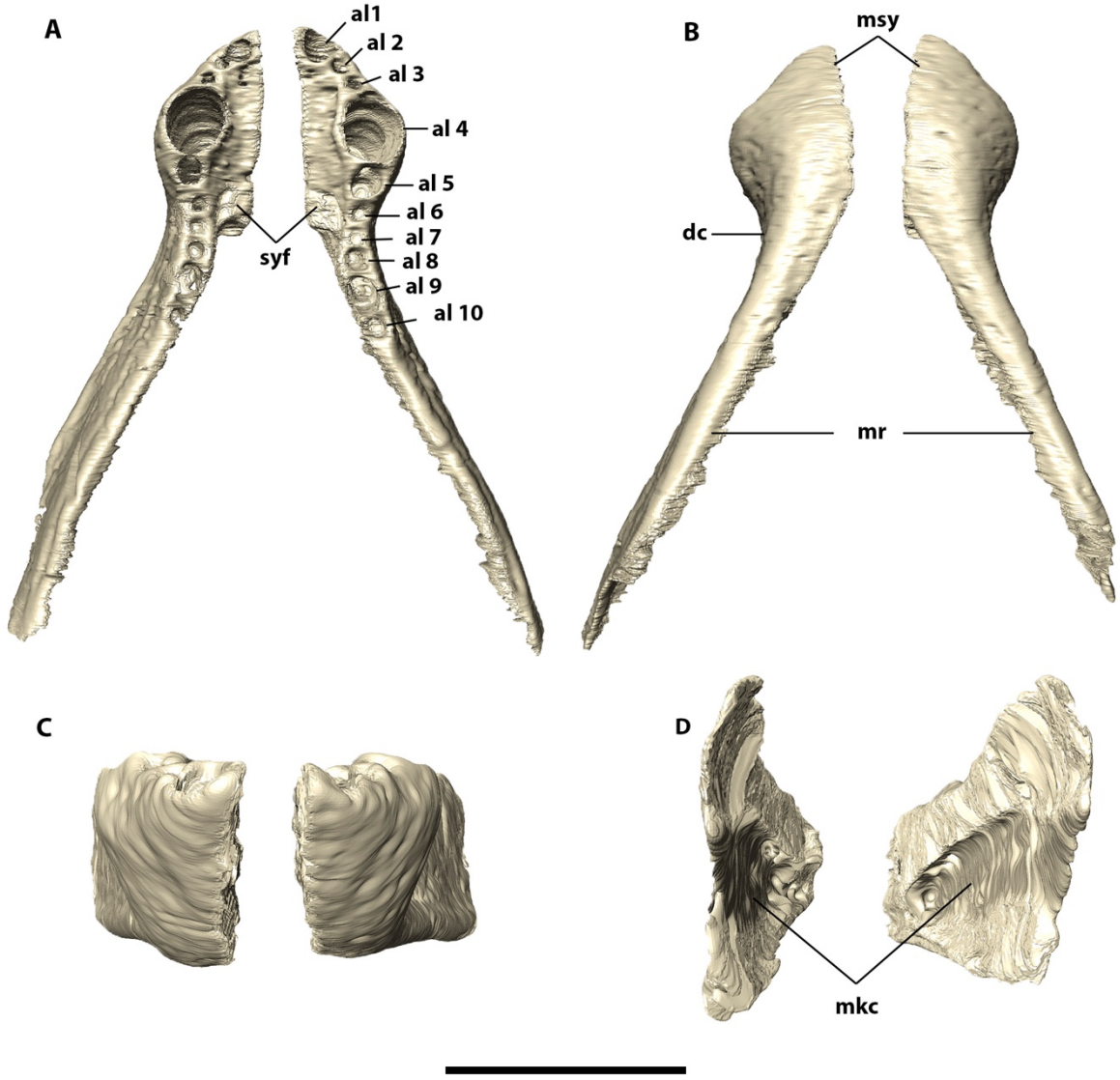


**Figure 38.** Digital reconstruction of left and right dentaries of LPRP 0697 in (A) dorsal, (B) ventral, (C) anterior, and (D) posterior views. Al, alveoli 1-10; dc, dentary mediolaterally constriction; mkc, Meckelian cavity; mr, mandibular rami; msy, mandibular symphysis; syf, symphyseal fossa. Scale bar: 10cm.

**Splenial:** The splenial is a lateromedially flattened bone positioned on the medial portion of the mandible, but also participating on its ventral surface of mandible. CT scan images reveal a thin, solid bone that forms the medial wall of the Meckelian cavity (Fig. 39). Its ventral surface is not rounded as that of the dentary, but is flattened instead, with a shallow splenial depressions medial to the splenial-dentary suture. The splenial ornamentation is restricted only to superficial small and inconspicuous dots and tiny grooves at the ventralmost surface, along with the ventral contact with the dentary. A marked ridge extends along the ventral surface of the symphysis, with a marked peg like protuberance at its posterior portion. The medial surface of splenial lacks ornamentation and posteriorly forms the anterior margin of the internal mandibular fenestrae, where the posterior portion of the bone is bifurcated by the fenestra concavity. More anteriorly at the medial surface, the *intramandibularis oralis* foramina are relatively small (approximately 10mm, vs. approximately 25 mm in *P. sera* LPRP 0020), elliptical and anteroposteriorly elongated.

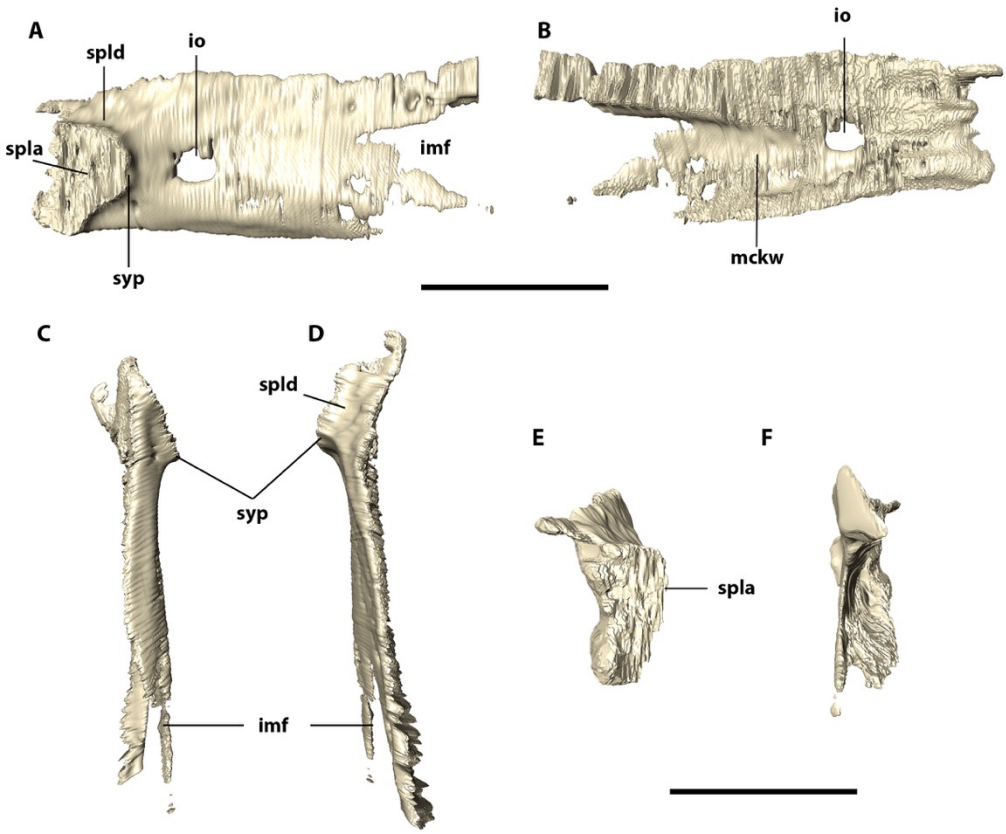


**Figure 39.** Digitally reconstructed right splenial of LPRP 0679 in (A) medial, (B) lateral, (C) ventral, (D) dorsal, (E) anterior and (F) posterior views. Imf, internal mandibular fenestra; io,

foramen *intramandibularis oralis*; mckw, Meckelian cavity medial wall; spla, splenial articulation area; spld, splenial depression; syp, mandibular symphysis peg projection. Scale bar: 5 cm.

**Surangular:** The surangular forms the posterodorsal portion of the mandible, contacting the dentary anteriorly via an interdigitated suture and the angular posteroventrally, forming the posterodorsal border of the external mandibular fenestrae. It is a solid bone, with only few foramina piercing its surface. It is mostly lateromedially flattened, but convex on its lateral surface. The surangular major axis is inclined, with the anterior portion of the bone more dorsally positioned than the posterior (Fig. 40). The ornamentation is restricted to its lateral surface, composed of by anteroposteriorly directed thin grooves anteriorly and of irregular and more inconspicuous grooves and ridges posteriorly. The posterior portion of the bone is flattened dorsoventrally and contacts the dorsal region of the angular via a sinuous suture. The medial surface of the bone composes the posterior border of the internal mandibular fenestra. CT scan images reveal that this portion of the surangular is dorsoventrally expanded and lateromedially thin, extending posteriorly between the angular and the articular. The anteroventral portion of such expanded surface is slightly pointed and extends anteriorly to the anterior tip of the articular bone. Also, this expanded surface extends posteriorly at the level of the anterior portion of the glenoid fossa of the articular, where it gradually becomes dorsoventrally constrict forming a posteriormost tip.

**Angular:** The angular is an elongated bone that composes mostly of the posterior half of mandible ventral surface, and forming the entire ventral border of the mandibular fenestrae. Anteriorly it contacts the posterior portion of the dentary-spelnial medial suture. This contact is better seen in CT scan images, which shows a thin anterior extension of the angular wedged between the posterior portion of the splenial and dentary (Fig. 41). This extension is dorsally concave and reaches the level of the tenth dentary tooth anteriorly. Posterodorsally, the contact of the angular with the surangular occurs via a sinuous suture extending from the posterior corner of the external mandibular fenestrae. At this contact, in lateral view, the dorsal margin of the angular is concave and more dorsally positioned, extending posteriorly to the posteriormost portion of the mandible, including the retroarticular process. At its posteriormost portion, the angular expands dorsoventrally, forming posteriorly convex posterolateral surface, which attaches to the articular.

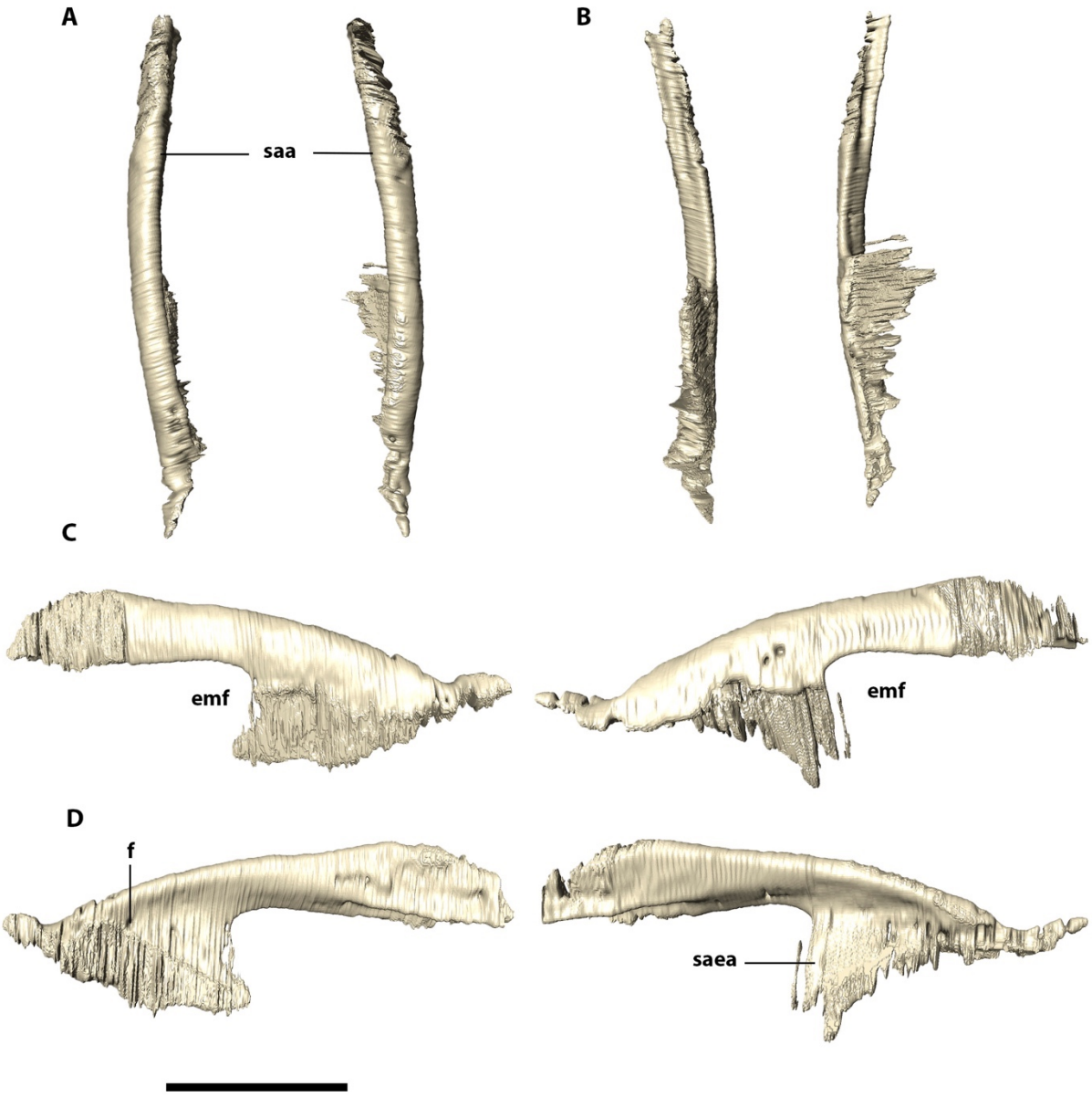


**Figure 40.** Digital reconstruction of left and right surangular of LPRP 0697 in (A) dorsal, (B) ventral, (C) lateral, and (D) medial views. Emf, external mandibular fenestra; f, foramen; saa, surangular major axis; saea, surangular expanded area. Scale bar: 5 cm

The entire lateral and ventral surfaces of the angular are ornamented, but more conspicuously at its lateral surface. Parallel to the posteroventral border of external mandibular fenestra, an elevated crest in the angular marks the insertion of *m. pterygoideous*.

The medial surface of the angular lacks ornamentations and is roughly cylindrical anteriorly. The dorsal margin of the internal mandibular fenestra possesses a subtriangular dorsal projection (torose margin, *sensu* Nascimento & Zaher, 2011), positioned slightly anterior to the center of the fenestra. Its profile gently slopes dorsally anteriorly and steeper posteriorly. In lateral view, the dorsal portion of this projection is rounded, but concave below that. At the middle portion of the angular, between its lateral and medial dorsal projections, there is the Meckelian canal, which corresponds to a longitudinal concavity extending along the bone, i.e. Meckelian groove, from the posterior contact with the articular to the anteriorly projected portion of the angular between the dentary and the splenial (Meckelian cavity).

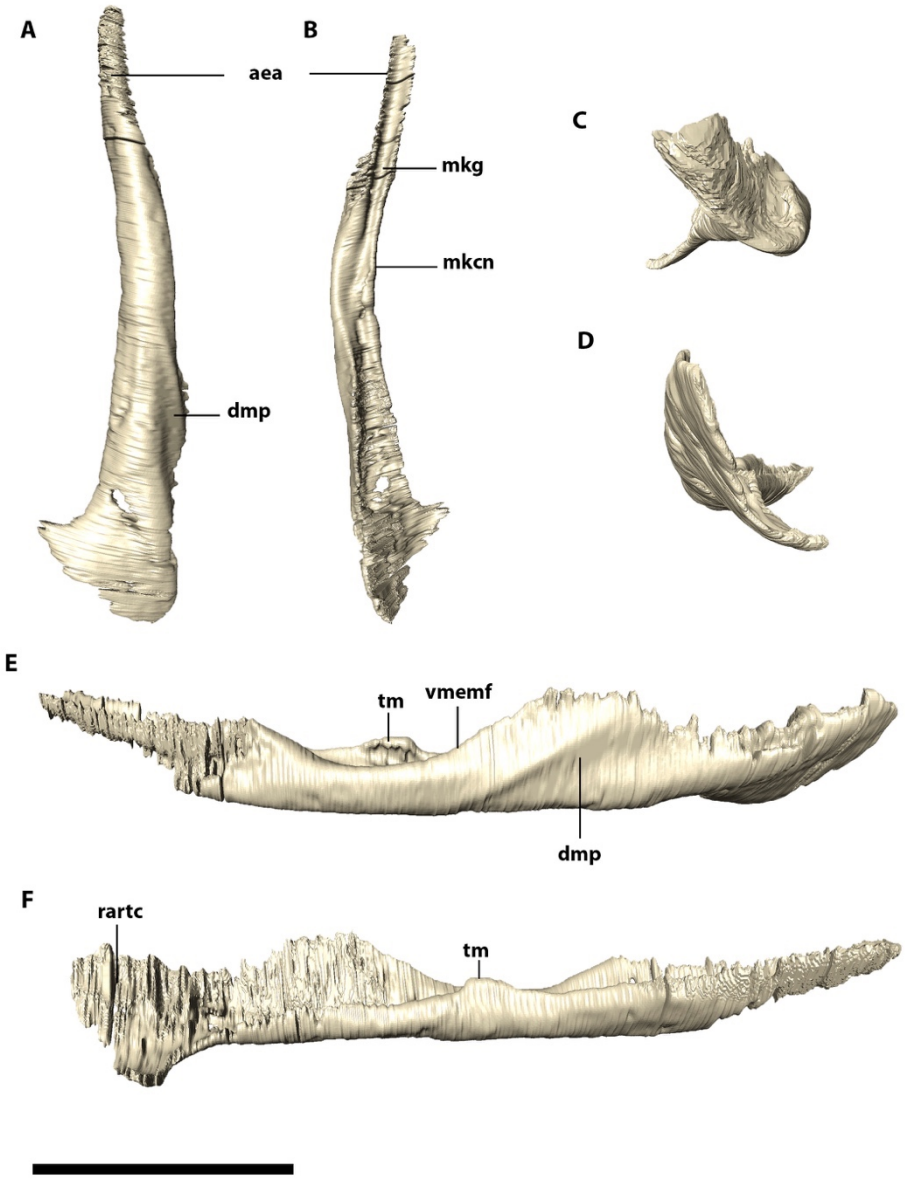


**Figure 41**. Digitally reconstructed left angular of LPRP 0697 in (A) ventral, (B) dorsal, (C) anterior, (D) posterior, (E) lateral, and (F) medial views. Aea, anterior expansion of angular;

dmp, depression for the insertion of *M. pterygoideous*; mkcn, Meckelian canal; mkg, Meckelian groove; rartc, retroarticular contact; tm, torose margin; vmemf, ventral margin of external mandibular fenestra. Scale bar: 10 cm

**Articular:** The articular contacts the angular anteroventrally and along the ventral margin, forming most of the retroarticular process posteriorly. The bone is subtriangular shaped, with an anteriorly projected portion and the posterior portion wider mediolaterally. The anterior projection of the articular is dorsoventrally thinner anteriorly and becoming deeper posteriorly. The dorsal and ventromedial surfaces of the articular are separated by a conspicuous ventral inflexion (Fig. 42). The dorsal portion of the articular is flattened anteriorly and inclined posterodorsally to anteroventrally. The glenoid fossa for articulation with the quadrate condyles is located right posterior to that flattened area, but it cannot be observed externally due to the quadrate articulation. However, the CT scan images reveal two depressions for the medial and lateral condyles of quadrate. The retroarticular process is lateromedially compressed with a rounded dorsolateral extension. The inflexion from the glenoid fossa to the posteromedial surface of the angular is well-marked, from a horizontal to a vertical surface (Fig. 45). The retroarticular expands posteriorly and is laterally covered by the angular. In this configuration, the retroarticular forms the acute posterior tip of the mandible. In lateral view, the posteroventral margin of the retroarticular process is rounded.

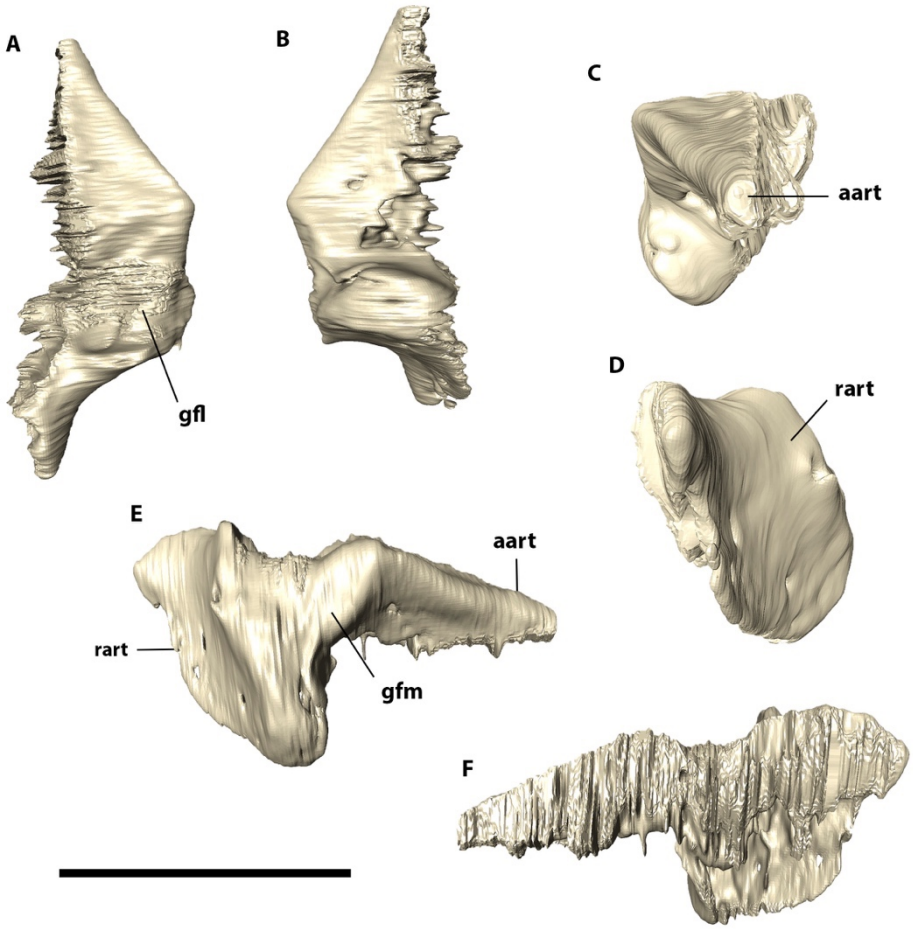


**Figure 42**. Digitally reconstructed left articular of LPRP 0697 in (A) dorsal, (B) ventral, (C) anterior, (D) posterior, (E) lateral, and (F) medial views. Aart- anterior projection of articular; gfl, glenoid fossa for articulation of lateral quadrate condyle; gfm, glenoid fossa for articulation of medial quadrate condyle; rart, retroarticular process. Scale bar: 5 cm.

4.2.4 Dentition

**Upper jaw dentition** (Fig. 43)**.** Four regularly spaced teeth are present in the premaxilla. The first tooth is positioned at the anteriormost portion of the bone, being incomplete in both premaxillae, so that its total length is uncertain. It is, however, conical in shape, posteriorly curved at the distal end, and has a serrated mesial carina, as seen in all premaxillary teeth. The second tooth is relatively thinner and elongated, preserved only on the left side. The third tooth is the largest, more rounded in cross section, whereas the fourth tooth is the smallest, arising from a more dorsally directed part of the premaxilla.

There are five maxillary teeth (m1-m5). The third tooth corresponds to a large caniniform, while the teeth anterior and posterior positioned in the tooth row are smaller. All teeth possess mediolaterally compressed crows in and more rounded roots in cross section, with serrated carinae in both mesial and distal margins. They are slightly curved backwards, except for the first tooth, which is less curved and more anteriorly positioned ventrally. The second maxillary tooth crown is broken on the right side and absent on left. The hypertrophied caniniform m3 reaches almost the level of the ventralmost extension of dentary in lateral view. The fourth and fifth teeth are subtriangular in lateral and medial views and are less distally curved (the fifth not recurved at all) and reduced in size.

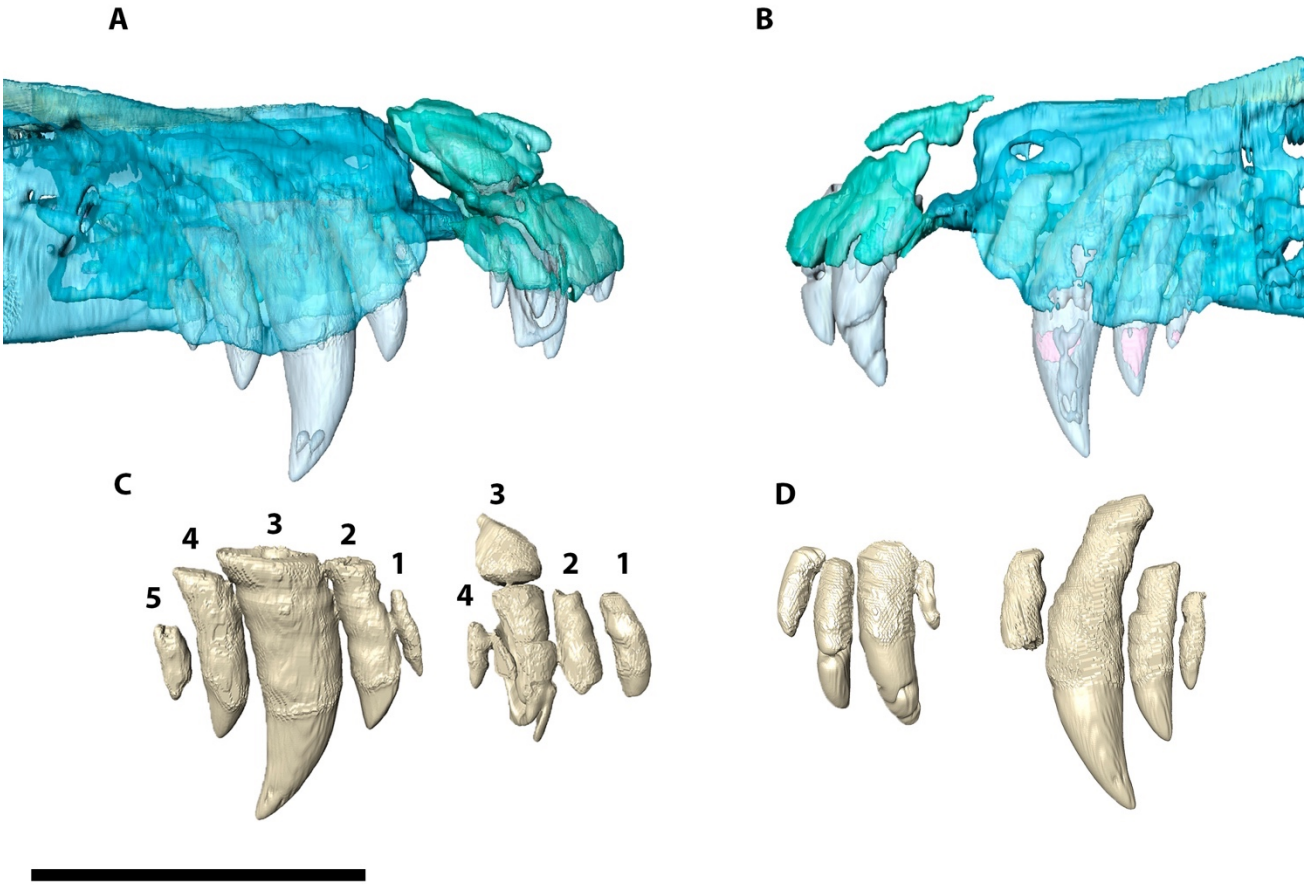


**Figure 43**. Upper jaw dentition of LPRP 0697. (A) and (B) shows right and left lateral views of semitransparent premaxillae and maxillae, (C) and (D) shows isolated teeth from each bone respectively. Numbers indicate the tooth. Scale bar: 10 cm.

**Lower jaw dentition** (Fig. 44)**.** The CT scan images allow the visualization of the entire lower tooth row composed by ten dentary teeth (D1-D10). D1 is procumbent, i.e. anteriorly inclined on its dorsal tip, but being more rounded in cross section and not as pointed as the remaining teeth. D4 is the largest dentary tooth being typicaly ziphodont (sensu Prasad and de Broin 2002), curved distally, with serrations on the anterior and posterior carinae. D9 is approximately of the same size as D1, but is less curved posteriorly. Also, the largest teeth present the largest roots, almost reaching the ventral surface of the dentary. The remaining teeth are smaller, subtriangular in shape, slightly mediolaterally compressed, with a more rounded cross section.

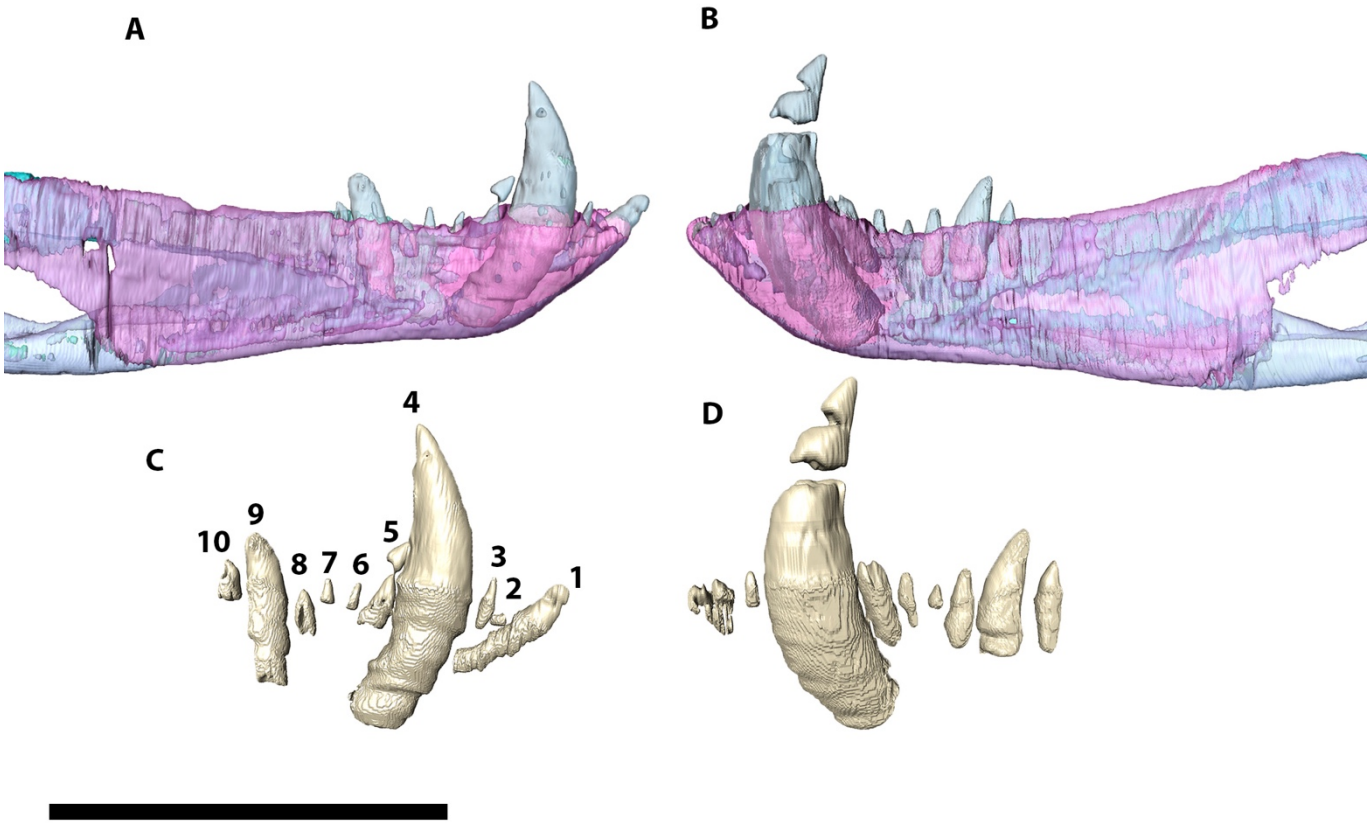


**Figure 44**. Lower jaw dentition of LPRP 0697. (A) and (B) shows right and left lateral views of semitransparent mandible, specifically the dentary in pink. (C) and (D) shows isolated teeth from each dentary. Numbers indicate the tooth. Scale bar: 10 cm.

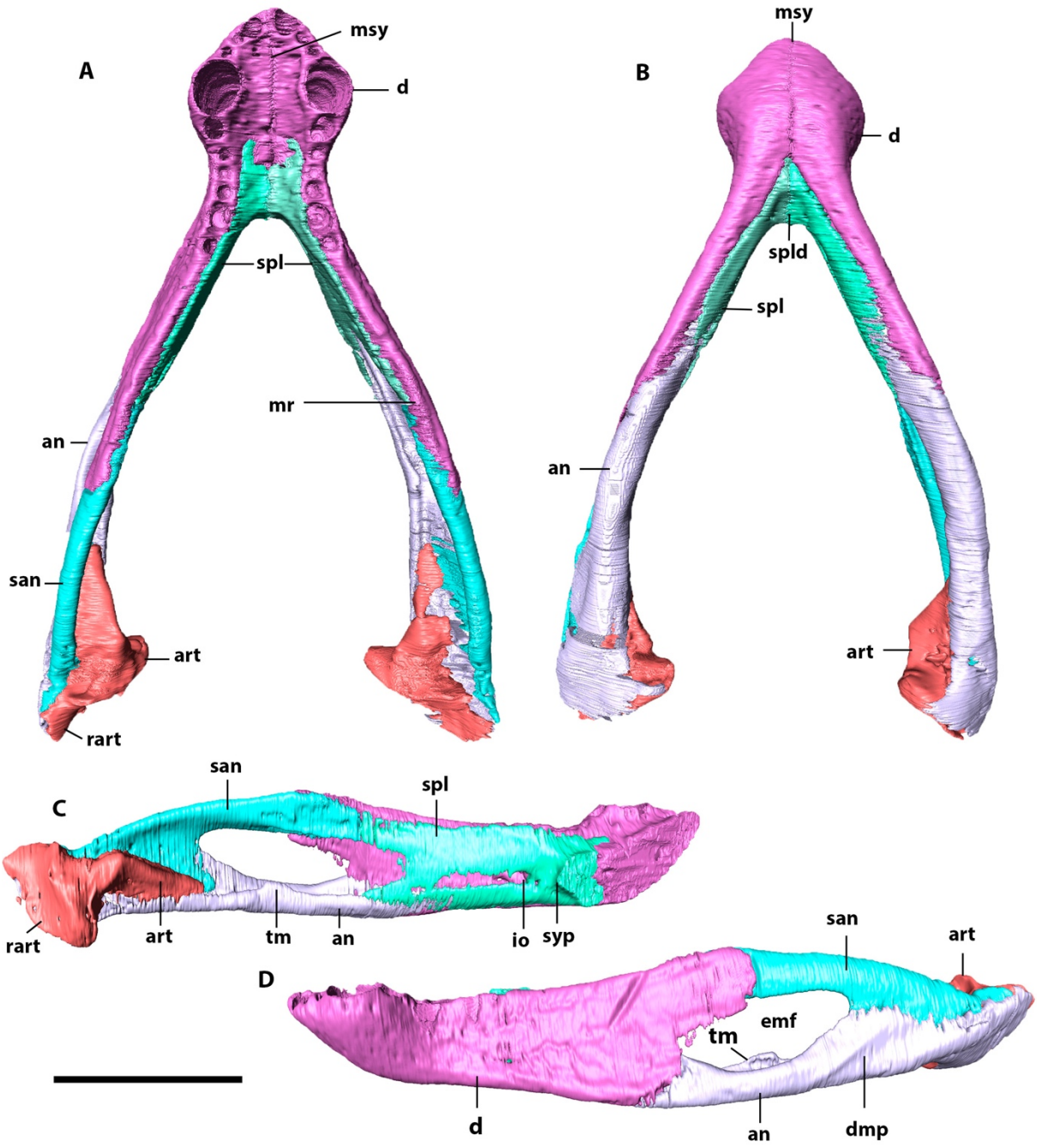


**Figure 45**. Digitally reconstructed and articulated mandible bones in (A) dorsal, (B) ventral view. Left mandible is reconstructed in (C) lateral, and (D) medial views. An, agular; art, articular; d, dentary; dmp, depression for the insertion of *M. pterygoideous*; emf, external mandibular fenestra; io, foramen *intramandibularis oralis*; mr, mandibular ramus; msy, mandibular symphysis; rart, retroarticular; san, surangular; spl, splenial; spld, splenial depression; syp, mandibular symphysis peg projection; tm, torose margin. Scale bar: 10 cm.

### *4.3 Phylogenetic position of LPRP 0697*

The scoring of LPRP 0697 in the original matrix of Godoy et al. (2014) resulted in three most parsimonious trees (mpts) with 131 steps each. In all trees, LPRP 0697 is recovered as the sister-taxon to all other Baurusuchinae (Fig. 46, node 8), and the other taxa have the same phylogenetic relationships as in the original study, except for the unresolved relationships of *A. sordidus*, *B. albertoi*, and *S. maxhechti*, which forms a polytomy on the strict consensus tree. The analysis of the expanded data matrix resulted in a single mpt with 143 steps, in which the new species is also recovered as the sister-taxon to all other Baurusuchinae (node 8). In addition, the polytomy including *S. maxhechti*, *B. albertoi*, and *A. sordidus* is resolved, with *B. albertoi* positioned as the sister taxon of the other *Baurusuchus* (node 11). That genus is, therefore, recovered as monophyletic in this analysis, with *S. maxhechti* as its sister-taxon (node 10), and *A. sordidus* (node 9) as sister of the *Baurusuchus* + *Stratiotosuchus* clade.

The modifications (addition of LPRP 0697, six characters, and changes in scoring) in the matrix of Godoy et al. (2014) resulted in disregarding characters 32:0 (dorsal extension of quadratojugal dorsal ramus in ventral view ending ventrally or at the same level of the dorsal tip of laterotemporal fenestra) and 47:1 (ridged ventral surface of the choanal septum) as synapomorphies of Baurusuchinae, because that specimen presents the opposite conditions. Yet, other synapomorphies were identified for the clade as a jugal with its antorbital portion deeper than the infraorbital portion (25:1), a relatively straight dorsal skull profile (67: 1), and a well-developed row of foramina dorsal to ectopterygoid-jugal suture (68:1). Likewise, Godoy et al. (2014) regarded character 30:1 (ventral border of quadratojugal forming a notch at the contact with the quadrate) as synapomorphic for Pissarrachampsinae, but this was not recovered in the present analysis, because this condition is also present in LPRP 0697 and as such regarded as a plesiomorphy of the Pissarrachampsinae + Baurusuchinae clade. Yet, three additional synapomorphies were found for Pissarrachampsinae: frontal longitudinal ridge extending anteriorly to the frontal mid-length (11.2), outer surface sculpture on dentary and slpenial (60:1), dorsal margin of mandibular fenestrae round (74.0). Finally, the *Baurusuchus* clade is supported by the lateralized orientation of the posterolateral surface of the squamosal prongs.

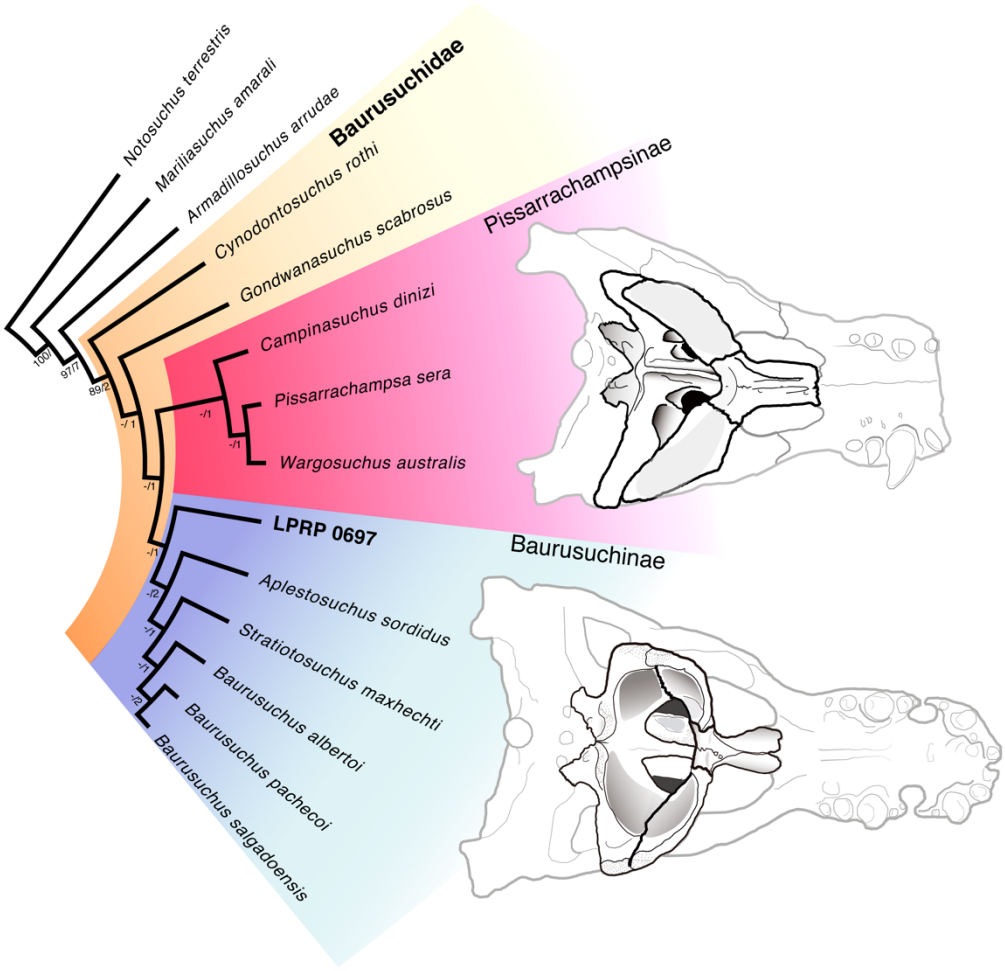


**Figure 46.** Phylogenetic position of the specimen LPRP 0697 within Baurusuchidae at the base of Baurusuchinae clade. The single most parsimonious tree (total length = 143 steps) recovered after an implicit enumeration analysis using the software TNT. The bootstrap (50% cut) and decay values are shown below the nodes. Silhouettes illustrates the 'choanal pattern' of Pissarrachampsinae and Baurusuchinae.

## 5. Discussion

### *5.1 Early baurusuchid evolution*

Among the morphological traits that Montefeltro et al. (2011) referred as diagnostic features for Baurusuchinae and Pissarrachampsinae, LPRP 0697 shares all the baurusuchine features except for the extensive medial contact of the prefrontals and the ridged ventral surface of choanal septum. On the other hand, LPRP 0697 bears two of the three Pissarrachampsinae

diagnostic features, lacking only the anterior longitudinal depression of the frontal. However, whereas the medial contact of the prefrontals occurs more anteriorly among pissarachampsines, it is more restricted and positioned at the anteroposterior mid-point in LPRP 0697.

During the first-hand revision of the above-mentioned diagnostic features, a not ridged ventral surface of the choanal septum was observed in the type material of *B. pachecoi*. That specimen bears a posterior small longitudinal groove in the area, whereas a completely smooth ventral surface of the choanal septum is present only in LPRP 0697. Nascimento (2014, page 180) on his unpublished master thesis defined the "*Baurusuchus* choana pattern", in which the ecopterygoid and pterygoid are ventrally concave and not pneumatized, and the "*Pissarrachampsa* choana pattern", in which the ectopterygoid bears parachoanal fossa, the pterygoid wings are pneumatized and have a straight ventral surface. For Nascimento (2014), baurusuchids with a "*Pissarrachampsa* choana pattern" usually also presents the anterior border of the supratemporal fenestrae up-lifted, two parasagittal sulci on the ventral surface of palatine, and the lateral "Eustaquian foramina" (here called pharyngeal tubes) larger than the central one (intertympanic foramen). The results of the comparative analysis conducted here are compatible with the patterns proposed by Nascimento (2014), and the following combination of traits were added as diagnostic of both groups; i.e. palatine inclined dorsolaterally from the ventral suture with its antimere, palatine-maxilla suture anteriorly convex, ectopterygoid and pterygoid wing ventrally projected bearing concavities on its ventral surface, and pterygoid anteroposteriorly expanded between the choanal septum and the contact with basisphenoid, for Baurusuchinae; flattened ventral surface of the palatine with a pair of conspicuous longitudinal row filled with foramina, straight palatine-maxilla suture, ectopterygoid and pterygoid posteriorly directed, ectopterygoid flattened, pterygoid forming parachoanal fenestrae, choanal septum lateromedially thin, and pterygoid anteroposteriorly short posterior to the choanal septum suffering a dorsal inflexion at the contact with basisphenoid, for Pissarrachampsinae.

It is clear that LPRP 0697 bears synapomorphic traits of both Baurusuchinae and Pissarrachampsinae, and that is somehow shown in our phylogenetic hypothesis by the placing of the specimen not much departed from that dichotomy along the baurusuchine branch. Accordingly, that evolutionary segment may be within a "zone of variability" sensu Bever et al. (2011), when plesiomorphies persist across speciation/cladogenetic events and may be read as homoplasies (e.g. pissarrachampsine traits of LPRP 0697) given the incompleteness of the fossil record. This seems more common during "early burst" radiation events, in cases when the increase in species richness occurred in the absence of significant changes in disparity, with

retention of similar body plans (Langer et al., 2019). Indeed, baurusuchids have restricted geographical and temporal ranges, consensually recorded only in the Adamantina and Bajo de la Carpa formations, in a Coniacian to Campanian inferred time span (Castro et al., 2018). Also, even though baurusuchids are one of the most diverse groups of Cretaceous Crocodyliformes, it is manifest that most species of the group have a very similar body plan. This indicates that the group radiated relatively fast during the early Late Cretaceous of South America, rapidly occupying a niche, i.e. medium to large sized terrestrial predators, previously unexplored by notosuchians, or even crocodilians in general.

### *5.2 LPRP 0697 as a new genus and species*

LPRP 0697 was recently mentioned in a revision of the osteoderm patterns in Baurusuchidae (Montefeltro, 2019) and in a Finite Element Analysis (FEA) of the skull, aimed to understand stress related to bite force (Montefeltro et al., 2019). Both works tentatively assigned the specimen to *B. pachecoi*, but did not back-up that inference with anatomical data. However, LPRP 0697 differs from *B. pachecoi*, as well as from all other baurusuchids, as discussed below.

LPRP 0697 differs from pissarrachampsines for the ventrally projected pterygoid and ectopterygoid with concavities on their ventral surfaces, the not flattened palatine, the dorsoventrally flattened choanal septum, and the lack a pneumatized pterygoid. Particularly, it differs from *W. australis* by lacking the frontal-nasal contact. LPRP 0697 also differs from *C. rothi* by presenting four maxillary teeth, palatines diverging laterodorsally from their ventromedial contact, and enlarged premaxillary teeth, and from *G. scabrosus* by lacking sulci on the outer surface of the teeth, presenting the palatines inclined and constricted posteriorly, the ventral tips of ectopterygoids ventrally directed and concave medioventrally, lacking a pair of foramina in the infratemporal ramus on the jugal, bearing the anterior corner of the external mandibular fenestra vertically aligned with the anteriormost portion of the orbit in lateral view, and prefrontals meeting medially, not allowing the nasal-frontal contact.

Among baurusuchines, LPRP 0697 differs from *S. maxhecthi* by the participation of the frontal on the supratemporal fossa and supraorbital fenestra, and from *B. salgadoensis* by the crested dorsal surface of its parietal, the crested lateral surface of the infra- and antorbital portions of the jugal extending anteriorly to the anterior lacrimal border, and the posterior portion of the squamosal prongs participating on the occipital wall. LPRP 0697 also differs

from *B. pachecoi* by presenting a curved alveolar margin of the maxilla (in lateral view) posterior to the enlarged caniniform tooth and posterior projections of the palatine aligned laterally ("T-shaped" palatine). LPRP 0697 differs from *A. sordidus* by the absence of the frontal longitudinal crest, by bearing a smooth choanal septum ventral surface, a posterior peg-like tuberosity on the mandibular symphysis, a depressed posterior portion of the nasal dorsal surface, and only one row of foramina on the lateral surface of the jugal. Finally, given the incompleteness of the skull of *B. albertoi* LPRP 0697 differs from the species by the absence of a well-developed crest running along the ventral portion of the quadrate until the basioccipital-otoccipital contact. That said, the uniqueness of LPRP 0697 relative to that taxon has to hinge on its postcranial anatomy that, unlike that of *B. albertoi*, includes a cervicodorsal gap between the nuchal and dorsal osteoderms shields (vs.continuous) and the absence of longitudinal keel in the nuchal osteoderms (vs. presence) (*sensu* Montefeltro, 2019). Those postcranial features were suggested as autapomorphic for LPRP 0697 in Montefeltro (2019) work, including even more evidence to the new species proposal of the specimen.

### *5.3 Comparative analysis of some LPRP 0697 traits*

The comparative analysis of LPRP 0697 and its positioning in the phylogenetic tree of baurusuchids revealed some interesting morphological patterns, which help understanding its taxonomic identity and relations. These are highlighted bellow.

**Nasal depression:** The nasal of LPRP 0697 has a depression on its posterior portion of its dorsal surface, where the lateral margins of the bone are clearly dorsally higher than its center. This is considered one of the diagnostics traits for Pissarrachampsinae (Montefeltro et al. 2011), but as it is also present in *G. scabrosus*, it most probably represents a baurusuchid plesiomorphy, retained in Pissarrachampsinae and modified along the baurusuchine lineage. A midline crest within the nasal depression has been considered a unique condition of *A. sordidus*, but is also observed in LPRP 0697, indicating that it either appeared convergently in those two species/specimens, or that it is a Baurusuchidae trait lost in the *Baurusuchus* + *Stratiotosuchus* clade.

**Medial contact of the prefrontals:** According to Montefeltro et al. (2011), the contact between the prefrontals occurs along most of their medial edges in Baurusuchinae, whereas in Pissarrachampsinae the approximation of the bones is restricted to their anterior portions. In

LPRP/USP 0697, this contact is restricted to the midpoint of medial margin of prefrontals, a condition very similar to that of *P. sera*. A prefrontal not contacting its antimere is observed in *G. scabrosus* and *C. dinizi*, so that the reduced contact in *P. sera* and LPRP/USP 0697 seems to be plesiomorphic relative to the full contact seen in other members of Baurusuchinae.

**Frontal dorsal crest:** Baurusuchids have a depressed frontal, with a sagittal crest along its dorsal surface. A sharp crest in seen in *A. sordidus*, *B. salgadoensis*, *C. dinizi*, *P. sera*, and *S. maxhechti*, whereas those of *B. salgadoensis* and *S. maxhechti* are smoother. The only species lacking such a crest is the Argentinean *W. australi*, which has a longitudinal dorsal depression instead. LPRP 0697 lacks both the crest and the depression, only bearing a few smooth longitudinal muscle scars in the area. The absence of a crest is considered an autapomorphic character for the new species (LPRP 0697).

**Jugal general morphology:** The jugal of LPRP 0697 presents a series of foramina along the ventral margin of the infraorbital ramus. This condition is highly variable among baurusuchids, with a similar condition observed in *B. salgadoensis*, *P. sera*, *A. sordidus*, and *C. dinizi* (CPP 1237). In *A. sordidus*, an extra row of foramina is present at the posterodorsal portion of the ramus, ventrally bordering the orbit, *S. machechti* lacks foramina altogether, and *G. scabrosus* has a paired row of foramina along the infratemporal ramus. The jugal of LPRP 0697 also presents a remarkable, autapomorphic condition, which is the infraorbital ridge (sensu Montefeltro et al., 2011) with a flattened dorsal surface and extending anteriorly until the anterior margin of the lacrimal.

**Quadrate and quadratojugal general morphology:** Two general constructions of the external auditory meatus at the anterodorsal process of the quadrate can be observed among baurusuchids (Montefeltro et al., 2016). Pissarrachampsines have a more anteroposteriorly expanded periotic fossa, so that the subtympanic foramina are more laterally exposed, whereas bauruschines have a more restricted periotic fossa, hence the foramina are internalized into a notch. Such conditions can be synapomorphic for each group and LPRP 0697 bears the baurusuchine condition, with only the anterior foramen exposed, as in *Baurusuchus* spp. and *S. maxhechti*. It is not possible to evaluate the presence of such small apertures in the badly preserved quadrate of *A. sordidus* and that bone is not preserved in *G. scabrosus*, *W. australis,* and *C. rothi*. The quadrate depression of LPRP 0697 is not restricted to the ventrolateral portion of that bone, but also expands anteriorly to include a posterior portion of the quadratojugal. This condition has been considered diagnostic of *P. sera*, but it is in fact homoplastic in the

phylogenetic scheme proposed here. Furthermore, the ventrolateral contact between the quadratojugal and quadrate is not continuous in LPRP 0697, forming a notch instead, due the projection of the posteroventral portion of the quadratojugal. This feature is also homoplastic, as it is seen also in *P. sera* and *C. dinizi*.

**Squamosal general morphology:** The squamosal prong of LPRP 0697 forms (in lateral view) a right angle in relation to the dorsal surface of the bone. Among baurusuchids, such condition is seen in *S. maxhechti* and in possible juvenile specimens of *P. sera* (LPRP 0049) and *C. dinizi* (CPP 1237), whereas a wider angulation is seen in the remaining species with this area preserved (i.e., *B. albertoi*, *B. salgadoensis*, *C. dinizi* , and *P. sera*). Clearly, such character is highly variable within Baurusuchidae, appearing in both of its main subgroups taxa, as well as in different specimens of *P. sera* and *C. dinizi*, the smaller forms of which present a higher angulation. Another interesting condition related to the squamosal prong is the convexity of its lateral margin, which can be better observed in posterior view. Such condition highlights the participation of the squamosal prong on the lateral portion of the occipital wall (e.g. lateral to the paroccipital process). In all the other baurusuchids with this area preserved, the lateral margin of the squamosal prong is almost straight in posterior view, so that the available evidence suggests that the condition of LPRP 0697 is autapomorphic.

**Parietal crest:** The parietal of LPRP 0697 presents a morphology shared only with *A. sordidus*: the interfenestral bar is crest shaped, lacking longitudinal grooves, and not expanded mediolaterally in its anterior end. Other baurusuchid present a mediolaterally wider dorsal surface (e.g., *B. salgadoensis*, *C. dinizi*, *P. sera*, and *S. maxhechti*), sometimes bearing a sagittal sulcus (e.g., *P. sera* and *S. maxhechti*). Again, the homoplastic crest-shaped interfenestral bar could have originated twice, in LPRP 0697 and *A. sordidus*, or can be a Baurusuchinae simapomorphy lost in the clade including *Baurusuchus* spp and *S. maxhechti*.

**Laterosphenoid:** Only Pinheiro et al. (2008) previously discussed the laterosphenoid anatomy of baurusuchids, mentioning possible contacts with the pterygoid and basisphenoid in a damaged skull they referred to *S. maxhechti*, but considered a Pissarrachampsinae indet. by Montefeltro et al. (2011). In living crocodilians, the laterosphenoid contacts the prootic posteriorly (Pinheiro, et al., 2008). The CT scan images only reveal that the laterosphenoid of LPRP 0697 meets its antimere ventrally, covering the anterior portion of the olfactory bulb, also meeting the prootic posteriorly.

**Basisphenoid and pharyngeal tubes**: The pharyngeal and pharyngotympanic tubes of LPRP 0697 are unique among Baurusuchinae because they are almost of the same size. The lateral tubes are elliptical and positioned slightly posteriorly to the medial tube, which is rounded. Among baurusuchids, such tubes are known for *C. dinizi*, *B. pachecoi*, *B. salgadoensis*, *P. sera*, and *S. maxhechti*, but the lateral tubes are not preserved in *B. pachecoi*. The medial pharyngeal tube is smaller than the lateral tubes in *C. dinizi*, the holotype of *P. sera*, and apparently also in *S. maxhechti* (which has only one pharyngotympanic preserved), whereas the opposite is seen in *B. salgadoensis*. In LPRP 0697 and one specimen of *P. sera* (LPRP 0049) all three pharyngeal tubes are almost of the same size. This distribution of this character is hard to fit in the phylogenetic scheme proposed here, and further data is required to fully evaluate its significance.

**Pterygoid morphology and patterns:** The mediolaterally broad and dorsoventrally flattened choanal septum of LPRP/USP 0697 is only shared with *B. pachecoi* among baurusuchids with this structure preserved. This condition is likely synapomorphic for Baurusuchinae, as *P. sera* and *C. dinizi* have a lateromedially thin choanal septum. Further, an abrupt dorsal inflexion of the pterygoid at the anterior contact with basisphenoid is seen in the species bearing a thin choanal septum, whereas the same area is anteroposteriorly expanded in Baurusuchinae. Although the choanal septum of *A. sordidus* is altered by taphonomic processes, which can lead to misinterpret its shape as crested, upon closely inspection it is possible to notice that its ventral surface was originally flattened, as typical of Baurusuchinae.

In taxa such as *P. sera* and *C. dinizi*, the sheets of bone that extend lateral to the choanal septum are confluent with the medial margin of the pterygoid wing, forming an inclined surface. These form the posteromedial border of two parachoanal fossae, one ventrally displaced, right above the dorsomedial suture between the ectopterygoid and the pterygoid, with a semicircular shape, and the other closer to the choanal septum and more anteroposteriorly elongated (Montefeltro et al., 2011). As for LPRP 0697, these sheets of bone are parallel to one another, displaced in relation to the choanal septum, and do not form a continuous surface with the pterygoid. Unfortunately, these elements are not preserved in any other Baurusuchinae, but based on the general shape of the pterygoid, we infer that bony sheets originating from the base of the pterygoid wings (forming also pterygoid fenestration) may be synapomorphic for Pissarrachampsinae, and bony sheets not extending from the pterygoid wings (pterygoid lacking fenestration) may be synapomorphic for Baurusuchinae. The CT scan of LPRP 0697 actually shows that those bony sheets converge dorsally from its ventral surface (the parallel

surfaces to the choanal septum), forming a triangular surface when observed in anterior or posterior views. Anteriorly, the sheets contact the posterior portion of palatino-vomer structure.

**Ectopterygoid concavity:** The ectopterygoid is ventrally pointed and presents a concave ventral surface in LPRP 0697, which is a common condition observed in *B. pachecoi*, *B. salgadoensis*, and *A. sordidus*. This can be considered synapomorphic for Baurusuchinae, given that ectopterygoid of Pissarrachampsinae is posteriorly oriented, with a more rounded ventral tip and a mediolaterally flattened ventromedial surface.

**Palatine morphology and vomer contact:** The palatine of LPRP/USP 0697 presents some similarities with those of *A. sordidus*, *B. pachecoi*, and *B. salgadoensis*, For example, the medial contact of the pair forms an inclined ventral surface and the suture with the maxilla is anteriorly convex, a synapomorphy for Baurusuchinae. On the other hand, the palatine of Pissarrachampsinae (e.g. *C. dinizi* and *P. sera*) is ventrally flattened, bearing a conspicuous parasagittal sulcus filled with a row of small foramina along the entire anteroposterior longitudinal ventral surface, and the anterior suture with the maxilla is straight (synapomoprhic characters for Pissarrachampsinae). Also, most baurusuchids present the posterior ramus of the palatine (which contacts to the ectopterygoid) diverging posterolaterally. Again, this ramus is strictly laterally oriented, forming a "T-shaped" palatine, only in LPRP 0697 and *A. sordidus*, suggesting that the condition appeared independently in both forms, or that it appeared in Baurusuchinae and was lost at the *S. maxhechti* + *Baurusuchus* clade. Finally, the CT scan images of LPRP 0697 show the dorsal surface of the palatine forming a roughly triangular airway in cross section. This triangular structure corresponds to the vomer, which is apparently fused with the palatine, as no suture could be observed. This assumption is based on the inferred anatomical position of the bone, based on the extant species *Caiman latirostris* (Reynolds, 1897. Fig. 45).

## 6. Conclusions

- LPRP 0697 can be diagnosed as a new species based on the following four autapomorphic character: posterior portion of the nasal depressed and bearing a crest; jugal infraorbital ridge extending until the anterior margin of the lacrimal; no crest or depression on dorsal surface of frontal; lateral convexity of the squamosal prong leading to a more conspicuous participation on the lateral portion of the occipital wall.
- The phylogentic study consistently places LPRP 0697 as a Baurusuchinae sister to all other members of the group, and recovers *Baurusuchus* as a monophyletic taxon.
- The CT scan images provided the first tridimensional digital atlas for the Baurusuchidae skull, allowing a better interpretation of the morphology of various bones, as well as the first descriptions for the vomer and laterosphenoid of the group.
- Morphological patterns and synapomorphies of Baurusuchinae and Pissarrachampsinae were revised and updated, allowing the suggestion of a "Zone of Variability" in the early radiation of Baurusuchidae, as partially recognized by the homoplastic features of LPRP 0697.

## 7. Literature cited

Araújo Júnior, H. I., & da Silva Marinho, T. (2013). Taphonomy of a Baurusuchus (Crocodyliformes, Baurusuchidae) from the Adamantina Formation (Upper Cretaceous, Bauru Basin), Brazil: implications for preservational modes, time resolution and paleoecology. *Journal of South American Earth Sciences*, *47*, 90-99.

Arruda, J.T., Carvalho, I.S. & Vasconcellos, F.M.V. (2004) Baurusuquídeos da Bacia Bauru (Cretáceo Superior, Brasil). *Anuário do Instituto de Geociências*, UFRJ, Rio de Janeiro. 27: 64-74.

Avilla, L.S., Fernandes, R. & Ramos, D.F. (2004) Bit marks on a crocodylomorph from the Upper Cretaceous of Brazil: evidence of social behavior? *Journal of Vertebrate Paleontology*. 24: 971-973.

Batezelli, A., Saad, A. R., de Jesús Perinotto, J. A., Fulfaro, V. J., & Etchebehere, M. L. D. C. (2003). Análise Estratigráfica aplicada à Formação Araçatuba (Grupo Bauru-Ks) no centro-oeste do Estado de São Paulo. *Geociências*, 22(1), 5-32.

Benton, M.J. and Clark, J.M. (1988) Archosaur phylogeny and the relationships of the Crocodylia. In: M. J. Benton (Ed.), The phylogeny and classification of the tetrapods, v.1: Amphibians, reptiles, birds. Systematics Assoc., Clarendon Press, Oxford, pp. 295-338. (Spec. v. nº 35 A)

Bever, G. S., Gauthier, J. A., & Wagner, G. P. (2011). Finding the frame shift: digit loss, developmental variability, and the origin of the avian hand. *Evolution & development*, *13*(3), 269-279.

Bremer, K. R. (1994). Branch support and tree stability. *Cladistics*, *10*(3), 295-304.

Busbey, A. B. (1995). The structural consequences of skull flattening in crocodilians. *Functional morphology in vertebrate paleontology*, 173-192.

Bronzati, M., Rauhut, O. W., Bittencourt, J. S., & Langer, M. C. (2017). Endocast of the Late Triassic (Carnian) dinosaur *Saturnalia tupiniquim*: implications for the evolution of brain tissue in Sauropodomorpha. *Scientific Reports*, *7*(1), 1-7.

Bronzati, M., Müller, R. T., & Langer, M. C. (2019). Skull remains of the dinosaur *Saturnalia tupiniquim* (Late Triassic, Brazil): With comments on the early evolution of sauropodomorph feeding behaviour. *PloS one*, *14*(9).

Bronzati, M., Langer, M.C. & Oliver W. M. Rauhut (2018) Braincase anatomy of the early sauropodomorph *Saturnalia tupiniquim* (Late Triassic, Brazil), Journal of Vertebrate Paleontology, 38:5,DOI: 10.1080/02724634.2018.1559173

Buffetaut, E. (1989) A new ziphodont mesosuchian crocodile from the Eocene of Algeria. *Palaeontographica*, v. 208, pp. 1-10.

Campos, D.A, Suarez, J.M., Riff, D. & Kellner, A.W.A. (2001) Short note on a new Baurusuchidae (Crocodyliformes, Metasuchia) from the Upper Cretaceous of Brazil. *Boletim do Museu Nacional*, Nova Série, Geologia. 57: 1-7.

Candeiro, C.R.A., Abranches, C.T., Abrantes, E.A., Avilla, L.S., Martins, V.C., Moreira, A.L., Torres, S.R. & Bergqvist, L.P. (2004) Dinosaur remains from western São Paulo State, Brazil (Bauru Basin, Adamantina Formation, Upper Cretaceous). *Journal of South American Earth Sciences*. 18: 1-10.

Candeiro, C.R.A & Martinelli, A.G. (2006) A review of paleogeographical and chronostratigraphical distribution of mesoeucrocodylian species from the upper Cretaceous beds from the Bauru (Brazil) and Neuquén (Argentina) groups, Southern South America. *Journal of South American Earth Sciences*. 22: 116-129.

Carvalho, I.S. & Bertini, R.J. (1999) *Mariliasuchus amarali*: um novo Crocodylomorpha (Notosuchia) do Cretáceo da Bacia Bauru, Brasil. *Geologia Colombiana*. 24: 83-105.

Carvalho, I.S., Campo, A.C.A. & Nobre, P.H. (2005) *Baurusuchus salgadoensis*, a new Crocodylomorpha from the Bauru Basin (Cretaceous), Brazil. *Gondwana Research*. 8(1): 11-30.

Carvalho, I. S., Teixeira, V. P., Ferraz, M. L., Ribeiro, L. C. B., Martinelli, A. G., Neto, F. M., Sertich, J.J.W., Cunha, G.C., Cunha, I.C. & Ferraz, P. F. (2011). Campinasuchus dinizi gen. et sp. nov., a new Late Cretaceous baurusuchid (Crocodyliformes) from the Bauru Basin, Brazil. *Zootaxa*, *2871*(2011): 19-42.

Castro, M. C., Goin, F. J., Ortiz-Jaureguizar, E., Vieytes, E. C., Tsukui, K., Ramezani, J., Batezeli, A., Marsola, J.C.A & Langer, M. C. (2018). A Late Cretaceous mammal from Brazil and the first radioisotopic age for the Bauru Group. *Royal Society open science*, *5*(5), 180482.

Colbert, E.H. (1946) Sebecus, representative of a peculiar suborder of fossil crocodilian from Patagonia. *Bulletin of American Museum of Natural History*. 87: 217-270.

Chapelle, K. E., & Choiniere, J. N. (2018). A revised cranial description of *Massospondylus carinatus* Owen (Dinosauria: Sauropodomorpha) based on computed tomographic scans and a review of cranial characters for basal Sauropodomorpha. *PeerJ*, 6:e4224.

Chapelle, K. E., Barrett, P. M., Botha, J., & Choiniere, J. N. (2019). *Ngwevu intloko*: a new early sauropodomorph dinosaur from the Lower Jurassic Elliot Formation of South Africa and comments on cranial ontogeny in Massospondylus carinatus. *PeerJ*, *7*, e7240.

Clark, J.M. (1997) Patterns of evolution in Mesozoic Crocodyliformes. In: Fraser, N.C. and Sues, H.D. (Eds.), In the shadow of the dinosaurs. Early Mesozoic tetrapods. Cambridge Univ. Press, pp. 84-97.

Cuesta, E., Vidal, D., Ortega, F., & Sanz, J. L. (2018). The cranial osteology of *Concavenator corcovatus* (Theropoda; Carcharodontosauria) from the Lower Cretaceous of Spain. *Cretaceous Research*, *91*, 176-194.

Dias-Brito, D., Musachio, E.A., Castro, J.C., Maranhão, M.S.S., Suárez, J.M. & Rodrigues, R. (2001) Grupo Bauru: uma unidade continental do Cretáceo no Brasil- concepções baseadas em dados micropaleontológicos, isótopos e estratigráficos. *Revue Paléobiologique*, Géneve. 20(1): 245-304.

Dufeau, D. L., & Witmer, L. M. (2015). Ontogeny of the middle-ear air-sinus system in *Alligator mississippiensis* (Archosauria: Crocodylia). *PLoS One*, *10*(9).

Fernandes, L.A. (1998) Estratigrafia e evolução geológica da parte oriental da Bacia Bauru (Ks, Brasil). Tese de Doutorado. Universidade de São Paulo.

Fernandes, L. A., & Coimbra, A. M. (1996). Bacia Bauru (Cretaceo superior, Brasil). *Anais da Academia Brasileira de Ciencias*, 68( 2 ): 195-205.

Fonseca, P. H. M., Martinelli, A. G., da Silva Marinho, T., Ribeiro, L. C. B., Schultz, C. L., & Soares, M. B. (2020). Morphology of the endocranial cavities of *Campinasuchus dinizi* (Crocodyliformes: Baurusuchidae) from the Upper Cretaceous of Brazil. *Geobios*.

Franzosa, J., & Rowe, T. (2005). Cranial endocast of the Cretaceous theropod dinosaur *Acrocanthosaurus atokensis*. *Journal of Vertebrate Paleontology*, *25*(4), 859-864.

Gasparini, Z. (1972) Los Sebecosuchia (Crocodilia) del territorio argentino. Consideraciones sobre su ‘‘status’’ taxonomico. *Ameghiniana*. 9: 23-34.

Gasparini, Z. (1981) Los Crocodylia fosiles de la Argentina. *Ameghiniana*. 18: 177-205.

Gasparini, Z.B., Chiappe, L.M. and Fernandez, M. (1991) A new Senonian peirosaurid (Crocodylomorpha) from Argentina and a sinopsis of the South American Cretaceous crocodilians. *J. Vertebrate Paleontol*., v. 11, pp. 316-333.

Gasparini, Z.B., Fernandez, M. and Powell, J. (1993) New tertiary Sebecosuchians (Crocodylomorpha) from South America: phylogenetic implications. *Historical Biol.,* v. 7, pp. 1-19.

Godoy, P.L., Montefeltro, F.C., Norell, M.A. & Langer, M.C. (2014) An additional baurusuchid from the Cretaceous of Brazil with evidence of interspecific predation among Crocodyliforms. PLoS ONE. 9:e97138.

Godoy, P.L., Bronzati, M., Eltink, E., Júlio, C.D.A., Cidade, G.M., Langer, M.C. & Montefeltro, F.C. (2016) Postcranial anatomy of *Pissarrachampsa sera* (Crocodyliformes, Baurusuchudae) from the Late Cretaceous of Brazil: insights on lifestyle and phylogenetic significance. *PeerJ*. 4: e2075.

Goloboff, P. A., Farris, J. S., & Nixon, K. C. (2008). TNT, a free program for phylogenetic analysis. *Cladistics*, *24*(5), 774-786.

Holliday, C. M., & Witmer, L. M. (2007). Archosaur adductor chamber evolution: integration of musculoskeletal and topological criteria in jaw muscle homology. *Journal of Morphology*, *268*(6), 457-484.

Hughes, M., Gerber, S., & Wills, M. A. (2013). Clades reach highest morphological disparity early in their evolution. *Proceedings of the National Academy of Sciences*, *110*(34), 13875-13879.

Iordansky, N. N. (1973). The skull of the Crocodilia. *Biology of the Reptilia*, *4*, 201-262.

Iori, F. V., Marinho, T. S., Carvalho, I. S., & Campos, A. C. D. A. (2013). Taxonomic reappraisal of the sphagesaurid crocodyliform *Sphagesaurus montealtensis* from the late Cretaceous Adamantina Formation of São Paulo State, Brazil. *Zootaxa*, 3686(2): 183-200.

Kellner, A. W., Pinheiro, A. E., & Campos, D. A. (2014). A new sebecid from the Paleogene of Brazil and the crocodyliform radiation after the K–Pg boundary. *PLoS One*, *9*(1).

Kley, N.J., Sertich, J.J.W., Turner, A.H., Krause, D.W., O'Connor, P.M. & Georgi, J.A. (2010) Craniofacial morphology of *Simosuchus clarki* (Crocodyliformes: Notosuchia) from the Late Cretaceous of Madagascar. *Journal of Vertebrate Paleontology*, 30, 13-98,

Langer, M. C., McPhee, B. W., Marsola, J. C. A., Roberto-da-Silva, L., & Cabreira, S. F. (2019). Anatomy of the dinosaur *Pampadromaeus barberenai* (Saurischia—Sauropodomorpha) from the Late Triassic Santa Maria Formation of southern Brazil. *PloS one*, 14(2).

Langston, W. (1965) Fossil crocodilians from Colombia and the Cenozoic history of the Crocodilia in South America. University of California Publications in Geological Science, 52: 1-157.

Larsson, H.C.E. & Sues, H.D. (2007) Cranial osteology and phylogenetic relationships of *Hamadasuchus rebouli* (Crocodyliformes: Mesoeucrocodylia) from the Cretaceous of Morocco. *Zoological Journal of the Linnean Society*, 149: 533-567.

Leardi, J. M., Pol, D., Novas, F. E., & Suárez Riglos, M. (2015). The postcranial anatomy of *Yacarerani boliviensis* and the phylogenetic significance of the notosuchian postcranial skeleton. *Journal of Vertebrate Paleontology*, 35(6): e995187.

Leardi, J. M., Pol, D., & Gasparini, Z. (2018). New Patagonian baurusuchids (Crocodylomorpha; Notosuchia) from the Bajo de la Carpa Formation (Upper Cretaceous;

Neuquén, Argentina): new evidences of the early sebecosuchian diversification in Gondwana. *Comptes Rendus Palevol*, *17*(8), 504-521.

Martinelli, A.G. & Pais, D.F. (2008) A new baurusuchid crocodyliform (Archosauria) from the Late Cretaceous of Patagonia (Argentina). *Systematic Palaeontology*. 7: 371-381.

Marinho, T.S., Iori, F. V., de Souza Carvalho, I., & de Vasconcellos, F. M. (2013). *Gondwanasuchus scabrosus* gen. et sp. nov., a new terrestrial predatory crocodyliform (Mesoeucrocodylia: Baurusuchidae) from the Late Cretaceous Bauru Basin of Brazil. *Cretaceous Research*, 44: 104-111.

Montefeltro, F.C., Larsson, H.C.E. & Langer, M.C. (2011) A new baurusuchid (Crocodyliformes, Mesoeucrocodylia) from the late Cretaceous of Brazil and phylogeny of Baurusuchidae . PLoS ONE. 6: e21916.

Montefeltro, F. C., Larsson, H. C., de França, M. A., & Langer, M. C. (2013). A new neosuchian with Asian affinities from the Jurassic of northeastern Brazil. *Naturwissenschaften*, 100(9): 835-841.

Montefeltro, F. C. (2019). The osteoderms of baurusuchid crocodyliforms (Mesoeucrocodylia, Notosuchia). *Journal of Vertebrate Paleontology*, *39*(2), e1594242.

Montefeltro, F. C., Lautenschlager, S., Godoy, P. L., Ferreira, G. S., & Butler, R. J. (2019). A unique predator in a unique ecosystem: modelling the apex predator from the Late Cretaceous crocodyliform-dominated fauna in Brazil. *BioRxiv*, 843334.

Nascimento, P. M., & Zaher, H. (2010). A new species of *Baurusuchus* (Crocodyliformes, Mesoeucrocodylia) from the Upper Cretaceous of Brazil, with the first complete postcranial skeleton described for the family Baurusuchidae. *Papéis avulsos de Zoologia*, 50(21): 323-361.

Nascimento, P. M., & Zaher, H. (2011). The skull of the Upper Cretaceous baurusuchid crocodile Baurusuchus albertoi Nascimento & Zaher 2010, and its phylogenetic affinities. *Zoological Journal of the Linnean Society*, *163*(suppl_1), S116-S131.

Nascimento, P. M. (2014). *Revisão da família Baurusuchidae e seu posicionamento filogenético dentro do clado Mesoeucrocodylia* (Doctoral dissertation, Universidade de São Paulo).

Oliveira, C.E.M., Santucci, R.M. Andrade, M.B., Fulfaro, V.J., José, A.F. & Benton, M.J. (2011) Crocodylomorph eggs and eggshells from the Adamantina Formation (Bauru Group), Upper Cretaceous of Brazil. *Paleontology*. 54(2): 309-321.

Ortega, F., Buscalioni, A.D. and Gasparini, Z. (1996) Reinterpretation and new denomination of Atacisaurus crassiproratus (Middle Eocene, Issel, France) as cf. Iberosuchus (Crocodylomorpha, Metasuchia). *Geobios*, v. 29, pp. 353-364.

O'connor, P. M., Sertich, J. J., Stevens, N. J., Roberts, E. M., Gottfried, M. D., Hieronymus, T. L. & Temba, J. (2010). The evolution of mammal-like crocodyliforms in the Cretaceous Period of Gondwana. *Nature*, 466(7307), 748.

Ősi, A., Pereda-Suberbiola, X., & Földes, T. (2014). Partial skull and endocranial cast of the ankylosaurian dinosaur *Hungarosaurus* from the Late Cretaceous of Hungary: implications for locomotion. *Palaeontologia Electronica*, Article-nr.

Paula e Silva, F. (2003) Geologia e subsuperfície e hidrostatigrafia do Grupo Bauru no Estado de São Paulo. Tese de Doutorado. Instituto de Geociências e Ciências Exatas, Universidade Estadual Paulista (UNESP), Rio Claro, 166p.

Paula e Silva, F., Kiang, C. H., & CAETANO-CHANG, M. R. (2003). Perfis de referência do Grupo Bauru (K) no estado de São Paulo. *Geociências*, 22(1): 127-139.

Paula e Silva, F., Chang, H.K. & Caetano-Chang, M.R. (2005) Estratigrafia de subsuperfície do Grupo Bauru (K) no Estado de São Paulo. *Revista Brasileira de Geociências*. 35(1): 77-88.

Pinheiro A.E.P., Pereira, P.V.L.G.C., de Souza, R.G., Brum, A.S., Lopes, R.T., Machado, A.S., Bergqvist, L.P. & Simbras, F.M. (2018) Reassessment of the enigmatic crocodyliform"*Goniopholis" paulistanus* Roxo, 1936: Historical approach, systematic, and description by new materials. *PLoS ONE* 13(8): e0199984

Pol, D. 2005. Postcranial remains of *Notosuchus terrestris* (Archosauria: Crocodyliformes) from the upper Cretaceous of Patagonia, Argentina. *Ameghiniana,* 42(1):1-17.

Pol, D & Powell, J.E. (2011) A new sebecid mesoeucrocodylian from the Rio Loro Formation (Paleocene) of north-western Argentina. *Zoological Journal of the Linnean Society*. 163: S7-S36.

Pol, D., Leardi, J. M., Lecuona, A., & Krause, M. (2012). Postcranial anatomy of *Sebecus icaeorhinus* (Crocodyliformes, Sebecidae) from the Eocene of Patagonia. *Journal of Vertebrate Paleontology*, 32(2): 328-354.

Pol, D., Nascimento, P. M., Carvalho, A. B., Riccomini, C., Pires-Domingues, R. A., & Zaher, H. (2014). A new notosuchian from the Late Cretaceous of Brazil and the phylogeny of advanced notosuchians. *PLoS One*, *9*(4).

Prasad, G.V.R. & Lapparent de Broin F. (2002) Late Cretaceous crocodile remains from Naskal (India): comparisons and biogeographic affinities. *Annales de Paléontologie.* 82: 19-71.

Price, L.I. (1945) A new reptile from the Cretaceous of Brazil. *Notas Preliminares e Estudos. Divisão de Geologia e Mineralogia*. Ministério da Agricultura. Rio de Janeiro, Brasil. 25: 1-8.

Raselli, I. (2018). Comparative cranial morphology of the Late Cretaceous protostegid sea turtle Desmatochelys lowii. *PeerJ*, 6:e5964.

Reynolds, S.H. (1897) The vertebrate skeleton. Cambridge (UK): Cambridge University Press. P. 535.

Riff, D.A & Kellner A.W.A. (2001) On the dentition of *Baurusuchus pachecoi* Price (Crocodyliformes, Metasuchia) from the Upper Cretaceous of Brazil. *Boletim do Museu Nacional*. 59: 1-15.

Rogers, S. W. (1998). Exploring dinosaur neuropaleobiology: computed tomography scanning and analysis of an *Allosaurus* fragilis endocast. *Neuron*, *21*(4), 673-679.

Santucci, R. M., & Bertini, R. J. (2001). Paleogeographical and biochronological distributions of the Bauru Group titanosaurids (Saurischia, Sauropoda) Upper Cretaceous of southeastern Brazil. *Rev Bras Geoci*, *31*, 307-314.

Sereno, P.C. & Larsson, H.C.E. (2009) Cretaceous Crocodyliforms from the Sahara. *Zookeys*, 28: 1-143.

Sertich, J.J.W. & O'Connor, P.M. (2014) A new Crocodyliform from the middle Cretaceous Galula Formation, southwestern Tanzania. *Journal of Vertebrate Paleontology* 34(3): 576-596.

Soares, P.C., Landim, P.M.B., Fulfaro, V.J. & Neto, A.F.S. (1980) Ensaio de caracterização estratigráfica do Cretáceo no Estado de São Paulo: Grupo Bauru. *Revista Brasileira de Geociências*. 10: 177-185.

Smith, J. B., & Dodson, P. (2003). A proposal for a standard terminology of anatomical notation and orientation in fossil vertebrate dentitions. *Journal of Vertebrate paleontology*, *23*(1), 1-12.

Turner, A. (2004) Crocodyliform biogeography during the Cretaceous: biogeographical analysis. *Proceedings of the Royal Society of London* B, 271:2003-2009

Turner A. & Calvo, J.O. (2005) A new sebecosuchian crocodyliform from the Late Cretaceous of Patagonia. *Journal of Vertebrate Paleontology*. 25: 87–98.

Turner, A. & Sertich, J.J.W. (2010) Phylogenetic history of *Simosuchus clarki* (Crocodyliformes: Notosuchia) from the Late Cretaceous of Madagascar. *Journal of Vertebrate Paleontology*. Memoir 10: 177-236.

Tykoshi, R.S., Rowe, T.B., Ketcham, R.A. and Colbert, M.W. (2002) *Calsoyasuchus valliceps*, a new crocodyliform from the Early Jurassic Kayenta Formation of Arizona. J. Vertebrate Paleontol., v. 22, pp. 593-611.

Vasconcellos, F.M. (2009) Análise morfofuncional e hábitos de vida de *Baurusuchus* (Crocodyliformes, Mesoeucrocodylia) na Bacia Bauru. Tese de Doutorado. Universidade Federal do Rio de Janeiro.

Walker AD (1968) *Protosuchus*, *Proterochampsa*, and the origin of phytosaurs and crocodiles. Geological Magazine 105: 1–14.

Wilson, J.A., Malkani, M.S., Gingerich, P.D. 2001. New crocodyliform (Reptilia, Mesoeucrocodylia) from the Upper Cretaceous Pab Formation of Vitakri, Balochistan

(Pakistan). Contributions from the Museum of Paleontology of the University of Michigan. 30 (12): 321-336.

Witmer L.M., Ridgely R.C., Dufeau D.L., Semones M.C. (2008) Using CT to Peer into the Past: 3D Visualization of the Brain and Ear Regions of Birds, Crocodiles, and Nonavian Dinosaurs. In: Endo H., Frey R. (eds) Anatomical Imaging. Springer, Tokyo

**APPENDIX 1**

**List of taxa**

**Outgroup:**

*Armadillosuchus arrudae*, Marinho & Carvalho (2009)

*Mariliasuchus amarali*, Carvalho & Bertini (1999)

*Notosuchus terrestris*, Woodward (1896)

**Ingroup**

*Aplestosuchus sordidus*, Godoy et al. (2014)

*Baurusuchus albertoi*, Nascimento & Zaher (2010)

*Baurusuchus pachecoi*, Price (1945)

*Baurusuchus salgadoensis*, Carvalho et al. (2005)

*Campinasuchus dinizi*, Carvalho et al. (2011)

*Cynodontosuchus rothi*, Woodward (1896)

*Gondwanasuchus scabrosus*, Marinho et al. (2013)

*Pissarrachampsa sera*, Montefeltro et al. (2011)

*Stratiotosuchus maxhechti*, Campos et al. (2001)

*Wargosuchus australis*, Martinelli & Pais (2008)

## APPENDIX 2

### List of skull characters (modified from Godoy et al., 2014)

**Character 1**. Premaxilla-maxilla suture: in the lateral surface of rostrum (0), internalized in a notch for the reception of lower caniniform (1) [1].

**Character 2**. Nasals: paired (0), partially or complete fused (1) [2].

**Character 3**. Posterior portion of the nasal elevated above the dorsal surface of the maxillae, forming a sagittal bar: absent (0); present posteriorly (1) [3].

**Character 4**. Dorsal surface of the nasal, posterior portion: rounded or flat (0), bearing a rugose broad depression (1) [3].

**Character 5**. Prefrontal-prefrontal medial contact (+): absent (with a broad contact between nasal and frontal) (0) medial margin of prefrontals anteriorly convergent, almost touching each other (with a tiny contact between nasal and frontal) or touching each other anteriorly (1), contact present along mostly of the dorsal medial edge (2) [3].

**Character 6**. Dorsal surfaces of prefrontal and anterior palpebral: continuous (0), central portion of the dorsal surfaces elevated, with a marked groove between them (1) [3].

**Character 7**. Frontal: participates in the supratemporal fenestrae (0), excluded from the supratemporal fenestrae (1) [1].

**Character 8**. Width of frontals between orbits relative to mid-length width across nasals: narrow (similar to width of nasals) (0); or broad (about twice the width of nasals) (1) [1].

**Character 9**. Dorsal surface of frontal, posterior to orbits: flat or slightly concave (0), or markedly concave transversely (1) [4].

**Character 10**. Midline longitudinal depression on anterior portion of frontal: absent (0), present (1) [3].

**Character 11**. Frontal longitudinal ridge (+): absent (0), restricted to the posterior portion (1), extending anteriorly to the frontal mid-length (2) [1].

**Character 12**. Support for the anterior palpebral bone (+): marked depression on prefrontal (0), marked depression on prefrontal and lacrimal forming an incipient lateral projection (1), marked depression on prefrontal and lacrimal forming a great lateral projection for the support of anterior palpebral (2) [5].

**Character 13**. Supratemporal rims raised and hypertrophied: restricted to the median edge of the external supratemporal fenestra (0), extended to anterior edge of the external supratemporal fenestrae (1) [3].

**Character 14**. Postorbital-quadratojugal contact in lateral view: restricted (0), broad contact between quadratojugal and the posterior portion of the postorbital descending flange (1) [1].

**Character 15**. Lateral surface of the postorbital descending flange: flat (0), or concave (1) [3].

**Character 16**. Postorbital-squamosal suture at the skull table in lateral view: straight line (0), squamosal anteriorly convex (1) [6].

**Character 17**. Lateral margins of squamosal and postorbital in dorsal view: parallel (0), or diverging posteriorly (1) [7].

**Character 18**. Squamosal prong horizontal extention: well developed (0), restricted (1) [1].

**Character 19**. Squamosal lateral descending flange: obliquely directed (0), vertically directed with lateral edge medially concave and laterally convex (1), vertically directed and medially convex and laterally concave (2) [1].

**Character 20**. Lacrimal duct external aperture: ventral to the corner formed by the dorsal and lateral lacrimal surfaces (0), at the corner (1) [3].

**Character 21**. Contact between anterior and posterior palpebrals: only laterally, forming a supraorbital foramen (0), along the whole length without a foramen (1) [1].

**Character 22**. Alveolar margin of maxilla in lateral view (+): almost straight (0), arched only anteriorly, below the enlarged caniniform tooth (1), arched along the entire alveolar margin (2) [1].

**Character 23**. Maxillary palatal sagittal contact: smooth (0), bearing a longitudinal series of foramina (1) [3].

**Character 24**. Dorsoventral depth of the jugal orbital portion in relation to infratemporal portion: almost the same depth (0), orbital portion twice the depth of the infratemporal portion (1) [1].

**Character 25**. Dorsoventral depth of the jugal antorbital portion in relation to infraorbital portion: equal or lower (0), antorbital portion deeper than infraorbital portion (1) [8].

**Character 26**. Posterior portion of the jugal orbital border: without a notch (0), with a marked ventral notch (1) [3].

**Character 27**. Jugal outer surface (+): confluent along the entire length (0), infratemporal portion of jugal laterally displaced but not reaching the level of orbital anterior edge (1), infratemporal portion of jugal laterally displaced and reaching the level of orbital anterior edge (2) [8].

**Character 28**. Jugal infratemporal bar: laterally flat (0), rod-shaped (1) [1].

**Character 29**. Anterodorsal ramus of quadrate in ventral view: developed, forming more than 50% of the lateral edge of the internal supratemporal fenestra (0), restricted, forming less than 50% of the lateral edge of the internal supratemporal fenestra (1) [3].

**Character 30**. Ventral border of quadratojugal and quadrate (lateral view): continuous (0), quadratojugal ventrally displaced, forming a notch between the bones (1) [3].

**Character 31** Anterior margin of distal portion of body of the quadrate: at a right angle to the anterolateral portion of the bone (0), slopes gently towards the anterolateral portion of the bone (1) [3].

**Character 32**. Quadratojugal dorsal ramus in medial view ( +): ending ventrally, or at the same level, of the dorsal tip of laterotemporal fenestra (0), overcoming the dorsal tip of laterotemporal fenestra but not reaching the supratemporal fossa (1), overcoming the dorsal tip of laterotemporal fenestra and reaching the supratemporal fossa (2) [3].

**Character 33**. Quadrate lateral depression: absent (0), present with the major axis dorsoventrally oriented (1), present with the major axis anteroposteriorly oriented and with quadratojugalquadrate suture within the depression (2) [3].

**Character 34**. Quadrate fenestrae: visible in lateral view (0), internalized in otic notch (1) [3].

**Character 35**. Lateral quadrate condyle: almost as anteroposteriorly wide as the medial condyle (0), or lateral quadrate condyle hemispherical (1) [3].

**Character 36**. Muscle scar in the medial quadrate surface (ridge 'A'): curved or almost straight (0), sigmoidal (1) [3].

**Character 37**. Supraoccipital dorsal exposure: along the midline portion of posterior region of skull table (0), restricted to a thin surface attached to the posteriormost portion of parietal and squamosal (1) [3].

**Character 38**. Posterior region of the auditory fossa: posteriorly open (0), bound posteriorly by a posteroventrolateral extension of the squamosal and exoccipital (1) [9].

**Character 39**. Foramen incisivum: absent or small (0), enlarged (1) [3].

**Character 40**. Anterior extension of palatine: passes the anterior margin of the suborbital fenestrae (0), does not reach the level of the anterior margin of suborbital fenestrae (1) [8].

**Character 41**. Ventral face of palatine bar: flat and wide (0), flat and wide posteriorly and ventral surface restricted and dorsal portion cylindrical posteriorly (1) ventral surface restricted and dorsal portion cylindrical through (2) [3].

**Character 42**. Medial palatal contact: smooth (0), rugose (1) [3].

**Character 43**. Dorso-lateral surface of the ectopterygoid near jugal contact: smooth (0), bearing a series of irregularly-sized foramina (1) [3].

**Character 44**. Row of foramina flanking the medial contact of the palatines: absent (0), present (1) [3].

**Character 45**. Ridge on the ectopterygoid-jugal articulation: absent (0), present and continuous with the ventral ridge of the infratemporal portion of jugal (1), present but separated from the ventral ridge of the infratemporal portion of jugal by a notch at the posterior margin of the articulation (2) [3].

**Character 46**. Ectopterygoid-jugal contact behind pterygoid wing in ventral view: rounded (0), medially angled (1) [3].

**Character 47**. Ventral surface of the choanal septum: smooth (0), ridged (1) [3].

**Character 48**. Major surface of the pterygoid wing: lateroventrally oriented (0), ventrally oriented (1) [3].

**Character 49**. Posttemporal fenestrae: present (0), absent (1) [3].

**Character 50**. Pterygoid parachoanal fenestra and depressions: absent (0), present (1) [10].

**Character 51**. Basisphenoid ventral surface: continuous to surrounding bones (0), ventrally displaced and separated from the neighboring elements by a posteroventral step formed by a groove that separated the bone from the main occipital plane (forming a postchoanal pterygoidbasisphenoid tuberosity) (1) [3].

**Character 52**. Anterior wall of the lateral Eustachian foramina: present, separating each foramen from the sulcus (0), absent, foramina open into the sulcus (1) [3].

**Character 53**. Lateral Eustachian foramen: smaller than medial one (0), as large or larger than medial one (1) [3].

**Character 54**. Paired ridges located medially on the ventral surface of the basisphenoid (originating at the anterior margins of lateral Eustachian foramina): absent (0), present and anteroventrally convergent (1), present and sub-parallel (2) [11].

**Character 55**. Tooth mesial and distal carinae: smooth (0), bearing a pebbled surface (1), serrated (2) [12].

**Character 56**. Premaxillary teeth: four (0), three (1) [13].

**Character 57**. Enlarged premaxillary teeth: present (0), absent (1) [1].

**Character 58**. Last premaxillary tooth hypertrophy: present (0), absent (1) [1].

**Character 59**. Maxillary teeth: five or more (0), only four (1) [13].

**Character 60**. Mandibular outer surface sculpture: present on dentary (0), present on dentary and splenial (1) [3].

**Character 61**. Foramen intramandibularis oralis: small or absent (0), big and slot-like (1) [7].

**Character 62**. Mandibular symphysis, orientation of anterior part: horizontal or slightly dorsally directed (0), forming an angle of approximately 45 degrees to the main axis of the jaw (1) [9].

**Character 63**. Peg at the posterior surface of the mandibular symphysis formed by a ridged splenial suture: absent (0), present (1) [14].

**Character 64**. Posteroventral symphyseal depressions: absent (0), present (1) [3].

**Character 65**. M. pterygoideous posterior insertion: reaching the anterior external mandibular fenestra (0), in a marked depression on surangular-angular lateral surface on posterior edge of external mandibular fenestra (1) [1].

**Character 66**. Ridged border of the angular medial face: overcomes the anterior edge of the mandibular fenestra (0), does not overcome the anterior edge of mandibular fenestra (1) [3].

**Character 67**. Dorsal skull profile: rostrum downturned with the inflexion point just in front of the orbit (0), profile relatively straight (1).

**Character 68**. Row of foramina dorsal to ectopterygoid-jugal suture: absent or small foramina (0), foramina well developed (1).

**Character 69**. Longitudinal sulcus in intertemporal bar: absent (0), present (1).

**Character 70**. Maxillae-palatines suture: round (0), transverse (1).

**Character 71**. Cylindrical portion of the palatine bar: same wideness through (0), constricted in the posterior portion (1).

**Character 72**. Maxillae-palatines transverse suture: without posterior process of maxillae (0) with a V-shaped posterior process of maxillae at midline (1).

**Character 73**. Series of foramina in angular below the mandibular fenestrae: absent (0), present (1).

**Character 74**. Dorsal margin of Mandibular fenestrae: round (0), straight line formed by surangular (1).

**Character 75. (NEW) Convexity of dorsal surface of squamosal participating on the skull roof in lateral view**: straight (0), slightly convex (1), markedly convex (2).

**Character 76. (NEW) Angulation of squamosal prongs:** forming a right angle, 90º (0), higher angulation, more than 90º (1)

**Character 77. (NEW) Position of posterolateral surface of squamosal prongs in occipital view:** more lateralized (0), posterolaterally oriented participating of the occipital wall (1).

**Character 78. (NEW) Marked jugal crest/ridge along the ventral border of the orbit, anterior to the infratemporal bar:** absent (0), present (1).

**Character 79. (NEW) Dorsal surface of parietals between the supratemporal fenestrae:** enlarged mediolaterally anteriorly and posteriorly, forming two subtriangular surfaces, providing an hourglass shape (0), forming only a posterior slightly mediolaterally expanded subtriangular surface with a conspicuous thin crest extending anteriorly until the contact with frontal (1).

**Character 80. (NEW) Shape of choanal septum ventrally:** mediolaterally constricted/ thin (0), dorsoventrally flattened (1)

## APPENDIX 3

### List of modified characters codification

Below are listed the taxa and characters states modified from Godoy et al. (2014). The modifications were based on the firsthand analysis of the species material.

*Aplestosuchus sordidus*

Char. 18:1 → 0

Char. 50: 1 → 0

*Baurusuchus pachecoi*

Char. 20: ? → 0

Char. 24: 1 → 0

*Gondwanasuchus scabrosus*

Char. 6: ? → 0

Char. 8: 0 → ?

Char. 10: 1 → ?

Char. 15: ? → 1

Char. 28: ? → 1

Char. 30: 0 → ?

Char. 43: ? → 0

Char. 73: 0 → ?

## APPENDIX 4

### Data Matrices

Character states (0-2) are given for outgroup and ingroup taxa. Brackets enclose variable conditions; question marks indicate missing data; and dashes indicate inapplicable characters. The nexus file will be available for publication.

### Scoring of LPRP 0697 for the 74 characters in the dataset of Godoy et al. (2014)

1 1 0 1 1 1 0 0 1 0 0 2
0 1 1 1 1 1 1 0 0 2 ? 1
1 0 2 1 1 1 1 [1&2] 2 1 ? 0
1 1 0 1 2 1 0 ? 1 0 0 0
? 0 1 ? 1 1 2 0 0 1 0 0
0 1 1 1 1 ? 1 1 0 1 1 1
1 1

### Modified dataset of Godoy et al. (2014)

80 characters x 14 taxa

*Armadillosuchus arrudae*

0 1 0 0 0 0 0 0 0 0 0 1
0 0 1 1 1 1 0 0 - ? ? ?
? 0 1 1 1 0 0 1 0 0 1 1
0 0 ? ? ? ? ? ? ? ? ? ?
? ? 0 1 1 0 1 ? ? ? ? ?
? ? 1 ? ? ? 0 ? 0 ? ? ?
? ? 0 1 1 0 1 ?

*Mariliasuchus amarali*

0 0 0 0 0 0 1 0 0 0 0 1
0 0 0 [0&1] 0 1 0 0 - 0 0 0
- 0 1 0 0 0 0 1 0 0 1 -
0 0 0 0 0 0 0 0 0 0 0 1

0 1 0 0 0 0 1 0 0 1 0 0
0 0 1 0 0 0 0 0 0 0 - -
0 0 0 1 1 0 0 0

*Notosuchus terrestris*

0 0 0 0 0 ? 1 0 0 0 2 0
0 0 0 0 0 1 0 - - 0 0 0
- 0 0 0 0 0 0 ? 0 0 0 ?
0 0 0 0 0 0 ? 0 0 ? 0 1
1 0 0 0 0 0 0 0 0 0 0 0
0 0 0 0 0 ? 0 0 0 0 - -
0 1 0 1 1 0 0 0

*Aplestosuchus sordidus*

1 1 ? 0 1 0 0 0 1 0 2 ?
0 ? ? 0 1 0 ? ? 0 2 ? 1
1 ? 2 1 ? ? ? ? [1&2] [0&1] ? 0
1 1 ? 1 2 1 ? 1 2 ? 1 0
? 0 1 ? ? 1 2 0 0 1 0 0
1 1 0 1 1 1 ? 1 0 1 0 0
1 1 ? ? ? 1 1 0

*Baurusuchus albertoi*

? ? ? ? ? ? ? ? ? ? ? ?
? 1 1 1 1 0 2 ? 0 ? ? 1
1 0 2 1 1 0 1 0 1 1 1 0
1 1 ? ? ? ? 0 ? 2 ? ? 0
1 ? ? ? ? ? ? ? ? ? ? ?
? ? ? ? 1 0 ? 1 ? ? ? ?
1 1 1 1 0 1 ? ?

*Baurusuchus pachecoi*

1 1 ? ? ? ? ? ? ? ? ? ?
? 1 1 1 0 0 [1&2] 0 ? 1 1 0
1 0 2 1 ? 0 1 0 1 1 1 0
? 1 0 1 2 1 ? 1 1 ? 1 0

0 ? 1 1 ? 2 2 0 0 1 0 ?

1 1 1 ? 1 0 1 0 ? 1 1 1

1 0 1 - 0 1 ? 1

*Baurusuchus salgadoensis*

1 1 1 0 2 0 0 1 1 0 1 2

0 1 1 1 1 0 1 0 0 2 ? 1

1 0 2 1 1 0 1 0 1 1 1 0

1 1 0 1 2 1 0 1 1 ? ? 0

0 ? 1 1 0 1 2 0 0 1 0 1

1 1 1 1 1 1 1 1 0 1 1 1

0 0 2 1 0 1 0 ?

*Campinasuchus dinizi*

1 1 1 1 1 ? 0 ? 1 ? 2 2

1 1 1 1 1 0 [1&2] 0 ? 2 ? 1

0 0 2 1 ? 1 1 ? 1 0 1 ?

1 1 0 1 2 1 ? 1 2 ? 0 1

1 1 ? 1 ? ? 2 0 0 1 0 1

1 1 1 1 1 ? 0 0 1 1 0 0

0 0 [1&2] [0&1] 1 1 0 [0&1]

*Cynodontosuchus rothi*

1 ? ? ? ? ? ? ? ? ? ? ?

? ? ? ? ? ? ? ? ? [1&2] ? ?

? ? ? ? ? ? ? ? ? ? ? ?

? ? 1 1 0 0 ? 0 ? ? ? ?

? ? ? ? ? ? 2 1 1 - 0 ?

? 1 1 1 ? ? ? ? ? 1 - 0

? ? ? ? ? ? ? ?

*Gondwanasuchus scabrosus*

1 0 1 1 1 0 ? ? ? ? ? 2

? 1 1 ? ? ? ? ? 0 1 1 1

0 0 2 1 ? ? ? ? ? ? ? ?

? ? ? 1 0 0 0 1 1 ? ? ?

? ? ? ? ? ? 2 0 0 1 0 0

1 1 0 1 ? ? 0 0 ? 1 0 0

? 1 ? ? ? 1 ? ?

*Pissarrachampsa sera*

1 1 1 1 1 0 0 0 1 1 2 2

1 1 1 [0&1] 1 0 [1&2] 1 0 2 1 1

0 0 2 1 1 1 1 2 2 0 0 1

1 1 ? 1 2 1 1 1 2 1 0 1

1 1 1 1 1 2 2 1 0 0 1 1

1 1 1 1 ? ? 0 0 1 1 0 0

? 0 1 0 0 ? 0 0

*Stratiotosuchus maxhechti*

1 1 0 0 2 0 1 1 1 0 1 2

0 1 1 0 1 0 1 0 1 2 1 1

0 1 2 1 1 0 1 0 1 1 0 0

1 1 1 1 2 1 ? ? 2 0 1 ?

1 ? ? ? 0 ? 2 1 0 0 0 1

1 ? 1 1 ? ? 1 0 1 1 0 0

? ? 1 0 1 0 0 0

*Wargosuchus australis*

1 1 ? 1 1 1 ? ? ? 1 ? 2

? ? ? ? ? ? ? 0 ? ? ? ?

? ? ? ? ? ? ? ? ? ? ? ?

? ? ? ? ? ? ? ? ? ? ? ?

? ? ? ? ? ? 2 ? 0 0 ? ?

? ? ? ? ? ? ? ? ? ? ? ?

? ? ? ? ? ? ? ?

LPRP 0697

1 1 1 1 1 1 0 0 1 0 0 2

0 1 1 1 1 0 1 0 0 2 ? 1

1 0 2 1 1 1 1 ? [1&2] 1 1 0

1 1 0 1 2 1 0 0 1 0 0 0

| | | | | | | | | | | | |
|---|---|---|---|---|---|---|---|---|---|---|---|
| 0 | 0 | 1 | 1 | 1 | 2 | 2 | 0 | 0 | 1 | 0 | 0 |
| 0 | 1 | 1 | 1 | 1 | ? | 1 | 1 | 0 | 1 | 1 | 1 |
| 0 | 1 | 1 | 0 | 1 | 1 | 1 | 1 | | | | |

## APPENDIX 5

### List of synapomorphies

a. Common synapomorphies from the three most parsimonious tree of the original dataset (74 x 14).

**Node 1**

Char. 6: 1 → 0

Char. 14: 0 → 1

Char. 16: 0 → 1

Char. 27: 0 → 1

Char. 28: 0 → 1

Char. 51: 0 → 1

Char. 52: 0 → 1

**Node 2** (Baurusuchidae)

Char. 0: 0 → 1

Char. 54: 1 → 2

**Node 3**

Char. 40: 0 → 1

Char. 43: 0 → 1

**Node 4**

Char. 21: 1 → 2

Char. 40: 1 → 2

Char. 41: 0 → 1

**Node 5** (Pissarrachampsinae)

Char. 10: 01 → 2

Char. 12: 0 → 1

Char. 68: 0 → 1

Char. 73: 1 → 0

**Node 6**

Char.57: 1 → 0

**Node 7** (Baurusuchinae)

Char. 24: 0 → 1

Char. 33: 0 → 1

Char. 35: 1 → 0

Char. 47: 1 → 0

Char. 66: 0 → 1

Char. 67: 0 → 1

**Node 8**

Char. 3: 1 → 0

Char. 46: 0 → 1

**Node 11**

Char. 44: 2 → 1

Char. 48: 1 → 0

Char. 70: 0 → 1

Char. 71: 0 → 1

b. Common synapomorphies from one most parsimonious tree of the modified dataset (80 x 14) with new characters present.

**Node 1**

Char. 6: 1 → 0

Char. 14: 0 → 1

Char. 16: 0 → 1

Char. 27: 0 → 1

Char. 28: 0 → 1

Char. 51: 0 → 1

Char. 52: 0 → 1

**Node 2** (Baurusuchidae)

Char. 0: 0 → 1

Char. 54: 1 → 2

**Node 3**

Char. 43: 0 → 1

**Node 4**

Char. 21: 1 → 2

Char. 40: 0 → 2

Char. 41: 0 → 1

**Node 5** (Pissarrachampsinae)

Char. 10: 01 → 2

Char. 12: 0 → 1

Char. 59: 0 → 1

Char. 68: 0 → 1

Char. 73: 1 → 0

**Node 6**

Char.57: 1 → 0

**Node 7** (Baurusuchinae)

Char. 24: 0 → 1

Char. 33: 0 → 1

Char. 35: 1 → 0

Char. 47: 1 → 0

Char. 66: 0 → 1

Char. 67: 0 → 1

**Node 8**

Char. 3: 1 → 0

Char. 46: 0 → 1

Char. 72: 0 → 1

**Node 9**

Char. 4: 1 → 2

Char. 7: 0 → 1

Char. 59: 0 → 1

**Node 10** (*Baurusuchus*)

Char. 75: 0 → 1

Char. 76: 1 → 0

**Node 11**

Char. 44: 2 → 1

Char. 48: 1 → 0

Char. 73: 1 → 0